THE UNIVERSITY OF MICHIGAN RESEARCH INSTITUTE
ANN ARBOR

# INVESTIGATION OF NARROWBAND WAVEFORMS GENERATED BY CLOCKED PULSES

Technical Report No 112

Cooley Electronics Laboratory
(formerly Electronic Defense Group)
Department of Electrical Engineering

By M. P. Ristenbatt

Approved by: A. B. Macnee

Project 2899

TASK ORDER NO. CEL-3
CONTRACT NO. DA-36-039 sc-78283
SIGNAL CORPS, DEPARTMENT OF THE ARMY
DEPARTMENT OF THE ARMY PROJECT NO. 3A99-06-001-01

Submitted in partial fulfillment of the requirements for the
Degree of Doctor of Philosophy in The University of Michigan

October 1960

ACKNOWLEDGEMENTS

The author wishes to express sincere appreciation to all the members of the Doctoral Committee for their technical guidance and comments on this material. Especial thanks are owed to the Chairman, Professor Alan B. Macnee, and to Professor Gunnar Hok for the extended conferences with them and their technical support.

Sincerest appreciation is due Mr. T. G. Birdsall, who was in close contact with all this work and who provided a constant stream of ideas and technical guidance. Also, credit is due Mr. Edmund P. Gould, who conducted all the experimental work, and Mr. Gordon Roberts who first noted a spectral property of great interest to this work.

Finally the author wishes to thank Mr. Robert E. Graham, Miss Ann Rentschler, and Mr. Earl DeRienzo for their skilled and intensive efforts in preparing the material for publication.

The research reported on in this paper was supported by the U.S. Army Signal Corps.

TABLE OF CONTENTS

TABLE OF CONTENTS--Continued

LIST OF ILLUSTRATIONS

LIST OF ILLUSTRATIONS--Continued

LIST OF ILLUSTRATIONS--Continued

LIST OF ILLUSTRATIONS--Continued

# LIST OF SYMBOLS

| Symbol | Description |
|---|---|
| $a_n$ | Sign of individual pulse; either positive or negative |
| $e(t)$ | Output of transmitting filter |
| $e_1(t)$ | Output of transmitting filter with sequence as input |
| $e_2(t)$ | Output of analyzing filter |
| $f_c$ | Clock frequency ($1/f_c$ equals clock interval) |
| $f_o$ | Center frequency of transmitting filter |
| $g(t)$ | Pulse response of analyzing filter or an elementary pulse |
| $h(t)$ | Pulse response of transmitting filter |
| $r$ | Number of poles-pairs of a filter |
| $t_1$ | Width of finite pulse |
| $u_o$ | Rectangular area whose limit is an impulse |
| $x(t)$ | Clocked sequence of pulses |
| $y(t)$ | General multiplying waveform |
| $A_m$ | Fourier coefficients |
| $A_{N'}$ | Coefficient of particular sum of sine waves |
| $E_1(t)$ | Output of analyzing filter with sequence as input |
| $E_2(t)$ | Output of transmitting filter |
| $E_3(t)$ | Output of transmitting filter with heterodyning |
| $E\{\ \}$ | Expected value |
| $F(t)$ | Envelope of pulse response |
| $F^2(\omega)$ | Finite Fourier transform |
| $G(j\omega)$ | Frequency characteristic of analyzing filter |
| $G_t(\omega)$ | Short-time power spectrum |
| $G_{xx}(f)$ | Power spectral density of random process |

LIST OF SYMBOLS--Continued

| Symbol | Description |
|---|---|
| $H(j\omega)$ | Frequency characteristic of transmitting filter |
| $K(t)$ | Coherent, multiplying waveform |
| L | Digit length of period |
| M | Magnitude |
| $N = N(t)$ | Integer that advances by one with each clock pulse |
| N' | Particular value of N |
| $R_x(\tau)$ | Auto-correlation of random process x(t) |
| $\mathcal{R}(\tau)$ | Finite, time auto-correlation |
| $S_N(f)$ | Fourier transform of ensemble of random processes |
| T | Total period of a time waveform. It is used both for period of sequences ($T = L/f_c$) and for clock period ($T = 1/f_c$) in this work. |
| T' | Integrating time |
| $\alpha$ | Damping coefficient of exponential decays |
| $\beta$ | Angle associated with sampling phase |
| $\delta$ | Ideal impulse |
| $\theta$ | Angle associated with pulse response |
| $\theta_N$ | Angle associated with particular sum of pulse responses |
| $\sigma^2(\beta)$ | Sampled variance as a function of sampling phase $\beta$ |
| $\hat{\sigma}^2(\beta)$ | Estimate of sampled variance |
| $\sigma_c{}^2(\beta)$ | Sampled variance of clocked waveforms |
| $\sigma_{ac}{}^2(\beta)$ | ac portion of $\sigma_c{}^2(\beta)$ |
| $\sigma_{dc}{}^2(\beta)$ | dc portion of $\sigma_c{}^2(\beta)$ |
| $\sigma_N{}^2(\beta)$ | Sampled variance of noise waveform |
| $\theta_t(\tau)$ | Short-time auto-correlation function |

LIST OF SYMBOLS--Continued

| Symbol | Description |
|---|---|
| $\omega_c$ | Clock frequency |
| $\omega_d$ | Frequency difference from a multiple of half-clock |
| $\omega_o$ | Center frequency of transmitting filter |
| $a \nmid b$ | "a does not divide b" |
| $a \mid b$ | "a divides b" |
| $\ni$ | "such that" |
| $[\frac{t}{T}]$ | Largest integer less than $\frac{t}{T}$ |

ABSTRACT

This analytical and experimental study seeks to find those properties of narrowband waveforms which characterize the waveform as being clocked instead of Gaussian noise, where the waveforms are generated by hard-filtering sequences of constant-amplitude clocked pulses having a random (positive or negative) sign. First the ordinary frequency spectrum of both periodic and aperiodic sequences of pulses is calculated, using the usual methods.

The short-time spectrum of the narrowband waveforms, calculated by writing the output as a sum of filter pulse responses, exhibits a basic half-clock symmetry and other symmetry relations. If the filter passband is located at any of these symmetry points, the short-time spectrum will indicate the presence of clocking.

The variance of the magnitude of waveform samples taken coherently with the clock is calculated, versus phase between the sampling and clock positions. A maximum and a minimum variance relation is found, as a function of the clock-to-filter frequency, for the exponential filter. An analysis and corroborating experiments show that a waveform consisting of the "sum of weighted, sampled variances" can be used to characterize the waveforms as clocked if the waveform is run coherently with the clock.

Zero-crossing calculations for exponential filters show regularity of crossings under certain conditions. Probability density measurements of the zero-crossings show that an exponential filter produces a density distinguishable from noise, but this is not true, in general, for a non-exponential filter.

# CHAPTER I

## INTRODUCTION

The objective of the research in this thesis is the study of narrow-band waveforms which have been generated by passing sequences of clocked pulses through a relatively narrow-band filter. In general it will be our objective to note any characteristics of this narrow-band waveform that are associated with the clocked-pulsed input. A particular goal is the comparison of any output characteristics with the clocked input to the corresponding characteristics when the input is Gaussian noise. This aspect of the general investigation can be represented as shown in Fig. 1-1; the objective here is to note those characteristics which serve to identify the presence of the clocked pulses as the input, as opposed to the Gaussian input, looking only at the output.

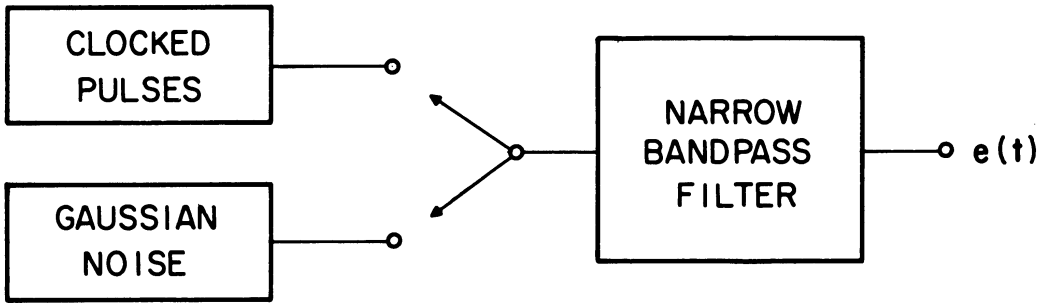


Fig. 1-1. The distinguishing aspect of the general investigation.

The sequence of pulses referred to here consists of pulses appearing at every clock position; these pulses are identical except that some are positive and some negative. For the purposes of this thesis the sign of the pulse at each clock position will be determined on a truly random

basis with the probability of a positive or negative being equally likely, hence, equal to one-half. One can consider such a sequence of pulses as resulting from sampling, at the clock rate, of one type of "random telegraph signal" (Ref. 1). When referring to such a sequence, we shall use the term "random telegraph wave."

When such a sequence of pulses is passed through a narrow-band (high Q) filter, one can analytically view the filter output as a superposition of a number of the filter's pulse responses. The narrow-band property is defined by the requirement that ten or more pulse responses will give significant contributions to the output for any time t. Although a certain amount of structure is imparted to the output by virtue of the "clocking" of the input pulses, this output structure tends to disappear for two reasons: (1) the randomness of the sign of the pulse; and (2) the expected incommensurability of the clock rate and periodicities in the pulse response. Hence, grossly speaking, the filter output "scrambles" ten or more of the input pulses and depends upon the particular positive-negative sequence that immediately preceded time t.

At this point it is useful to note that the output, with a Gaussian noise input (Fig. 1-1), can also be conceptually regarded as resulting from a superposition of elementary pulses. One of the most familiar examples of Gaussian noise is the filtered shot effect, taken in a limiting sense. In turn, the shot effect is viewed conceptually as the superposition of elementary pulses, in which the density of pulses is allowed to approach infinity while the magnitude of the individual pulse tends toward zero (Ref. 2). Taking note of the differences between the above "sequence of pulses" and the shot-effect model we note that: (1) the time of occurrence of the pulses in the shot effect is a random variable, compared to

the clocking of the pulses; (2) the expected number of pulses within a given time interval follows a Poisson distribution for the shot effect, but is constant for the clocked process; and (3) the density of pulses in the shot effect approaches infinity, compared to a finite clocking rate.

## 1.1 Areas of Investigation

This investigation of the narrow-band clocked waveforms is divided into four major parts: (1) the ordinary power spectrum description of the filtered and unfiltered clocked sequences; (2) short-time spectrum calculations and experiments; (3) statistical amplitude considerations; and (4) zero-crossing properties. The ordinary spectrum considerations will be studied first, since they are the most familiar description of signals and provide the most basic information about the clocked processes. In dealing with these calculations the clocked processes will be considered as a periodic phenomenon and also as a random process.

The short-time spectrum considerations will be found to be useful in distinguishing the clocked process from Gaussian noise. From these short-time considerations one can state properties of all clocked waveforms and also distinguishing properties under a variety of conditions. Also the short-time spectrum considerations will include the possible use of short-time autocorrelation as a means of identifying the input. If the clocked inputs are considered as samples of an ensemble of a random process, then it is clear that the above two considerations, ordinary spectrum and short-time spectrum, are calculations and measurements of the second-order statistic. Such an approach, involving second-order statistics, is by far the most familiar and most often used property in dealing with either random processes or deterministic processes.

The third area of investigation involves statistical amplitude considerations. Concerning the amplitude statistics, it can readily be shown that these statistics are "cyclo-stationary"; that is, the statistics are not stationary in the common sense but do exhibit a repetitive behavior having the period of one clock interval. This repetitive statistical behavior leads one to consider the variance of the amplitude, taken at different positions within a clock interval.

For the zero-crossing case, the investigation looks for particular behavior of the zero-crossing intervals when the waveform is clocked and narrow-band. From this investigation, one can state the properties of the "zero-crossing-interval" probability distribution for given combinations of filters and clock frequencies. In addition, information is obtained about the correlation of "excessive" zero-crossing intervals with the clock. Experimental verification of both of these studies has been obtained.

At this point it is worthwhile to point out two approaches which have not been investigated in this study. The first is the testing of the output for non-Gaussianness. Although any clocked process is inherently nonstationary, one can construct a stationary ensemble from the samples by assuming a random phase relationship (i.e., a random time origin) among the samples. With such a stationary process it is possible to approximate the amplitude probability density by calculating the first four moments and using well-known approximation techniques (Ref. 3). The chief reason for not pursuing this attack was the dim prospect for successful results. Middleton (Ref. 4) and Mazelsky (Ref. 5) have shown that the amplitude probability density becomes very nearly Gaussian when a sufficiently narrow-band filter is used, as is dealt with in this investigation.

Another method that might at first appear profitable is the consideration of the inverse-filter possibility. This method was not pursued primarily because, for narrow-band signals, the corresponding inverse filter becomes extremely difficult to realize since theoretically it would require gain outside the signal passband and attenuation within this passband. Thus the noise would far outweigh the signal. Further, if an inverse-filter achievement were successful it would mean that it would be possible not only to identify the input as clocked but also to directly decode the input pulses. Thus this appears to be a more difficult problem than identifying the input as clocked. Since we wish to simply identify the presence of clocked input pulses under difficult conditions, the inverse filter was not considered feasible.

## 1.2 Maximal Sequences as Simulation of Truly Random Sequences

One way to generate a clocked sequence of pulses (described earlier) is to divide the time axis into discrete intervals and, at each clock position, decide the sign (positive or negative) of the pulse by purely probabilistic means (the equivalent of flipping a coin). Generated in such a way, the resulting sequence will have statistics given by probability considerations. Over a sufficiently long time, the number of "heads" is approximately equal to the number of "tails"; about one-half the consecutive runs have length one, one-quarter have length two, etc.

A very convenient tool, when dealing with clocked sequences experimentally, is the use of deterministic sequences which have, over a period, statistics very close to those described above. Such sequences are called "maximal sequences" (Ref. 6) or "pseudo-noise sequences" (Ref. 7). The statistics of these sequences over a period are very close to

those mentioned; in particular:

(1) The number of heads per period is always one more than the number of tails.

(2) Half the runs (consecutive states of same sign) are of length one, one-fourth of length two, etc., as long as the number of runs concerned exceeds one.

(3) The finite autocorrelation of these sequences closely resembles that of a truly random sequence.

In this work, maximal sequences were used as experimental signals for simulating truly random sequences. This permits a repeatable waveform to be displayed on the oscilloscope which, at the same time, has the necessary statistics. Furthermore, the relative ease with which these sequences can be generated makes them especially attractive.

Maximal sequences are generated by using a binary shift-register generator to which a binary feedback loop is attached. The feedback link uses modulo-two logic and connects various stages of the register (including the last) back to the input stage. By using this method, called a "linear shift-register generator," one can obtain a sequence of length $2^n-1$ from a register of n stages.

To illustrate this method, Fig. 1-2 shows a four-stage linear shift-register, its output sequence, and its run statistics. The output sequence can be justified by assuming any four digits (except all zeros) as the initial state and then adding modulo-two the last two digits to obtain the next input digit, etc. For the run statistics there are a total of eight runs in the period, which gives the statistics shown.

For the actual experiments a shift register of twelve stages was used, which resulted in a period of $4 \times 10^3$ digits. It is by this means, then, that the clocked sequences were obtained experimentally to study the characteristics of narrow-band clocked waveforms.

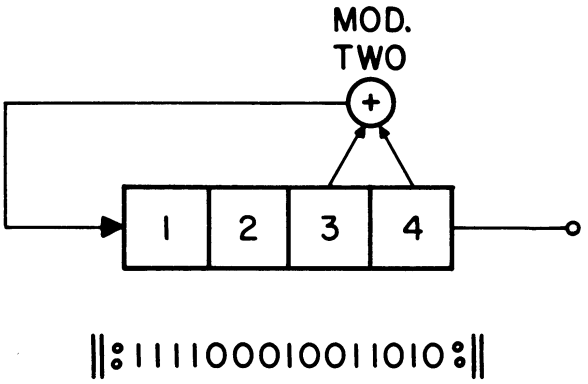


| Run Statistics (out of 8) | | |
|---|---|---|
| Length | Number of runs in period | Ratio to total runs |
| 1 | 4 | 1/2 |
| 2 | 2 | 1/4 |
| 3 | 1 | 1/8 |
| 4 | 1 | 1/8 |

Fig. 1-2. Generation of maximal sequences and their run statistics.

## 1.3 Format

The format of the thesis follows the order of investigation mentioned above. Chapter II considers the ordinary spectrum calculations, where the waveform is considered both as being periodic and as a sample of a random process. In each case the objective is to note under what conditions it is possible to use the particular method being considered to identify the input process. Chapter III is devoted to short-time frequency spectrum considerations; both analytical calculations and experiments including sound spectrographs are reported. Chapter IV concerns a statistical evaluation of the amplitude of clocked waveforms. Finally, Chapter V deals with zero-crossing information, and a number of experimental results are reported here.

In general, when reporting the results of experiments, we will describe the experiment briefly and show the results within the text at the appropriate place. The actual equipment used in the experiment, circuit diagrams of new equipment, and a detailed description will be relegated

to Chapter VI, the final chapter. Thus there will be one section of Chapter VI for each major experiment performed.

# CHAPTER II

# ORDINARY SPECTRUM DESCRIPTION

It is the objective of this chapter to display the long-time power spectral density of the filtered and unfiltered pulse sequences that are being dealt with in this report. The long-time spectrum considerations consist of two points of view: (1) analyzing the pulse sequence in terms of a periodic sequence of pulses; and (2) analyzing the pulse sequence as a nonperiodic member of an ensemble of possible pulse sequences. As will be noted, the two points of view yield similar results, but the method of obtaining them is quite different. In the first part we will consider the periodic point of view and in the second part the member-of-an-ensemble point of view.

## 2.1 Periodic Clocked Sequences--Maximal Sequences

If one is dealing with a periodic clocked sequence, then there are a finite number of possible sequences for a given period length. However, out of all possible sequences of a given length, in this investigation we are interested in those which simulate a truly random sequence by having the three randomness properties described in Section 1.2. Restricting oneself thus, one is forced to consider linear shift-register generated sequences of the type described, since there are no other sequences having these properties. Therefore, in considering periodic "random-like" sequences, we shall be dealing with such maximal sequences.

It will seem below that one can calculate the power spectral density for all maximal sequences with one general expression--which is a function of the period and the particular pulse shape. This can be done by

noting that the finite-time autocorrelation function is the same for all maximal sequences.

Before considering the power spectral density for maximal sequences, consider the simplest description of any periodic waveform, the Fourier series representation. Using the complex form of a Fourier series representation, any waveform having a finite number of maxima and minima and an absolutely convergent integral in the fundamental range is written:

$$f(t) = \sum_{m=-\infty}^{\infty} A_m e^{\frac{i2m\pi}{T} t} , \qquad (2\text{-}1)$$

where:

$$A_m = \frac{1}{T} \int_0^T f(t) e^{\frac{-i2m\pi}{T} t} dt , \text{ and}$$

$T$ = period of pulse sequence.

Since the particular $f(t)$ being considered in this section is a sequence of pulses, the $f(t)$ can be written as:

$$f(t) = \sum_{n=0}^{L} a_n \, g(t - \frac{n}{f_c}) , \qquad (2\text{-}2)$$

where:

$a_n$ = sign of pulse at $t = n \times \frac{1}{f_c}$ ,

$L$ = digit length of period = $Tf_c$, and

$g(t)$ = particular pulse shape of an elementary pulse.

Upon the substitution of Eq. 2-2 into Eq. 2-1, $A_m$ can formally be written:

$$A_m = \frac{f_c}{L} \sum_{n=0}^{L} a_n \int_0^T g(t - \frac{n}{f_c}) e^{\frac{-i2m\pi}{T} t} dt , \qquad (2\text{-}3)$$

where:

$A_m$ is the mth component of a Fourier series.

Any attempt to evaluate Eq. 2-3 to find the Fourier coefficients, in amplitude and phase, requires that each $a_n$ for the pulse sequence be known. However, here we are interested in the power spectral density, which involves only the magnitude of the Fourier coefficients. It is well known (Ref. 8) that the power spectral density of a periodic waveform[1], which can be expanded as in Eq. 2-1, is given by:

$$\delta(f) = \sum_{n=-\infty}^{\infty} |A_m|^2 \, \delta(f - nf_o) \qquad \left(f_o = \frac{1}{T}\right) \quad , \tag{2-4}$$

where:

$\delta(f)$ = power spectral density of periodic function, and

$A_m$ = Fourier coefficients given by Eq. 2-1.

We wish to find, then, the value of $|A_m|^2$ for all maximal sequences. This is done by considering the finite-time autocorrelation for the maximal sequences. It is remembered that the time correlation functions equal the statistical correlation functions if the process is ergodic (Ref. 9).
The finite-time autocorrelation is defined as:

$$\mathcal{R}(\tau) = \frac{1}{T} \int_o^T x(t)x(t + \tau)dt \quad , \tag{2-5}$$

where:

$\mathcal{R}(\tau)$ = finite-time autocorrelation function, and

$T$ = period of waveform.

---

1 The power spectral density of a periodic waveform considered here should not be confused with the spectral density of a periodic, wide-sense, stationary random process. In the former we deal with only the time autocorrelation function, whereas in the latter a statistical correlation is used.

Considering the properties of maximal sequences in Section 1.2, the fact that there is always one more "head" than "tails" means that this correlation function will be the same for all maximal sequences. For the case of rectangularly-shaped pulses the general function is depicted in Fig. 2-1. The pulse parameters in Fig. 2-1 have been normalized so that the

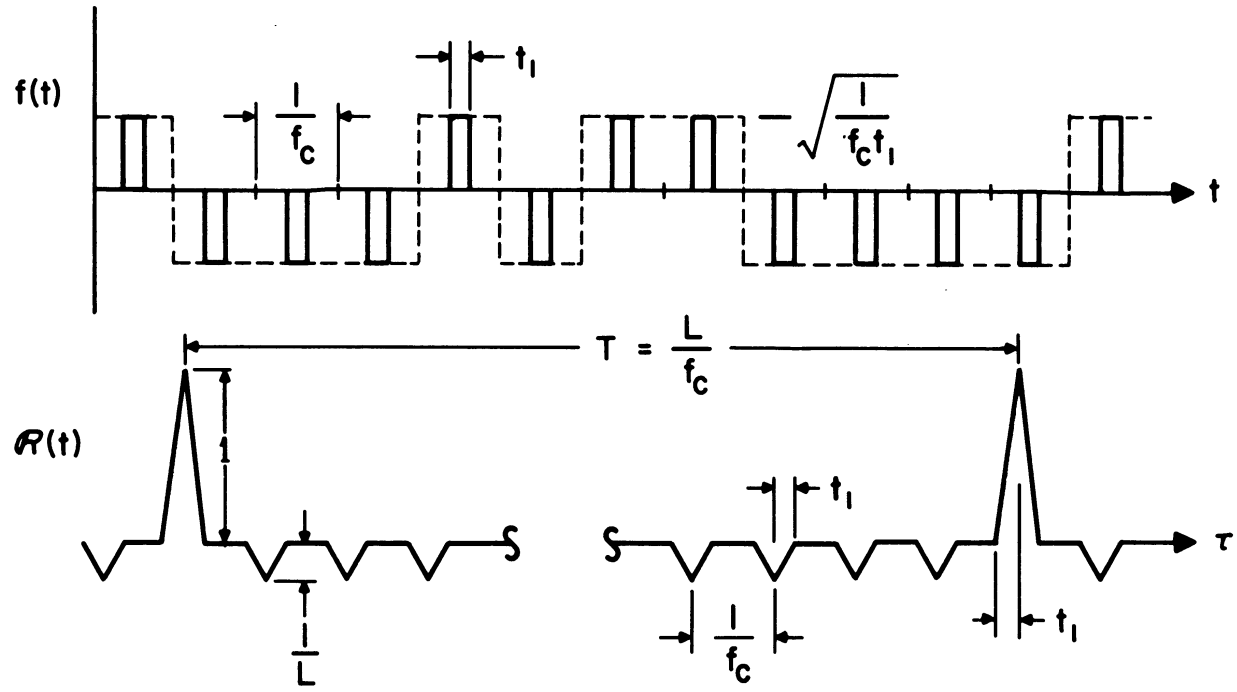


Fig. 2-1. Finite, time autocorrelation for all maximal sequences with rectangular pulses.

major peak [R(o)] equals one, and the subsidiary peaks [$R(\frac{k}{f_c})$] equal $\frac{1}{L}$ (L is the length of the period in clock intervals). It may be noted that the form of the major and subsidiary peaks are the same, but differ by a scale factor. This will be true for all pulse shapes. If the pulse shapes were triangular, then the correlation function would be parabolic, etc.

The issue here is that this $R(\tau)$ is the same for all maximal

sequences and therefore we wish to find the power spectral density in terms of this correlation function. This can be done by finding the relation between $\mathbb{R}(\tau)$ and the values of $|A_m|^2$. We begin by defining a finite transform of $\mathbb{R}(\tau)$ for discrete frequencies:

Let

$$F^2(\omega) = \frac{1}{T}\int_0^T \mathbb{R}(\tau)e^{-i\omega\tau}d\tau \qquad (2\text{-}6)$$

for

$$\omega \ni \omega T = 0 \pmod{2\pi},$$

where:

$F^2(\omega)$ = finite Fourier transform.

Note that in Eq. 2-6 the $F^2(\omega)$ is defined for only those $\omega$'s for which $\omega T = 0 \pmod{2\pi}$; for $\omega$'s restricted in such a way the $F^2(\omega)$ is always real. Substituting Eq. 2-5 into Eq. 2-6 one obtains:

$$F^2(\omega) = \frac{1}{T^2}\int_0^T\int_0^T x(u)x(u+\tau)e^{-i\omega\tau}d\tau\,du \qquad (2\text{-}7)$$

$$= \frac{1}{T^2}\int_0^T\int_0^T x(u)e^{i\omega u}\,x(u+\tau)e^{-i\omega(\tau+u)}d\tau\,du \quad .$$

Now change variable by letting $v = \tau + u$.

Then:

$$F^2(\omega) = \frac{1}{T^2}\int_0^T\int_0^T x(u)e^{i\omega u}\,x(v)e^{-i\omega v}\,dudv \qquad (2\text{-}8)$$

$$= \left(\frac{1}{T}\int_0^T x(u)e^{i\omega u}du\right)\left(\frac{1}{T}\int_0^T x(v)e^{-i\omega v}dv\right) \quad .$$

But for values of $\omega$ limited to multiples of $2\pi/T$ using Eq. 2-1 it is seen that Eq. 2-8 consists of the product of $A_m$ and its complex conjugate:

$$F^2(\omega) = A_m A_m^* = |A_m|^2 \quad , \tag{2-9}$$

where:

$A_m$ = the Fourier coefficients given by Eq. 2-1.

It is remembered from Eq. 2-1 that $A_m$ is defined for both positive and negative values of m; hence we have a power spectral density for both positive and negative frequencies. If one wishes to speak only about spectral density for positive frequencies, then the values of Eq. 2-9 must be multiplied by two.

As a result of Eq. 2-9 one can find the power spectral density for any periodic maximal sequence of pulses. We will now do this for the general autocorrelation of maximal sequences with rectangular pulses given in Fig. 2-1. Our procedure will be to evaluate $F^2(\omega)$ at the proper $\omega$. Figure 2-1 is repeated in Fig. 2-2 with proper notation.

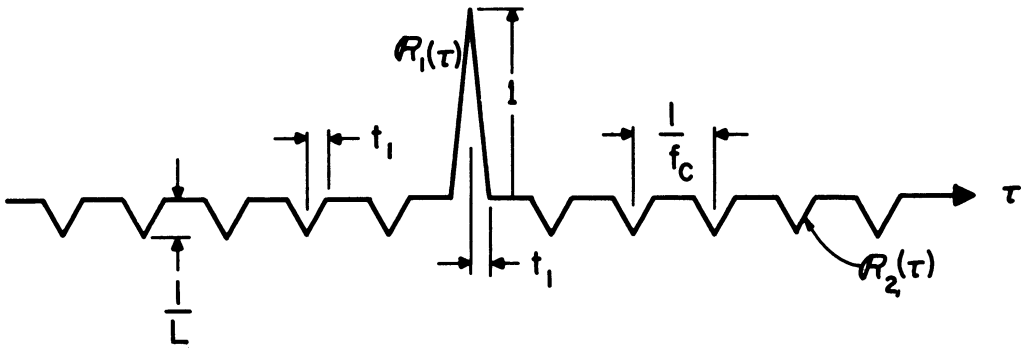


Fig. 2-2. $\mathcal{R}(\tau)$ for all maximal sequences with rectangular pulses; a repeat of Fig. 2-1.

Using Eq. 2-6 and writing $\mathcal{R}(\tau)$ as the sum of its major peak and its minor peaks, one writes:

$$F^2(\omega) = \frac{1}{T}\int_{-t_1}^{+t_1} R_1(\tau)e^{-i\omega\tau}d\tau - \frac{1}{T}\sum_{n=1}^{L-1}\int_{n/f_c-t_1}^{n/f_c+t_1} R_2(\tau)e^{-i\omega\tau}d\tau . \quad (2\text{-}10)$$

But $R_2(t) = \frac{1}{L}R_1(\tau)$. Noting this, and adding and subtracting $R_2(\tau)$ at $\tau = 0$, one obtains:

$$F^2(\omega) = \frac{1}{T}\int_{-t_1}^{+t_1} R_1(\tau)e^{-i\omega\tau}d\tau + \frac{1}{L}\left[\frac{1}{T}\int_{-t_1}^{+t_1} R_1(\tau)e^{-i\omega\tau}d\tau\right] \quad (2\text{-}11)$$

$$- \frac{1}{T}\sum_{n=0}^{L-1}\frac{1}{L}\int_{n/f_c-t_1}^{n/f_c+t_1} R_1(\tau)e^{-i\omega\tau}d\tau .$$

Let $\tau' = \tau - \frac{n}{f_c}$ ; then drop the primes in the 2nd summation:

$$F^2(\omega) = \frac{1}{T}\left[\frac{L+1}{L}\int_{-t_1}^{t_1} R_1(\tau)e^{-i\omega\tau}d\tau - \sum_{n=0}^{L-1}\frac{1}{L}\int_{-t_1}^{+t_1} R_1(\tau)e^{-i\omega(\tau+\frac{n}{f_c})}d\tau\right] \quad (2\text{-}12)$$

$$= \frac{1}{T}\left[\frac{L+1}{L}\int_{-t_1}^{+t_1} R_1(\tau)e^{-i\omega\tau}d\tau - \frac{1}{L}\int_{-t_1}^{+t_1} R_1(\tau)e^{-i\omega\tau}\sum_{n=0}^{L-1} e^{-i\omega\frac{n}{f_c}}d\tau\right].$$

Since $F^2(\omega)$ is defined only for $\omega_m = \frac{m2\pi f_c}{L}$ ,

$$F^2(\omega_m) = \frac{1}{T}\left[\frac{L+1}{L}\int_{-t_1}^{+t_1} R_1(\tau)e^{-i\omega_m\tau}d\tau - \frac{1}{L}\int_{-t_1}^{t_1} R_1(\tau)e^{-i\omega_m\tau}\sum_{n=0}^{L-1} e^{\frac{imn2\pi}{L}}d\tau\right] . \quad (2\text{-}13)$$

Concerning the summation on the right, note the following:

$$\sum_{n=1}^{L} e^{\frac{-i2\pi mn}{L}} = L \text{ if } m = 0 \pmod L, \text{ and}$$

$$\sum_{n=1}^{L} e^{\frac{-i2\pi mn}{L}} = 0 \text{ if } m \neq 0 \pmod L. \quad (2\text{-}14)$$

Therefore, for all m = 0 (mod L) the summation on the right of Eq. 2-13 equals L. For all other m, the summation equals zero. Consequently one may write, for $F^2(\omega)$:

$$|A_m|^2 = F^2(\omega_m) = \frac{1}{T}\left(\frac{L+1}{L}\right)\int_{-t_1}^{+t_1} \mathcal{R}_1(\tau)e^{-i\omega\tau}d\tau \qquad \text{if } \omega_m = \frac{2\pi m f_c}{L} \neq 0 \pmod{2\pi}; \text{ or} \tag{2-15}$$

$$|A_m|^2 = F^2(\omega_m) = \frac{1}{T}\left(\frac{1}{L}\right)\int_{-t_1}^{+t_1} \mathcal{R}_1(\tau)e^{-i\omega\tau}d\tau \qquad \text{if } \omega_m = \frac{2\pi m f_c}{L} = 0 \pmod{2\pi}.$$

Note that in Eq. 2-15 there is a factor of L + 1 between the components at multiples of clock frequency relative to the other frequencies. We can use Eq. 2-15, then, to find the power spectral density for any type of pulse shape for all maximal sequences; the triangular $\mathcal{R}(\tau)$ shown in Figs. 2-1 and 2-2 pertains specifically to square-top pulses. For other pulse shapes one merely uses the proper $\mathcal{R}(\tau)$ in Eq. 2-15. It is noted that one must always evaluate the two conditions, the case in which multiples of clock are involved and the other cases.

From Eq. 2-15 it can be seen that each of the components in the spectral density will be multiplied by the transform of the particular $\mathcal{R}(\tau)$ and that one can think of this transform as being the envelope of the discrete components in the spectral density. For the square-top waveforms one gets a triangular autocorrelation as shown in Figs. 2-1 and 2-2, and therefore the corresponding $F^2(\omega)$ can be shown to be:

$$|A_m|^2 = F^2(\omega_m) = \frac{L+1}{L} \times \frac{t_1}{T}\left(\frac{\sin\frac{m\pi t_1}{T}}{\frac{m\pi t_1}{T}}\right)^2 \qquad \text{for } \frac{2\pi m}{T} \neq 0 \pmod{2\pi}; \text{ and} \tag{2-16}$$

$$|A_m|^2 = \frac{1}{L} \times \frac{t_1}{T} \left( \frac{\sin \frac{m\pi t_1}{T}}{\frac{m\pi t_1}{T}} \right)^2 \quad \text{for} \quad \frac{2\pi m}{T} = 0 \pmod{2\pi} \quad .$$

If the particular sequence of pulses consisted of ideal impulses, then the integrals in Eq. 2-15 would result in a flat transform. From the foregoing considerations the entries in Fig. 2-3 can be justified.

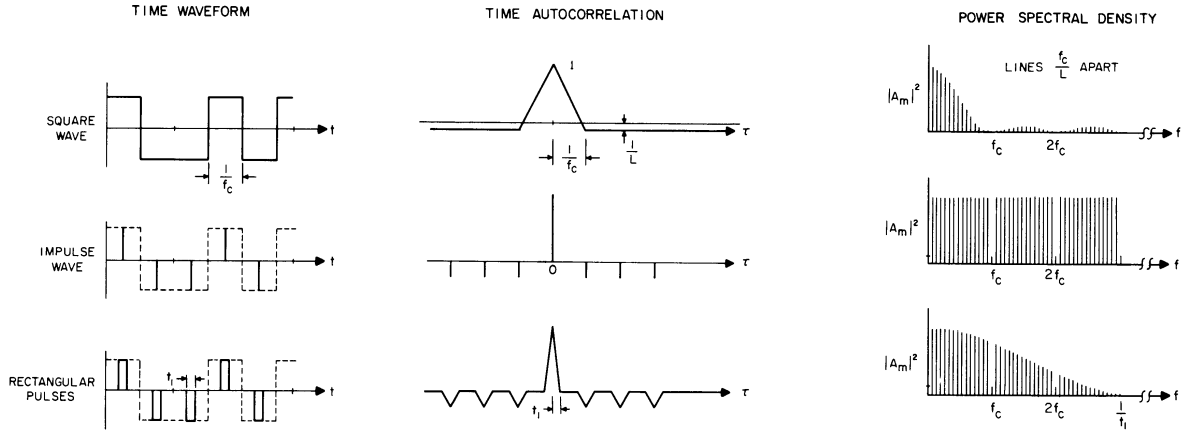


Fig. 2-3. Power spectral density for various pulse shapes, for any maximal sequence.

Part (a) gives the results for the case in which the pulses are as wide as the clock interval, and it is seen that the components follow a $\left(\frac{\sin x}{x}\right)^2$ - shaped envelope. For the impulse case it is seen that the components are flat except for multiples of clock frequencies. In relation to this case it may be noted that one can obtain equal components, including the components at multiples of clock, simply by unbalancing the impulses; i.e., by adding a train of impulses, all of the same sign, to the original train. This can be verified when one considers that the Fourier transform is a linear operation, so if waveforms are added in the time domain one may add the transforms

in the frequency domain. Consequently a flat component envelope could be obtained in Part (b) if the impulses were unbalanced properly in the positive direction. Part (c) considers the case for a finite pulse wave but where the width is less than the clock intervals. This is the case which is of most interest to us. It is noted that the component envelope follows a $\left(\frac{\sin x}{x}\right)^2$-shaped curve, and the first zero occurs when $m = \frac{T}{t_1}$. For other pulse shapes one would find other envelope relationships.

If the maximal clocked sequences treated above are passed through a filter with a transfer characteristic, $H(j\omega)$, the resultant spectral density is obtained, as usual, by multiplying the sequence density by $|H(j\omega)|^2$.

One can see the spectral effect of passing a sequence through a narrow-band filter by considering Fig. 2-3. In the usual case there will be a large number of components (spaced $f_c/L$ apart) even in a narrow band of frequencies. In dealing with such spectra experimentally, it is implied that analyzing equipments have an effective integrating time which is of the order of ten or more times the period of the sequence. Therefore, if the sequence were short enough one could hope to ascertain the fact that separate components exist, and they would bear the relation shown in Fig. 2-3. Under such an ideal condition one could of course identify the pulse input as opposed to the Gaussian noise input without any further ado; however this is a situation which requires no further comment since it is one of a number of singular cases that yield a simple solution. Our purpose here has been to portray these fundamental properties of maximal sequences.

## 2.2 Aperiodic Random Sequence of Pulses

In Section 2.1 we considered the power spectral density for maximal sequences of pulses which are repeated in order to form a periodic sequence. Here we wish to consider the power spectrum of the random process

composed of sequences of pulses which occur when no period considerations are present. We take the point of view here that the sequence of pulses is a member of an ensemble of possible such sequences.

There are two general methods for calculating power spectra of nonperiodic phenomena. The first consists of a direct evaluation of the general formulas; the second, applicable only if the process is stationary over the continuous time domain, consists of finding first the autocorrelation function and then using the Fourier transform to obtain the power spectra. Consider for a moment the stationarity of our process consisting of a sequence of pulses. If a random process $x(t)$ is stationary the joint probability distribution for $x(t_1)$ and $x(t_2)$ depends only on the time difference $\tau$ and not on the particular values $t_1$ and $t_2$. Then the autocorrelation function is a function only of the time difference $\tau$, hence it is independent of t (Ref. 10).

$$R_x(t_1, t_2) = R_x(t, t-\tau) = E\left\{x_1, x_2\right\} = R_x(\tau) \qquad (2\text{-}17)$$

where:

$R_x(\tau)$ = autocorrelation function of process $x(t)$,

$x_1$ = value of $x(t)$ at $t = t_1$,

$x_2$ = value of $x(t)$ at $t = t_2$.

From this definition it can be seen that a sequence of pulses such as we have is not a stationary process with time as a continuous parameter. For example, if the $\tau$ separation is less than a pulse interval the joint probability of $x_1$ and $x_2$ will depend on whether the $\tau$ lies within a pulse interval or spans across two pulse intervals. In any event it can be shown rigorously that a sequence of clocked pulses such as we have does not constitute a stationary process. This is done by showing that the autocorrelation of

the ensemble x(t) does not reduce to an expression which is independent of time and therefore would violate Eq. 2-17.

Since one is not able, a priori, to use the stationary property, the power spectrum must be found by the direct method mentioned above.[1] However, after the results have been obtained it will be seen that the same result would have been obtained if the process were either assumed to be stationary or made to be stationary by the construction of a new ensemble function (allowing the phases of the members of the ensemble to be random).

A method for calculating the power spectrum of sequences of pulses without making use of the stationary property has been described by Bennett (Ref. 11). Because the development below is similar to Bennett's, only the major steps will be outlined here.[2]

To begin, define the ensemble $x_N(t)$ to include only the pulses from n = -N to n = +N:

$$x_N(t) = \sum_{n=-N}^{N} a_n \, g\left(t - \frac{n}{f_c}\right) , \qquad (2\text{-}18)$$

where:

$x_N(t)$ = ensemble of functions x(t) defined from $\frac{-N}{f_c}$ to $\frac{N}{f_c}$, and

g(t) = shape of the individual or elementary pulse.

---

1 There is some confusion among authors about terminology of power spectral density of random processes. Some authors (Ref. 8) restrict discussion of power spectral density to wide-sense stationary random processes. Here, however, we use the more general concept that includes nonstationary random processes (Ref. 12), as described in Eq. 2-20 below. It can be shown that if a power spectral density exists for a nonstationary process then the operations of Eq. 2-20 converge to it.

2 Just prior to publication it was learned that a similar development is described by H. S. Tsien in Engineering Cybernetics (McGraw-Hill, 1954, p. 118-120) with the same results.

Then if we have unit pulses which possess a Fourier transform the transform of the ensemble $x_N(t)$ exists and is given by

$$S_N(f) = \sum_{n=-N}^{N} a_n G(f) e^{-in2\pi \frac{f}{f_c}} , \qquad (2\text{-}19)$$

where:

$S_N(f)$ = Fourier transform of $x_N(t)$ given above, and

$G(f)$ = Fourier transform of $g(t)$, the particular pulse shape of pulses in the sequence.

Now in general the power spectral density for a random process is defined as follows (Ref. 12):

$$G_{xx}(f) = \lim_{T \to \infty} G_{xx}(f,T) \qquad (2\text{-}20)$$

with

$$G_{xx}(f,t) = \left\langle G_T(f, {}^{N}x) \right\rangle \text{ av. over ensemble}$$

and

$$G_T(f, {}^{N}x) = \frac{|A_T(f, {}^{N}x)|^2}{T} ,$$

where:

$G_{xx}(t)$ = power spectral density of random process,

$G_{xx}(f,T)$ = ensemble average of finite power spectral density, and

$A_T(f, {}^{N}x)$ = finite Fourier transform of any sample of $x(t)$.

By a straight implementation of this definition it can be seen that the power spectrum we seek is given by:

$$G_{xx}(f) = \lim_{N \to \infty} \left[ \frac{\text{av} |S_N(f)|^2}{2N + 1} \times f_c \right] . \qquad (2\text{-}21)$$

To evaluate this, begin by writing the average of $|S_N(f)|^2$:

$$\text{av}|S_N(f)|^2 = \sum_{m=-N}^{N} \sum_{n=-N}^{N} \text{av}\left\{a_n\, a_m\right\} G(f)G^*(f)e^{i2\pi \frac{f}{f_c}(m-n)} \qquad (2\text{-}22)$$

$$= \sum_{m=-N}^{N} \sum_{k=m-N}^{m+N} R(k)|G(f)|^2 e^{i2\pi k \frac{f}{f_c}} ,$$

where:

$$k = m - n, \text{ and}$$

$$R(k) = \text{av}\left\{a_r\, a_{r+k}\right\} \text{ for fixed } r.$$

The order of summation of Eq. 2-22 can now be reversed by using the following conversion, which can be justified by considering the summation area in the k - m plane.

$$\sum_{m=-N}^{N} \sum_{k=m-N}^{m+N} = \sum_{k=-2N}^{0} \sum_{m=-N}^{k+N} + \sum_{k=1}^{2N} \sum_{m=k-N}^{N} \qquad (2\text{-}23)$$

Using this to change the order of summation in Eq. 2-22 one finds:

$$\text{av}|S_N(f)|^2 = \sum_{k=-2N}^{0} \sum_{m=-N}^{k+N} R(k)|G(f)|^2 e^{i2\pi k \frac{f}{f_c}} + \sum_{k=1}^{2N} \sum_{m=k-N}^{N} R(k)|G(f)|^2 e^{i2\pi k \frac{f}{f_c}} . \qquad (2\text{-}24)$$

Now, since the quantities under the summation depend only on k and not on m, one can evaluate the inner summation directly by simply totaling the number of terms. By a straightforward process this results in:

$$\text{av}|S_N(f)|^2 = \sum_{k=-2N}^{0} (k + 2N + 1)R(k)|G(f)|^2 e^{i2\pi k \frac{f}{f_c}} + \sum_{k=1}^{2N} (2N + 1 - k)R(k)|G(f)|^2 e^{i2\pi k \frac{f}{f_c}} . \qquad (2\text{-}25)$$

Using the fact that R(k) is equal to R(-k) for all cases and making a substitution of variables in either of the summations, the two summations can be combined to result in:

$$\text{av}|S_N(f)|^2 = 2\sum_{k=1}^{2N}(2N+1-k)R(k)|G(f)|^2\cos 2\pi k\frac{f}{f_c} + (2N+1)R(0)|G(f)|^2 \tag{2-26}$$

$$= (2N+1)|G(f)|^2\left\{R(0) + 2\sum_{k=1}^{2N}\left(1 - \frac{k}{2N+1}\right)R(k)\cos 2\pi k\frac{f}{f_c}\right\} .$$

From this step it can quickly be seen that dividing by 2N+1, multiplying by $f_c$, and letting N go to infinity (Eq. 2-21) yields the result:

$$G_{xx}(f) = \lim_{N\to\infty}\frac{|S_N(f)|^2}{2N+1} \times f_c = f_c|G(f)|^2\left\{R(0) + 2\sum_{k=1}^{\infty}R(k)\cos 2\pi k\frac{f}{f_c}\right\}, \tag{2-27}$$

where:

$G_{xx}(f)$ is the desired power spectral density.

Equation 2-27, then, is the result for the power spectral density of a sequence of pulses which are clocked and which have a zero mean. It is remembered that the pulse sequences we are considering have a zero mean. Note that Eq. 2-27 shows that the power spectral density is determined in two ways: by the basic spectrum of the unit pulse itself and by the statistics of the pulse train which makes up the process. We will now evaluate this expression for a few simple cases.

The case of direct interest to us is that in which the individual $a_n$'s are independent. For this condition the power spectral density of Eq. 2-27 reduces to

$$G_{xx}(f) = f_c|G(f)|^2 a^2 , \tag{2-28}$$

where:

$a$ = height of pulse, and

$R(0) = \text{av}\left\{a_n^2\right\} = a^2$.

Here it is seen that the power spectrum is determined primarily by the shape of the spectrum of the individual pulse itself. It is for this case of independent $a_n$'s that one could have obtained the same result by regarding the process as stationary. That is, one could have regarded the phases of the individual members of the ensemble as being randomly distributed. The procedure then would be: (1) find the auto-correlation function for a representative sample of the process; (2) find the expected value (over the ensemble) of this autocorrelation; and (3) take the Fourier transform of this average autocorrelation to find the power spectral density. It can be shown that, if the $a_n$'s are independent, this procedure yields the same result as Eq. 2-28. We have used the non-stationary method here because this lack of stationarity will be used to show statistical identification methods for the clocked process (Sec. 4.2). Also, the stationary calculation would not show the dependence of the spectrum upon the statistics of the pulse sequence.

Using Eq. 2-28 one can depict the continuous power spectral density for various pulse shapes. Figure 2-4 shows the result for two cases of rectangular pulses. These two densities should be compared to parts (a) and (c) of Fig. 2-3. It is seen that the density here forms the continuous envelope of the frequency spikes of Fig. 2-3.

It should be noted at this point that if the sequence of values $a_n$ did not have a zero mean then the power spectrum as calculated above might contain discrete contributions (spikes) at each of the multiples of clock frequency; in fact there would be such discrete contributions unless

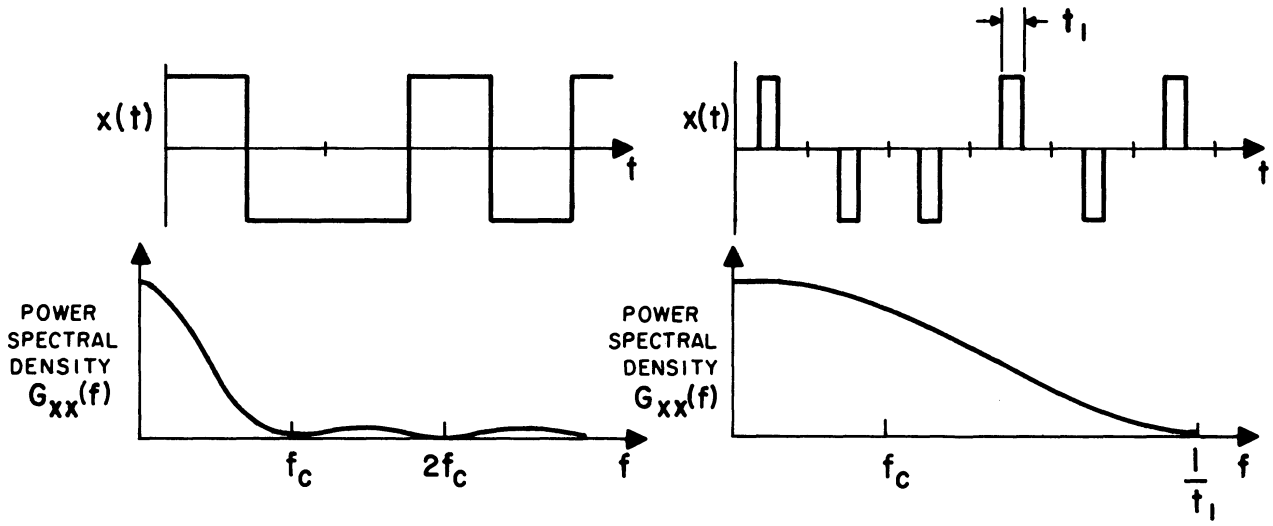


Fig. 2-4. Power spectral density for random sequence of pulses with $a_n$'s independent.

the spectrum of the individual pulse itself had zeros at multiples of clock frequency. Thus, for the general case in which the pulse sequence does not have a zero mean the spectrum will have both a continuous power spectral density as calculated in Eq. 2-27 and line spectral components at each multiple of clock frequency. Since for our case we do not consider anything other than sequences having a zero mean these line components did not appear.

It is of interest to consider the power spectral density when the $a_n$'s are not independent but form a Markoffian process. If the sequence of $a_n$'s forms a wide-sense Markoffian process then the R(k) can be written:

$$R(k) = E\left\{a_n\, a_{n+k}\right\} = a^2 e^{-|k|\alpha} \quad . \tag{2-29}$$

Under these conditions, utilizing Eq. 2-27, the power spectrum is found to be:

$$G_{xx}(f) = f_c |G(f)|^2 \left\{ a^2 + 2 \sum_{k=1}^{\infty} a^2 e^{-k\alpha} \cos 2\pi k \frac{f}{f_c} \right\} \quad . \tag{2-30}$$

Note that the continuous power spectrum now contains periodic components whose period is $f_c$. For example, if $\alpha \geq 2.3$, so that $e^{-2\alpha}$ is one-tenth or less of $e^{-\alpha}$, than a good approximation to $G_{xx}(f)$ is given by the first two terms of Eq. 2-30:

$$G_{xx}(f) = a^2 f_c |G(f)|^2 \left\{1 + 2e^{-\alpha} \cos 2\pi \frac{f}{f_c}\right\} \quad \alpha \geq 2.3 . \quad (2\text{-}31)$$

Thus a periodic phenomenon is superimposed on the spectrum of the unit pulse itself. This periodic phenomenon, here coming from the relation of one $a_n$ to another, is similar to the behavior which occurs in the short-time spectrum for independent $a_n$'s, which will be considered in the next section.

As is always true, the power spectral density after passing any of the above sequences through a linear filter is given by multiplying the appropriate sequence spectrum by $|H(j\omega)|^2$, where $H(j\omega)$ is the transfer characteristic of the filter.

In summary, then, we have found that the power spectral density resulting from considering the pulse sequence as one member of an ensemble of a random process is a continuous density which is similar to the discrete density when the pulse sequence is maximal and periodic. That is, for independent values of $a_n$, the power spectrum is determined, except for a constant, by the spectrum of the unit pulse itself. Thus this resulted in a continuous version of the same spectrum that occurred in a line spectrum for the periodic maximal case.

# CHAPTER III

## SHORT-TIME SPECTRUM CONSIDERATIONS

In the preceding chapter the long-time spectral properties of pulse sequences were investigated, both from the standpoint of the sequence being a periodic phenomenon and from the standpoint of it being a sample of an ensemble of possible pulse sequences. In each of the cases we noted the effect of passing this spectrum through a narrow-band filter and then discussed the possibilities of identifying the input based on the long-time spectrum at the output of the filter. Here we will be interested, not in a long-time spectral property, but rather in short-time spectral considerations.

Although the concept of "short-time spectra" may be conceptually clear, it is best to be as precise as possible. For long-time or ordinary spectra, the averaging time is over a period (if the waveform is periodic) or over an infinite interval (for transient waveforms or random processes). In both of these cases the result of the averaging is a constant--for a particular frequency--hence independent of time. For short-time spectra, on the other hand, one chooses to average over a time which is short compared either to any period present or to infinity. The result is an average which is a function of time, and it is this time dependence which is desired.

When attempting to approximate long-time power spectra experimentally, one inherently thinks about filtering, and the process is as follows: (1) pass the waveform through a variable narrow-band "analyzing" filter; (2) pass this signal through a power-averaging circuit (for example, a thermocouple); and (3) read the dc output of the averaging circuit. [It

is not necessary to obtain spectra in this way; it is possible to find spectra experimentally using a computational procedure--for example, see Blackman and Tukey (Ref. 13)]. In contrast to this long-time spectrum, the short-time spectra defined for this study does not utilize a power-averaging circuit. The square of the filter's output envelope is the measured variable. It may be noted that, if this squared envelope were smoothed to approximate the long-time spectra, the result does not converge to the desired long-time spectrum.[1]

The short-time spectrum considerations can thus be depicted as shown in Fig. 3-1. Although one is interested in the properties at the output of the "transmitting" filter [$e_1(t)$], one is in fact dealing with

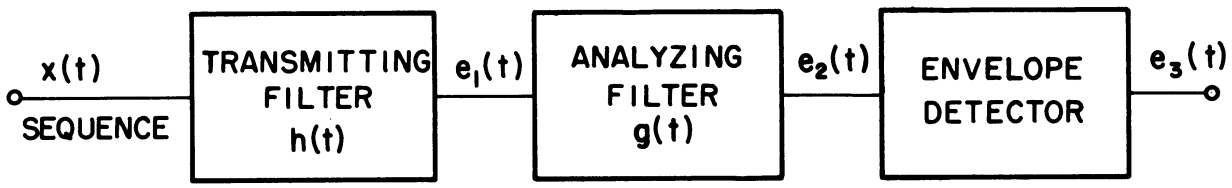


Fig. 3-1. Basic block diagram to study short-time spectrum properties of N.B. pulsed waveforms.

the envelope at the output of the analyzing filter when investigating the short-time spectra of $e_1(t)$.

For reasons to appear shortly, we must restrict the possible analyzing filters to those of the type stated below. We can now state specifically what we mean by "short-time spectra":

---

1 In the past a number of experimental procedures for obtaining long-time spectra used the procedure of averaging the squared envelope of the analyzing filter. However, it has been shown (Ref. 8, p. 107) that this average does not converge to the desired long-time spectrum for a large class of signals: i.e., for real Gaussian random variables.

(1) The analyzing filter has a pulse response[1] of the form:

$$g(t) = F(t)\cos(\omega_o t + \theta) \qquad t \geq 0 \qquad (3\text{-}1)$$

$$g(t) = 0 \qquad t < 0 \ ,$$

where:

$F(t)$ = any envelope such that $\int_{-\infty}^{\infty} |g(t)|\, dt < +\infty$,

$\omega_o$ = ringing frequency of filter, and

$\theta$ = phase angle.

(2) The averaging time of the filter is much less than any period involved, or less than infinity.

(3) The short-time power spectrum $[G_t(\omega)]$ will consist of the square of the envelope out of this analyzing filter. The short-time spectrum is studied, then, in terms of these requirements.

Although Fig. 3-1 represents our problem, we shall, in the following material, reverse the positions of the two filters. That is, we shall consider the sequence as the input to the analyzing filter, and the transmitting filter will follow. This is legitimate since one can always interchange linear filters and retain the same output. The reason for doing this is as follows: for the class of analyzing pulse responses of Eq. 3-1 one is able to state certain symmetry properties about the clocked sequence; if a filter $H(j\omega)$ is at least as wide in frequency as $G(j\omega)$ these properties are not altered by subsequent filtering by $H(j\omega)$. By using this method one can exhibit the symmetry properties for any $H(j\omega)$ as above, while

---

1 The term "pulse response" is used throughout the analytical work of this report, as opposed to "impulse response." This is done because most of the results are valid for any pulse configuration as long as the response meets the requirements. However, in any practical situation, and in the experiments, the pulse length is sufficiently short relative to any periodicity in the response, so we can consider the response as the true impulse response.

the permissible g(t)'s are given by Eq. 3-1. This makes sense in light of the fact that the analyzing filter g(t) is under our control, whereas the h(t) filter is not (referring to the situation depicted in Fig. 1-1).

## 3.1 Half-Clock Spectral Symmetry

We will now note an important property about all clocked waveforms. If a clocked waveform is put into an "analyzing" filter of the type in Eq. 3-1 and this filter is first centered at a frequency which is a specified distance above any multiple of one-half clock frequency and then placed the same distance below the multiple one-half clock frequency, the envelopes of the two outputs will be identical. The restriction that the pulse response be of the form $g(t) = F(t) \cos(\omega_o t + \theta)$ is not very severe since narrow-band filters tend to have equally-spaced zero crossings in their impulse responses. Figure 3-2 indicates this basic symmetry property along the frequency axis. The analyzing filter is first tuned to $\left(\frac{m\omega_c}{2} + \omega_d\right)$

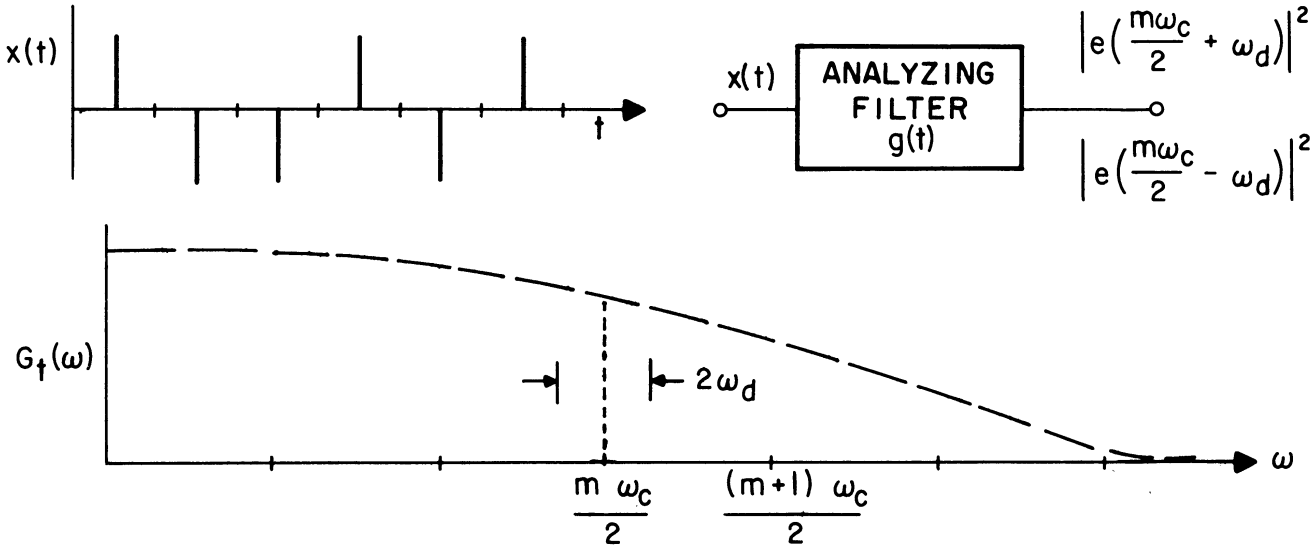


Fig. 3-2. Illustration of one-half clock symmetry.

and then to $\left(\frac{m\omega_c}{2} - \omega_d\right)$, where $\omega_c$ is the clock frequency and $\omega_d$ is the frequency interval away from the multiple of half-clock frequency. From the previous study it is known that the long-time power spectral density of a rectangular pulse sequence is as shown by the dashed lines. The symmetry property states that, about any multiple of one-half clock $\left(\frac{m\omega_c}{2}\right)$, identical envelopes will be observed if an analyzing filter is tuned to equal intervals on either side of the multiple.

This spectral symmetry will now be derived. The output, when a clocked sequence of pulses is the input to a filter, can be written as:

$$E(t) = \sum_{n=-\infty}^{N(t)} a_n \, g(t - \frac{n}{f_c}) \quad \text{for } t \ni N < t < N+1 , \qquad (3\text{-}2)$$

where:

$N$ = integer $N < t < N+1$,

$a_n$ = +1 or -1, depending on positive pulse or negative pulse,

$g(t)$ = pulse response of analyzing filter,

$f_c$ = clock repetition rate, and

$\frac{1}{f_c}$ = interval between pulses.

It should be carefully noted that the upper limit, N, of the summation increases by one as t moves from one interval to the next clock interval; it is not a constant but is a function of time. Since the sequence does not actually begin at $t = -\infty$, the time reference can be changed so that $t = 0$ coincides with the beginning of a sequence. Henceforth, the output of the analyzing filter will be written as:

$$E(t) = \sum_{n=0}^{N(t)} a_n \, g(t - \frac{n}{f_c}) \quad \text{for } t \ni N < t < N+1 . \qquad (3\text{-}3)$$

Let the pulse response of the analyzing filter by given by:

$$g(t) = F(t)\cos(\omega t + \theta) = F(t)\,\mathrm{Re}\left\{e^{i(\omega t + \theta)}\right\} . \qquad (3\text{-}4)$$

Then the output voltage E(t) is:

$$E(t) = \sum_{n=0}^{N} a_n \,\mathrm{Re}\left\{F(t - \frac{n}{f_c})e^{i[\omega(t - \frac{n}{f_c}) + \theta]}\right\} . \qquad (3\text{-}5)$$

To test for symmetry, let two voltages be defined:

$$E_{la}(t) = E_l(t) \quad \text{when} \quad \omega_a = \frac{m\omega_c}{2} + \omega_d, \text{ and} \qquad (3\text{-}6)$$

$$E_{lb}(t) = E_l(t) \quad \text{when} \quad \omega_b = \frac{m\omega_c}{2} - \omega_d$$

where:

$\omega_d$ = frequency difference from a multiple of half-clock, and

$m$ = any integer.

Now, the $\Sigma\mathrm{Re}$'s = $\mathrm{Re}\left\{\Sigma\right\}$ ; therefore:

$$E_{la}(t) = \mathrm{Re}\left\{\sum_{n=0}^{N} a_n F(t - \frac{n}{f_c})e^{i[(\frac{m\omega_c}{2} + \omega_d)(t - \frac{n}{f_c}) + \theta]}\right\} \qquad (3\text{-}7)$$

$$= \mathrm{Re}\left\{e^{i[\frac{m\omega_c}{2} + \omega_d]t}\, e^{i\theta} \sum_{n=0}^{N} a_n F(t - \frac{n}{f_c})e^{-imn\pi}\, e^{-i\frac{n\omega_d}{f_c}}\right\} .$$

Writing in terms of envelope (or magnitude):

$$E_{la}(t) = \left|\sum_{n=0}^{N} a_n F(t - \frac{n}{f_c})e^{-imn\pi}\, e^{-i\frac{n\omega_d}{f_c}}\right| \mathrm{Re}\left\{e^{i\omega_a t}\, e^{i\theta_N}\right\} , \qquad (3\text{-}8)$$

where:

$\omega_a = \frac{m\omega_c}{2} + \omega_d$ , and

$\theta_N$ = phase angle, dependent on N.

In an identical manner, $E_{lb}(t)$ is written:

$$E_{lb}(t) = \left| \sum_{n=0}^{N} a_n F(t - \frac{n}{f_c}) e^{-imn\pi} e^{i\frac{n\omega_d}{f_c}} \right| \mathrm{Re}\left\{ e^{i\omega_b t} e^{i\theta'_N} \right\} , \quad (3\text{-}9)$$

where:

$$\omega_b = \frac{m\omega_c}{2} - \omega_d .$$

Looking at Eqs. 3-8 and 3-9, at the magnitude of both of these terms, it is seen that both magnitudes are summations of terms involving n and t and that each term in the summations is the complex conjugate of the corresponding term in the other voltage. Therefore, the envelopes or magnitudes of both voltages are equal:

$$|E_{la}(t)| = |E_{lb}(t)| . \quad (3\text{-}10)$$

Since the magnitudes are equal, the squares of the magnitudes are equal, and therefore the power as a function of time is the same for the two voltages. Since the voltages $E_{la}$ and $E_{lb}$ were taken at symmetrical points about an arbitrary multiple of one-half clock frequency, this is the proof, then, that all clocked waveforms possess this half-clock symmetry.

It has been shown above that a clocked sequence of pulses exhibits half-clock spectral symmetry when a proper but common type of analyzing filter is used. To illustrate this, Fig. 3-3 shows a "sound spectrograph" of a sequence of rectangular pulses, from a twelve-stage maximal generator at 2000 cps. The multiples of half-clock frequency are shown by dashed lines. The symmetry of the spectra about these lines is clearly visible. The sound spectrograph is a device which measures the short-time spectra as defined above. Its filter is very close to that of the form in Eq. 3-1, and the darkness of the record is monotone with the magnitude-squared of the output envelope (see Section 6.2).

We are now interested in this half-clock symmetry when a general

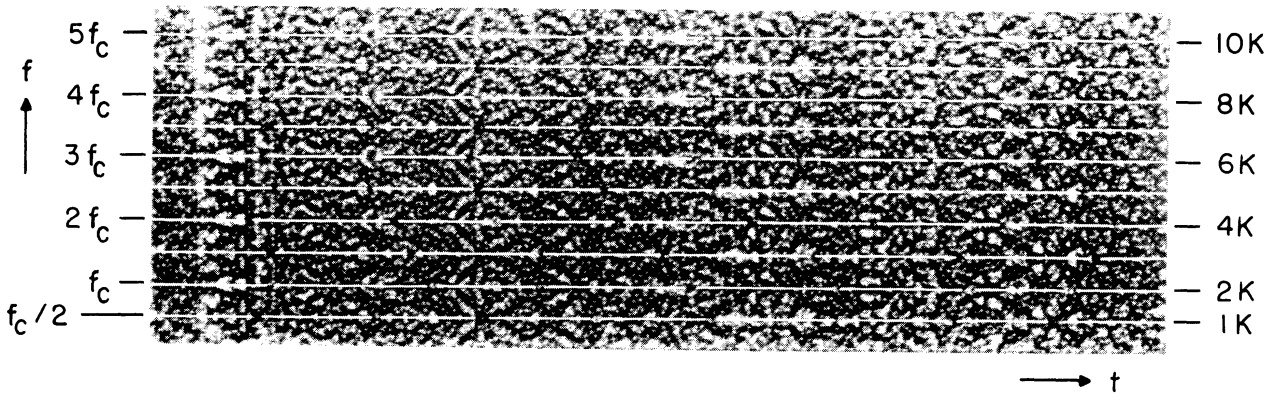


Fig. 3-3. Sound spectrograph of a clocked sequence of rectangular pulses.

narrow-band filter $H(j\omega)$ (not necessarily of the form in Eq. 3-1)is interposed between the sequence and the analyzing filter (see Fig. 3-1). It will be found that, if the filter $H(j\omega)$ contains energy around some multiple of half-clock frequency, and if the analyzing filter (being narrower than the H filter) is consecutively placed at two symmetrical positions within the passband of $H(j\omega)$ then the basic symmetry property just noted can be viewed directly at the output. Thus, for the case in which $H(j\omega)$ is placed so that it transmits energy on both sides of a multiple of half-clock frequency, the output exhibits the property of having short-time power symmetry at two symmetrical positions within the passband.

To show this extension of the basic half-clock symmetry, consider Fig. 3-4. If the analyzing filter appears first, as shown in Fig. 3-4b, then the voltage $E_1(t)$ will possess half-clock symmetry by virtue of the previous proof, Eqs. 3-8 and 3-9. Now if this $E_1(t)$ is a narrow-band waveform, the transmitting filter will affect the envelope of $E_1(t)$ by essentially multiplying it by a constant. That is, the effect of the bandpass filter on the envelope of $E_1(t)$ can be approximated by simply multiplying

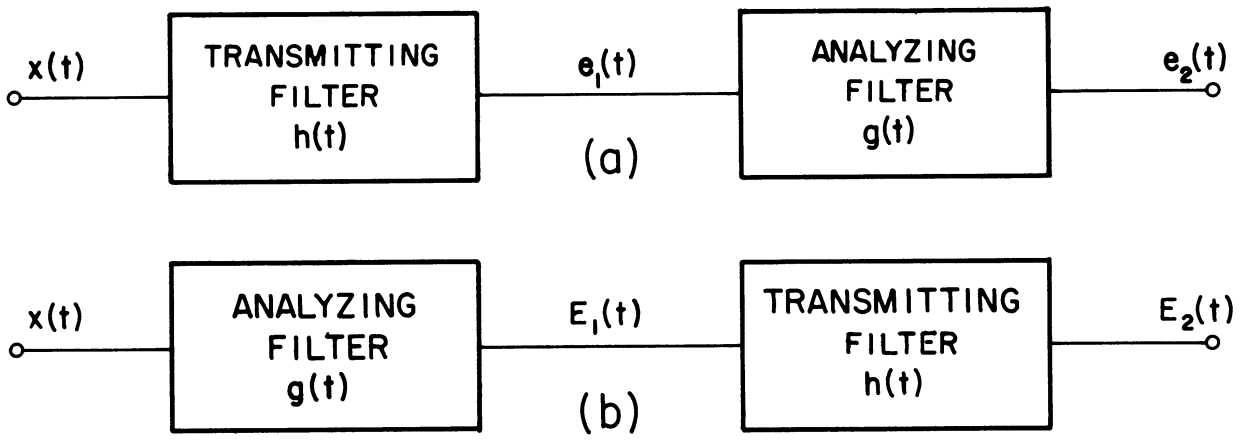


Fig. 3-4. Depiction of notation when reversing linear filters.

the envelope by the value of $|H(j\omega)|$, where $\omega$ is the frequency of the analyzing filter. Thus, referring to Eqs. 3-8 and 3-9, let $K(t, \omega_d)$ equal the amplitudes of $E_1(t)$ at both of the symmetrical frequencies. Then the two $E_2(t)$'s will be given by:

$$E_{2a}(t) = |H(j\omega_a)|\ K(t, \omega_d) \cos(\omega_a t + \theta_N) \quad , \tag{3-11}$$

where:

$|H(j\omega_a)|$ = magnitude of bandpass filter response at frequency $\omega_a$,

$\omega_a = \frac{m\omega_c}{2} + \omega_d$, and

$K(t, \omega_d)$ = amplitude of $E_1(t)$ (see Eqs. 3-8 and 3-9).

Also:

$$E_{2b}(t) = |H(j\omega_b)|\ K(t, \omega_d) \cos(\omega_b t + \theta_N') \quad , \tag{3-12}$$

where:

$$\omega_b = \frac{m\omega_c}{2} - \omega_d .$$

Thus one can expect the symmetry to be retained with the arrangement shown in Fig. 3-4b. Since it is well known that any cascaded linear filters can be interchanged it is evident that half-clock symmetry will be present in the situation of Fig. 3-4a, the case of interest here. This concludes the argument that $e_2(t)$ will exhibit half-clock envelope symmetry when the

$H(j\omega)$ filter includes energy around a multiple of half-clock frequency.

One can consider the implications of this result by referring back to Fig. 1-1. The conclusion is that we have found a property peculiar to the clocked input, consisting of half-clock symmetry in the output. Of course, there would be no such symmetry if Gaussian noise were the input to the filter. However, a restriction on this conclusion is that the $H(j\omega)$ filter must transmit energy on both sides of some multiple of half-clock frequency. If the bandpass filter is not so located one simply cannot test for this basic symmetry around a multiple of half-clock. The procedure for experimentally verifying this symmetry is first to place the analyzing filter a certain interval above the multiple of half clock, and then place a second filter the same frequency interval below the multiple of half-clock, and note the correspondence in the time behavior of the two outputs with square-law detection. This can be done either by using a sound spectrograph as depicted above or by correlating the two different frequency amplitudes and noting a peak in the correlation. Sound spectrographs have been obtained which clearly show this symmetry.

Figure 3-5 shows a sound spectrograph of the output when the same sequence used in Fig. 3-3, clocked at 2000 cps, was inserted into a filter with a 2100-cps bandwidth centered at 5950 cps. This filter was a 4-pole Tschebyscheff type, and its impulse response was quite unlike that of Eq. 3-1 (see Fig. 6-9).

Another version of the same experimental evidence is shown in Fig. 3-6. Here the two envelopes of $e_{2a}(t)$ and $e_{2b}(t)$ are superimposed, to exhibit the correlation, when the clocked sequence is the input. Thus these envelopes correspond to two symmetrical, single traces of the frequency-time diagram of Fig. 3-5. With the sequence clocked at 2000 cps,

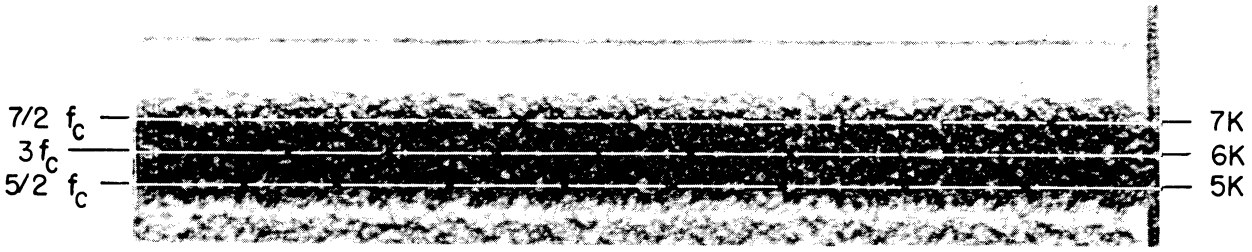


Fig. 3-5. Sound spectrograph of filtered clocked sequence.

the envelopes were taken at 5500 cps and 6500 cps. Also shown are the corresponding envelopes with a Gaussian noise input, to exhibit the complete lack of correlation (see Section 6.3 for experimental description).

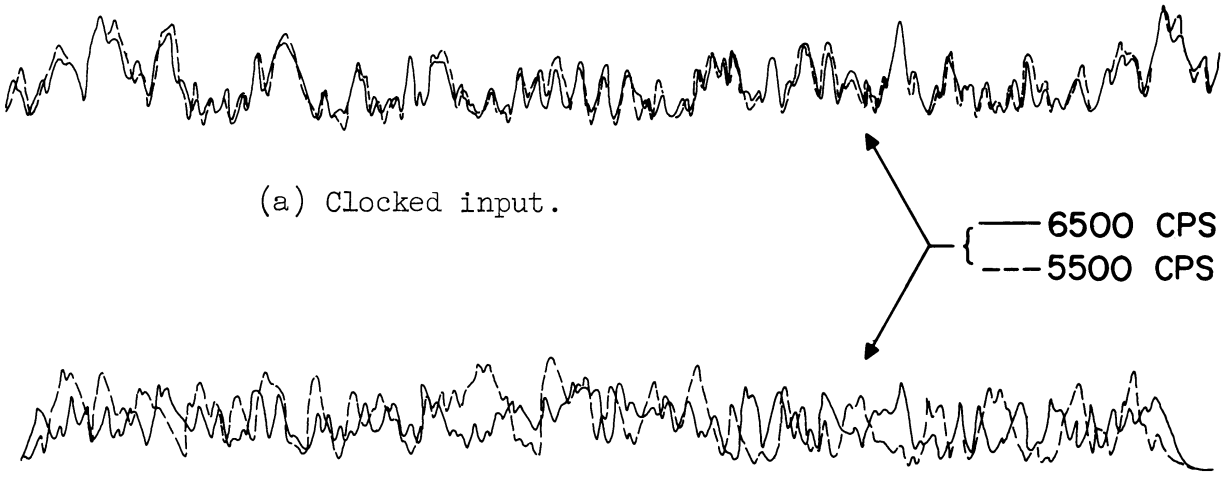


(a) Clocked input.

(b) Noise.

Fig. 3-6. Superimposed envelopes of two symmetrical frequencies with a clocked input and a Gaussian input.

From the above it is seen that this half-clock symmetry represents a singular case which yields a relatively simple solution.

## 3.2 Energy Midway Between Half-Clock

In the above section we noted that power spectral symmetry exists on either side of any multiple of half-clock frequency. This phenomenon can be observed at the output of an analyzing filter. This basic spectral symmetry is one general consequence of the fact that structure exists between spectral components when the input is a pulsed process. Therefore, the problem is to be able to extract some representation of this structure. In the above case it was a quite simple matter to note the equality of two envelopes.

A second case occurs when one considers spectral envelopes situated in symmetrical positions midway between half-clock positions. This situation occurs when one envelope is taken at a frequency interval ($\omega_d$) above a multiple of half-clock, and another is taken at an interval $\omega_d$ below the next half-clock position. This situation in the frequency plane is depicted in Fig. 3-7. To investigate this situation we proceed as before

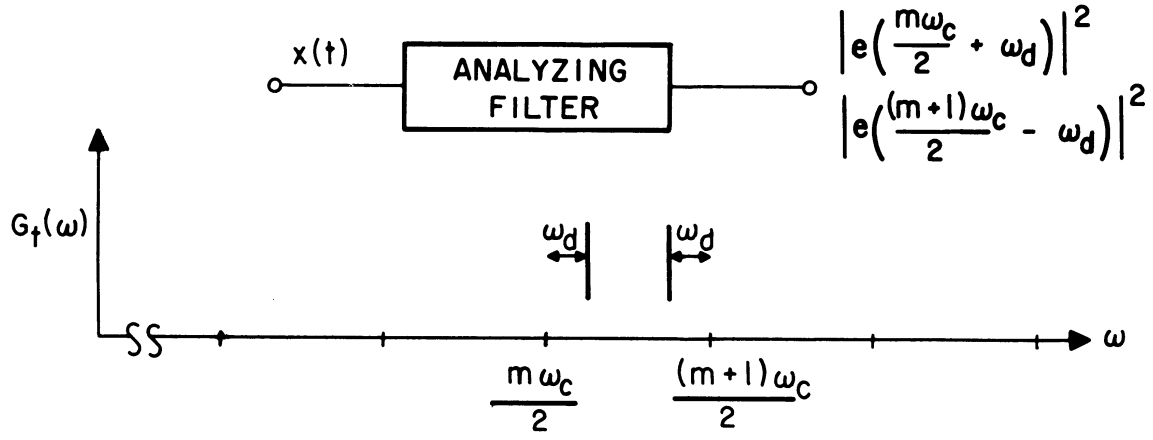


Fig. 3-7. Symmetry action for energy midway between half-clock frequencies.

by writing the output voltage for both cases in terms of an envelope and a carrier. Thus, for the case in which $\omega$ is a certain interval above a multiple $\frac{mf_c}{2}$ one has the same equation as in Eq. 3-8:

$$E_{la}(t) = \left| \sum_{n=0}^{N} a_n F(t - \frac{n}{f_c}) e^{-imn\pi} e^{-i \frac{n\omega_d}{f_c}} \right| \mathrm{Re}\left\{ e^{i\omega_a t} e^{i\theta_N} \right\}, \quad (3\text{-}13)$$

where:

$$\omega_a = \frac{m\omega_c}{2} + \omega_d, \text{and}$$

$$\theta_N = \text{phase angle, dependent on N.}$$

Now consider the voltage at the same distance $\omega_d$ from the next half-clock position; it is found that this $E'_{lb}(t)$ can be written:

$$E'_{lb}(t) = \left| \sum_{n=0}^{N} a_n F(t - \frac{n}{f_c}) e^{-i(m+1)n\pi} e^{+i \frac{n\omega_d}{f_c}} \right| \mathrm{Re}\left\{ e^{i\omega_b t} e^{i\theta'_N} \right\}, \quad (3\text{-}14)$$

where:

$$\omega_b = \frac{(m+1)}{2} \omega_c - \omega_d, \text{and}$$

$$\theta'_N = \text{phase angle, dependent on N.}$$

Taking out the term $e^{-jn\pi}$ causes Eq. 3-14 to appear as:

$$E'_{lb}(t) = \left| \sum_{n=0}^{N} a_n (-1)^n F(t - \frac{n}{f_c}) e^{-imn\pi} e^{i \frac{n\omega_d}{f_c}} \right| \mathrm{Re}\left\{ e^{i\omega_b t} e^{i\theta'_N} \right\}, \quad (3\text{-}15)$$

where:

$$\omega_b = \frac{(m+1)}{2} \omega_c - \omega_d.$$

Comparing the magnitudes of Eq. 3-13 and 3-15, it is seen that they are alike except that $a_n$ is the sequence in Eq. 3-13, and $a_n(-1)^n$ is the sequence in Eq. 3-15. Thus the envelopes behave according to two different sequences; but the sequences are closely related in that one is the

complement of the other (the sign of every other pulse is reversed). Although the two different envelopes were obtained by placing an analyzing filter at two different frequencies, since we are dealing only with magnitudes this can just as well be considered as one filter with two different inputs: a sequence and its complement.

If we write the magnitudes of the two envelopes in terms of real and imaginary quantities, for m even [for m odd, a term $(-1)^n$ multiplies all quantities in both equations and thus reverses the role of $a_n$ and $a_{nc}$], one obtains:

$$|E_{la}(t)|^2 = \left( \sum_{n=0}^{N} a_n F(t - \frac{n}{f_c}) \cos \frac{n\omega_d}{f_c} \right)^2 + \left( \sum_{n=0}^{N} a_n F(t - \frac{n}{f_c}) \sin \frac{-n\omega_d}{f_c} \right)^2 \tag{3-16}$$

$$|E_{lb}(t)|^2 = \left( \sum_{n=0}^{N} a_{nc} F(t - \frac{n}{f_c}) \cos \frac{n\omega_d}{f_c} \right)^2 + \left( \sum_{n=0}^{N} a_{nc} F(t - \frac{n}{f_c}) \sin \frac{n\omega_d}{f_c} \right)^2 ,$$

where:

$a_{nc}$ = complement of the sequence $a_n$.

First it may be noted that, if $\frac{\omega_d}{f_c} = 90^\circ$ (corresponding to both analyzing filters placed midway between half-clock positions), then the two envelopes are identical since those terms having different signs are zero. This must certainly be so since the filters are placed at exactly the same frequency. For other permissible angles ($0^\circ < \frac{\omega_d}{f_c} < 90^\circ$) no quantitative relation between the envelopes has been found. Experimental results in the form of envelopes taken at symmetrical positions about one-quarter clock frequency, for two cases, are shown in Fig. 3-8. While this experimental evidence gives some indication that the clocked envelopes show more of a tendency towards behaving oppositely than the noise envelopes, no firm conclusion can be based on this evidence. Any firm conclusion would be dependent on

a refined statistical study of such envelopes.

In Fig. 3-8 each pair of superimposed envelopes was taken at symmetrical positions about a "quarter-clock" position, as depicted in Fig. 3-7. A twelve-stage maximal sequence clocked at 2000 cps was inserted into a filter with a 2100 cps bandwidth centered at 5950 cps (same

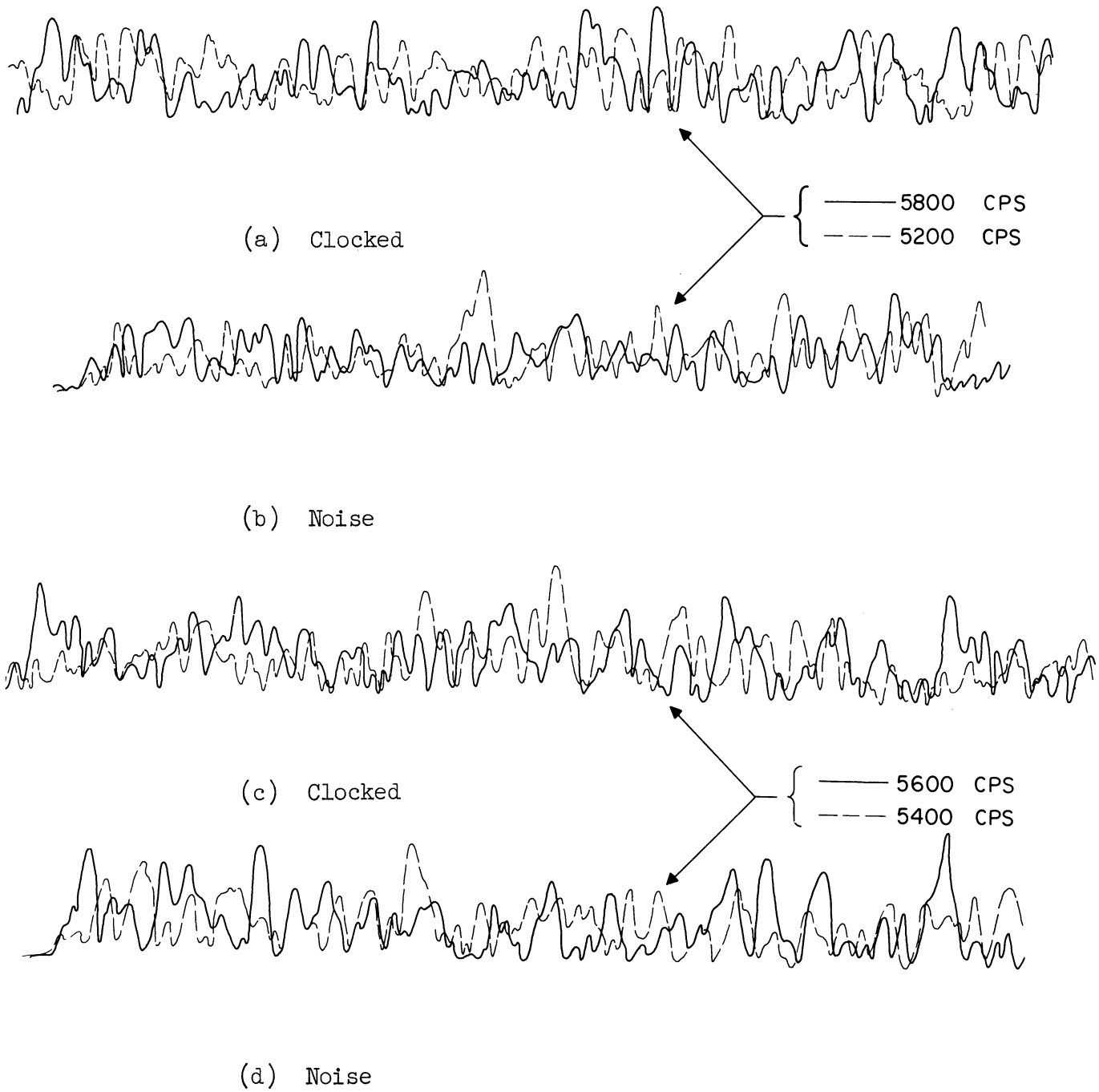


Fig. 3-8. Superimposed envelopes at frequencies symmetrical about quarter-clock frequency.

conditions as Figs. 3-5 and 3-6). The envelopes in parts (a) and (b) were taken at 5200 cps and 5800 cps; those in parts (c) and (d) were taken at 5400 cps and 5600 cps. Thus in part (a) the value of $\frac{\omega_d}{f_c}$ was $36^o$, and in part (c) the value was $72^o$; parts (b) and (d) show the two envelopes for a sample of Gaussian noise.

It is again seen that, if a filter $H(j\omega)$ is placed between the sequence and the analyzing filter (see Fig. 1-1), any possible differences in the statistical behavior of the envelopes will still be available. This follows by invoking the interchangeability of filters used in the previous section. Hence, this allows one to possibly identify a clocked input if energy is available as stated; this is an additional property to the one of the previous section where energy around a multiple of half-clock was required.

## 3.3 Energy Midway Between Quarter-Clock

In the preceding two sections we described properties of a narrow-band clocked sequence of impulses for two situations; (1) one in which energy is available on both sides of a multiple of half-clock frequency, and (2) one in which energy is available on both sides of midway between multiples of half-clock frequency. A third situation, about which one can study a relation between the envelopes is depicted in Fig. 3-9. It is seen that this is concerned with the case in which energy is centered midway between quarter-clock positions (or symmetrical about one-eighth clock). We now seek the relation between the envelopes when analyzing filters are placed at the two positions shown in Fig. 3-9.

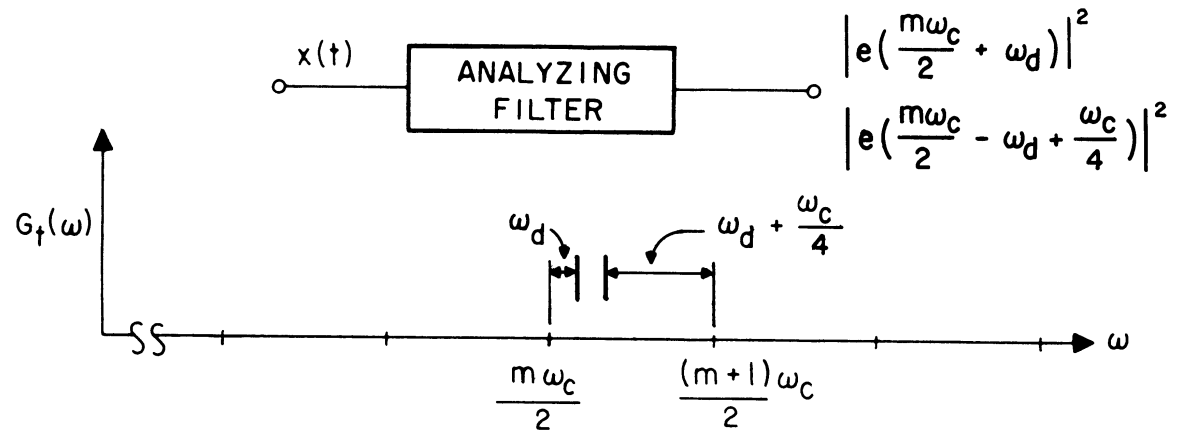


Fig. 3-9. Symmetry action for energy on both sides of one-eighth clock.

To investigate this, one again writes the first voltage waveform as shown in Eq. 3-17 (and in Eqs. 3-8 and 3-13 before):

$$E_{1a}(t) = \left| \sum_{n=0}^{N} a_n F(t - \frac{n}{f_c}) e^{-imn\pi} e^{-i\frac{n\omega_d}{f_c}} \right| \mathrm{Re}\left\{ e^{i\omega_a t} e^{i\theta_N} \right\}, \quad (3\text{-}17)$$

where:

$$\omega_a = \frac{m\omega_c}{2} + \omega_d.$$

By referring to Fig. 3-9 it will be seen that the other voltage will be written as:

$$E''_{1b}(t) = \left| \sum_{n=0}^{N} a_n F(t - \frac{n}{f_c}) e^{-i\left[\frac{m\omega_c}{2} + \frac{\omega_c}{4} - \omega_d\right]\frac{n}{f_c}} \right| \mathrm{Re}\left\{ e^{i\omega_b t} e^{i\theta''_N} \right\},$$

where:

$$\omega_b = \frac{m\omega_c}{2} + \frac{\omega_c}{4} - \omega_d.$$

$$E''_{1b}(t) = \left| \sum_{n=0}^{N} a_n F(t - \frac{n}{f_c}) e^{-imn\pi} e^{in\left(\frac{\omega_d}{f_c} - \frac{\pi}{2}\right)} \right| \mathrm{Re}\left\{ e^{i\omega_b t} e^{i\theta''_N} \right\} \quad (3\text{-}18)$$

Comparing the envelopes of Eqs. 3-17 and 3-18, the two envelopes can be written as:

$$\left| \sum_{n=0}^{N} a_n F(t, n) e^{-in\theta} \right| \text{ versus } \left| \sum_{n=0}^{N} a_n F(t, n) e^{+in(\theta - \frac{\pi}{2})} \right| . \quad (3\text{-}19)$$

As in the previous case no quantitative relations between the envelopes were found. Experimental envelopes taken for symmetrical positions about one-eighth clock are shown in Fig. 3-10. Here the sequence was clocked at 2000 cps, and the envelopes taken at 5100 and 5400 cps. Comparing Figs. 3-9 and 3-10 it appears that any statistical relation between the two envelopes is less pronounced for this case of one-eighth clock symmetry. As before, the presence of a narrow-band filter $H(j\omega)$ between the sequence and the analyzing filter will not affect the envelope situation as long

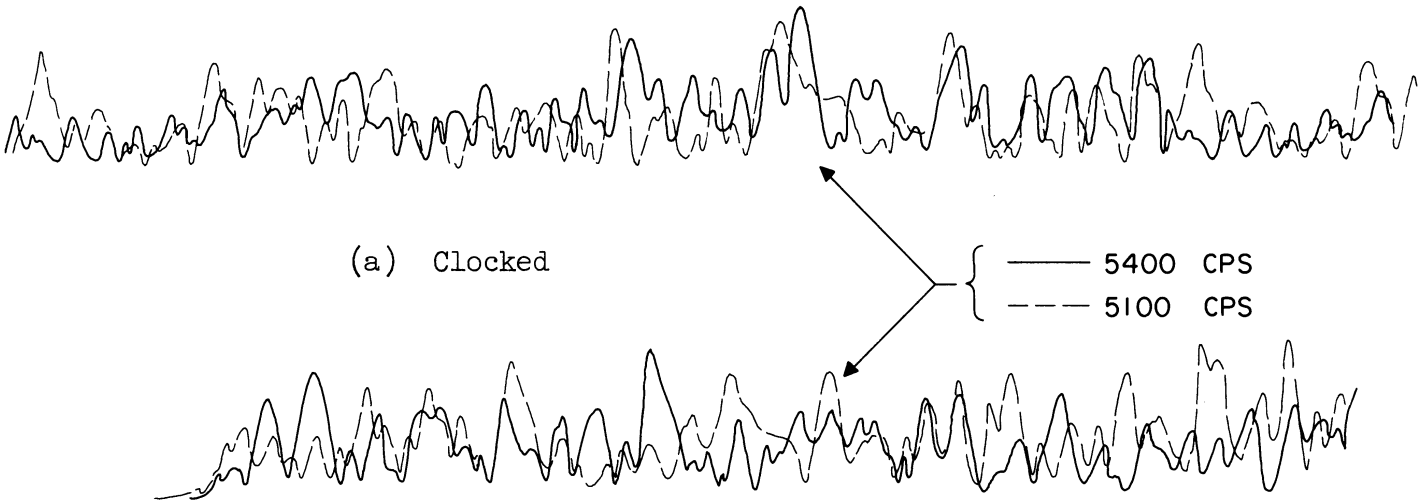


Fig. 3-10. Depiction of envelopes symmetrical about one-eighth clock frequency.

as the analyzing filter is sufficiently narrow.

## 3.4 Summary of Spectral Symmetry

The relationships between envelopes obtained from symmetrical frequency positions for three different cases have been noted. These cases are summarized on a frequency sketch in Fig. 3-11.

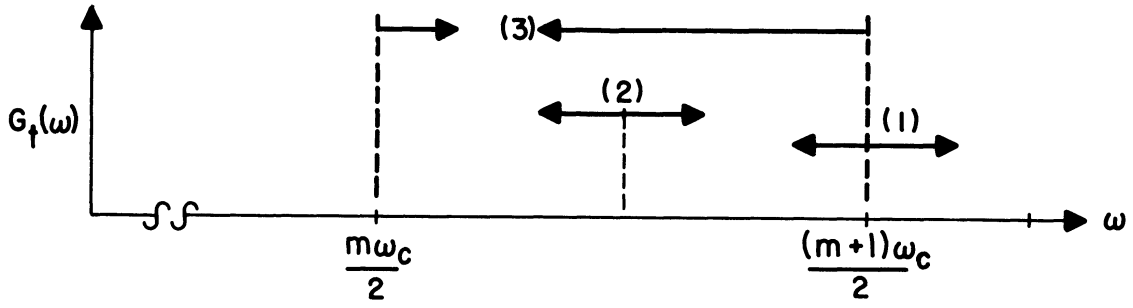


Fig. 3-11. Summary of symmetrical envelope relations.

For the first case, with envelopes taken symmetrical about a half-clock frequency, the envelopes are identical and give a firm positive identification. In the second case, symmetrical about a quarter-clock frequency, the envelopes behave as though they resulted from complementary sequences. In the third case, symmetrical about one-eighth clock frequency, the envelope relation is indicated by Eq. 3-19.

## 3.5 Reversing (Filter) Property when Heterodyning is Used

In the foregoing three sections the interchangeability of linear passive filters was used to show that the various symmetry properties of a pulsed waveform are present even when a filter $H(j\omega)$ appears between the sequence and analyzing filter. For the filters in those sections the bandpass of the two concerned filters were always within the same region; that is,

the filter g(t) was always within the bandpass of the filter h(t). This method of considering two filters as being reversed suggests exploring the possibility of reversing the filters when the two filters do not overlap, and hence one must use heterodyning. Consider, for example, the two filters with heterodyning shown in Fig. 3-12. No matter where the filter H(jω) is placed, the proper heterodyning frequency can be used to translate any desired part of the spectrum of x(t) to the passband of H(jω). Thus, for example, g(t) could be set to symmetrical points about a multiple of half-clock and then identical envelopes would appear at $E_3(t)$. If it were

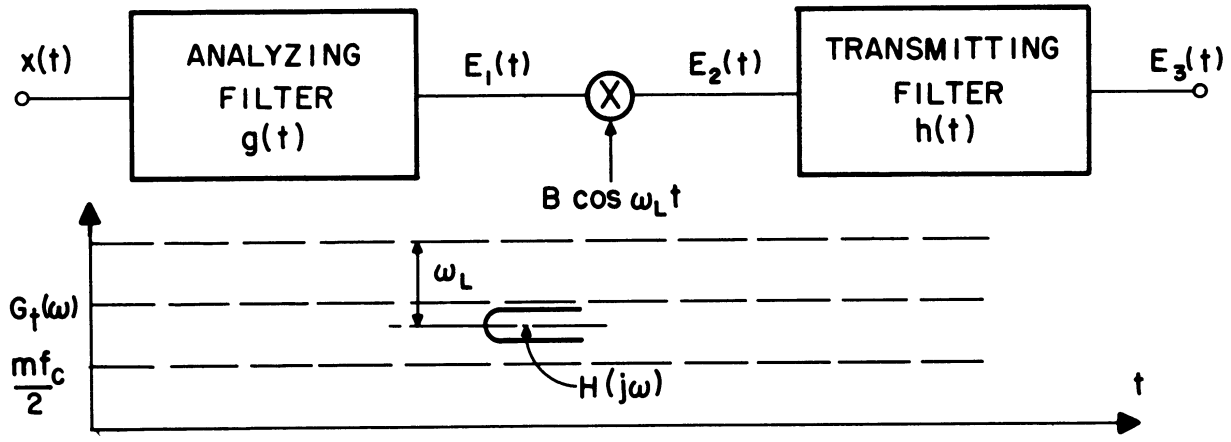


Fig. 3-12. Illustration of symmetry property when H(jω) is not at a half-clock symmetrical point.

possible to reverse the order of the filters, and obtain the same envelope, then it would be possible to test for half-clock symmetry no matter where the filter H(jω) was placed.

In the following we will show, as briefly as possible, the requirements for the envelopes to remain the same when the filters of Fig. 3-12 are interchanged. No satisfactory solution to fulfill these requirements has been found. However, as a result of this study, one can state

under what conditions the filters can be reversed--these conditions do not provide the symmetry which was desired.

Figure 3-13 depicts the reversing of the filters and shows the notation to be used in the following material. In short we will ask what coherent multiplication is required, in part (b), in order that the envelope

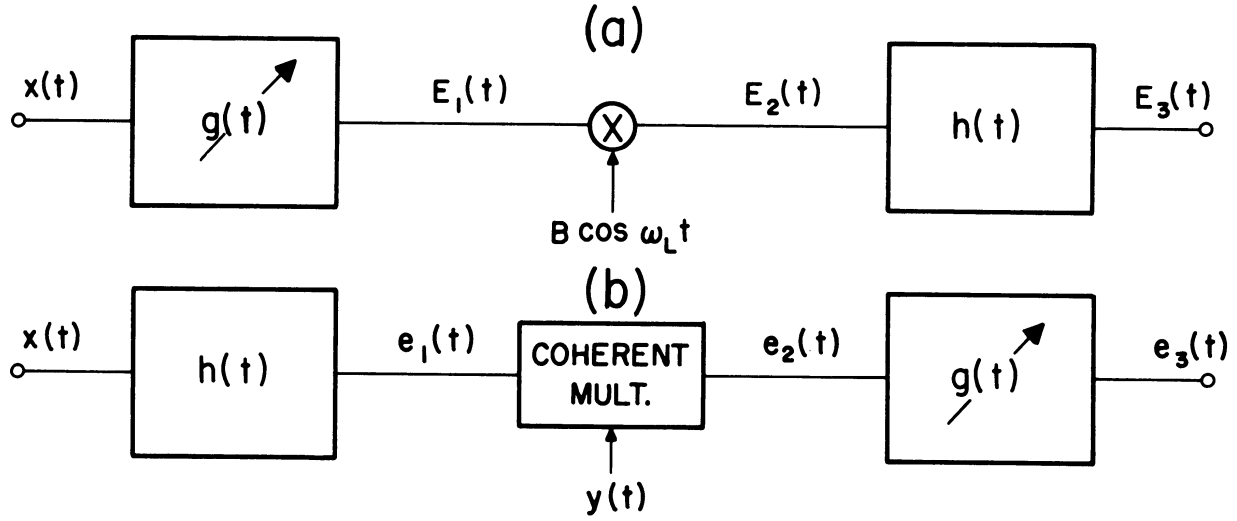


Fig. 3-13. Reversal of the filters when heterodyning is used.

of $e_3(t)$ be the same as that of $E_3(t)$. Using the summation of impulse responses[1] and the convolution integral, $E_3(t)$ can be written:

$$E_3(t) = B \int_0^t \sum_{n=0}^{N} a_n \, g(\tau - \frac{n}{f_c}) \cos \omega_L \tau \, h(t - \tau) \, d\tau, \qquad (3\text{-}20)$$

where:

$g(t)$ = impulse response of analyzing filter,

$h(t)$ = impulse response of transmitting filter, and

$\omega_L$ = heterodyning frequency necessary to move symmetry point within passband $h(t)$.

---

1 Note that here, when using the convolution integral, the impulse response must be used, rather than the more general pulse response sufficient in previous sections.

In order to put $E_3(t)$ into a form for comparison with $e_3(t)$, one can interchange order of integration and summation and change variables by letting $t - \tau' = \tau - \frac{n}{f_c}$. The result after interchanging again and dropping the primes is

$$E_3(t) = B \int_o^t \sum_{n=0}^{N} a_n \, g(t - \tau) \, h(\tau - \tfrac{n}{f_c}) \cos (\omega_L \tau - \tfrac{n\omega_L}{f_c} - \omega_L t) d\tau \, . \quad (3\text{-}21)$$

For comparison to this let us first write $e_3(t)$ without any coherent multiplication:

$$e_3(t) = B \int_o^t \sum_{n=0}^{N} a_n \, h(\tau - \tfrac{n}{f_c}) \, g(t - \tau) d\tau \quad . \quad (3\text{-}22)$$

Now suppose for a moment that it were possible to separate out each individual component of $e_1(t)$ and then multiply each such component by a sine waveform of the proper phase. If all such factors were then added one could obtain an $e_2(t)$ of:

$$e_2(t) = \sum_{n=0}^{N} a_n \, h(t - \tfrac{n}{f_c}) \cos (\omega_L t - \tfrac{n\omega_L}{f_c}) \quad . \quad (3\text{-}23)$$

If such were possible, then $e_3(t)$ would become:

$$e_3(t) = B \int_o^t \sum_{n=0}^{N} a_n \, h(\tau - \tfrac{n}{f_c}) \, g(t - \tau) \cos (\omega_L \tau - \tfrac{n\omega_L}{f_c}) \, d\tau \, . \quad (3\text{-}24)$$

Comparing Eq. 3-24 to Eq. 3-21 it will be seen that they are identical except for an $\omega_L t$ factor in the cosine term of Eq. 3-21. It can be shown that this difference is due to the fact that the output $E_3(t)$ is centered at a different frequency from that of $e_3(t)$. The two terms can be made identical by coherently detecting the waveform $e_3(t)$ (multiplying by $\cos \omega_L t$).

Of course, the difficulty lies in obtaining the $e_2(t)$ of Eq. 3-23. Since the waveform $e_1(t)$ consists of a sum of impulse responses it is required that each such response be separated out and then multiplied by a

sine waveform of the proper phase. One might attempt to separate out the individual components of $e_1(t)$ by use of delay line techniques, but this would amount to no less than attempting to decode the sequence itself (which is deemed impractical for purposes of this study). Consequently, there seems little hope of exploiting symmetry properties in a general way, for any position of $H(j\omega)$.

A rather extensive experimental test was run to determine whether or not a simple waveform might give results sufficiently similar to Eq. 3-23 to permit symmetry recognization. The waveform used to multiply was of the form:

$$y(t) = \cos\left(\omega_L t - \frac{N\omega_L}{f_c}\right) . \tag{3-25}$$

Here N is increased by one in step with the clock frequency. This results in a sine wave whose phase is "bumped" in step with the clock. The $e_2(t)$, then, was:

$$e_2(t) = \sum_{n=0}^{N} a_n \, h\left(t - \frac{n}{f_c}\right) \cos\left(\omega_L t - \frac{N\omega_L}{f_c}\right) . \tag{3-26}$$

No symmetry was obtainable with this attempted approximation. The coherent "phase-bumped" wave served merely to broad-band the $e_1(t)$ waveform so that, in general, only a simple heterodyning [by one component of $y(t)$] of the $e_1(t)$ waveform was accomplished when passed through the $g(t)$ filter.

One can see what conditions are necessary to be able to reverse the filters with heterodyning by comparing Eqs. 3-21 and 3-24. If the heterodyning frequency $\omega_L$ is any multiple of clock frequency, then the term $n\omega_L/f_c$ is always $2\pi$. Under this condition, the two waveforms differ only by the $\omega_L t$ term mentioned earlier, and this difference can be eliminated by coherently detecting $e_3(t)$. The result, then, is as follows: if the input

to two filters with heterodyning between them is a clocked sequence of impulses and if the heterodyning waveform is a multiple of the clocking frequency (and coherent with it) then one can reverse the positions of the two filters and retain the same output.

It can be seen that this reversible property does not help in our attempt to find symmetry irrespective of where $H(j\omega)$ is placed. To do this it is necessary to have $\omega_L$ take on values between multiples of clock frequency. If one is restricted to multiples, then one is merely reflecting a given symmetry point into another identical one.

## 3.6 Short-Time Autocorrelation Function

In the earlier parts of this chapter the distinctive properties of pulsed waveforms as exhibited by their short-time spectral properties were noted. Also, a rather precise definition of what is meant by short-time power spectra was given in Section 3. Whenever one deals with power spectra there appears the possibility of alternatively considering a time autocorrelation function (as opposed to a statistical autocorrelation function). Since we have dealt with a time-varying short-time power spectrum, one questions whether there is a corresponding time-dependent autocorrelation function.

The Fourier transform relation between long-time power spectra and the statistical autocorrelation function (for stationary random processes) is well known and is called Wiener's theorem. With such a relation, knowledge about the power spectra implies knowledge of the autocorrelation function, and vice versa. Hence one can work either in the spectrum (filter) plane or in the time (delay) plane.

Analagous to this relation for long-time spectra, Fano (Ref. 14)

has shown that, for a special case of short-time spectra, a time-varying autocorrelation exists which is the transform of the time-varying short-time power spectra. Referring to our previous definition of short-time spectra (p. 29) the special case applies to the situation in which the analyzing filter has an impulse response:

$$g(t) = e^{-\alpha t} \cos (\omega_o t + \theta) \quad . \tag{3-27}$$

In other words the general F(t) permissible before must now be given by $e^{-\alpha t}$. With such an analyzing filter, and with the measurements to be described below, the relation between short-time spectra and short-time autocorrelation is:

$$\begin{aligned} \theta_t(\tau) &= \frac{e^{\alpha|\tau|}}{2\pi} \int_{-\infty}^{\infty} G_t(\omega) \cos \omega\tau \, d\omega \\ G_t(\omega) &= \int_{-\infty}^{\infty} e^{-\alpha|\tau|} \theta_t(\tau) \cos \omega\tau \, d\tau \quad , \end{aligned} \tag{3-28}$$

where:

$\theta_t(\tau)$ = short-time autocorrelation function,

$G_t(\omega)$ = short-time power spectrum, and

$\alpha$ = time constant of analyzing filter.

As seen, these relations are similar to the relations which exist for the long-time quantities. It must be remembered, however, that it is necessary to use a particular type of analyzing filter, as noted above, in order for these relations to be valid. This is different from the case of the long-time quantities.

The measurements which are required in order to obtain $G_t(\omega)$ and $\theta_t(\tau)$ are as follows. For the short-time frequency spectrum, assuming that

Q is much greater than 1 (which is our interest here), the waveform is put through a filter which has an impulse response $e^{-\alpha t} \cdot \cos(\omega_o t + \theta)$. The output will be a sinusoid at the center frequency with slowly varying amplitude and phase. One now takes the envelope of this sinusoid and squares it to obtain $G_t(\omega)$. To emphasize, it is necessary to have this particular type of filter and also it is necessary that Q be much greater than 1 for this simple procedure to hold. If Q is not appreciably greater than 1, two filters are required which are essentially orthogonal to each other.

For the short-time autocorrelation measurement, which corresponds to the frequency measurement just described, one first multiplies the waveform by the same waveform delayed by $\tau$. This product is then passed through a low-pass filter which has an impulse response $2\alpha e^{-2\alpha t}$. The resulting output is then $\theta_t(\tau)$. Thus, if the measurements are done as described, then the two quantities that are measured will be related as shown in Eq. 3-28.

The essence of these relations is the same as for the case of the long-time relations in that one has the freedom to obtain the power spectrum either by direct measurement or by measuring the autocorrelation function and then using the transform. It is our interest here, however, not to obtain the $G_t(\omega)$ in detail but rather to note a particular characteristic about it. For example, the half-clock symmetry property noted in Sec. 3.1 means that

$$G_t\left(\frac{m\omega_c}{2} + \Delta\omega\right) = G_t\left(\frac{m\omega_c}{2} - \Delta\omega\right) , \qquad (3\text{-}29)$$

and

$$G_t(m\omega_c + \omega) = G_t(\omega) \quad (m = 0, 1, 2, 3, - - -) .$$

Thus, although the time behavior of the power spectrum is essentially a random process (because of the randomness of the $a_n$'s) we were able to find

that particular places in the frequency spectrum yielded the same random process as a function of time.

In considering how the symmetry properties in the $G_t(\omega)$ plane appear in the $\theta_t(\tau)$ plane, one can use the ordinary Fourier transform properties as a guide. Thus, if $G_t(\omega)$ consists of an infinite periodic function of $\omega$ for all t, then $\theta_t(\tau)$ will consist of a spike function of $\tau$ at multiples of the periodicity in $\omega$. For example, the $G_t(\omega)$ for a clocked train of impulses, for any time t, is a periodic function of period $\omega_c$ and extends to infinity. The $\theta_t(\tau)$ for this will be a series of parallel lines (corresponding to harmonics) spaced $\tau = \frac{1}{f_c} = \frac{2\pi}{\omega_c}$ apart with varying amplitude of the various lines for different t. The fact that $\theta_t(\tau)$ is everywhere zero except when $\tau = \frac{2\pi}{\omega_c}$ is obvious from considering the time waveform itself.

If the $G_t(\omega)$ is narrow in $\omega$ for all t, then the $\theta_t(\tau)$ will have nonzero amplitude for values of $\tau$ between the harmonic values mentioned above. Further, if a narrow $G_t(\omega)$ includes a symmetry point (as in Eq. 3-29) then the action in the $\theta_t(\tau)$ plane can be thought of as analogous to an amplitude-modulated, double-sideband wave. That is, the carrier itself will be evident in the time domain (in this case the $\tau$ domain), with a slowly varying amplitude. For any t, the action of $\theta_t(\tau)$ versus $\tau$ will be that the periodicity with $\tau$ will be evident; i.e., $\theta_t(\tau)$ will go through zero at the same values of $\tau$, for all t, but the heights of the "cycles" will vary slowly from cycle to cycle.

From the above it appears that, for narrow-band waveforms, dealing with symmetry properties in the $\theta_t(\tau)$ domain is not more convenient than in the $G_t(\omega)$ domain. However, any final conclusion in this respect would be dependent on further study.

# CHAPTER IV

# STATISTICAL AMPLITUDE CONSIDERATIONS

In the previous two chapters the long-time and the short-time spectrum properties of clocked narrow-band waveforms were considered. In this section the statistics of the clocked waveforms will be studied; in particular, the sampled variance. Variance in general can be considered as the average, over frequency, of all the spectral content.

To deal with the sampled variance of a clocked waveform it is necessary to consider first the stationarity of the waveform. It will be shown that the waveform is "cyclo-stationary"; that is, the statistics are repetitive with the clock period. One can obtain a stationary set of values by sampling the clocked waveform coherently with the clock. The variance of these samples (called sampled variance) will then be studied. It will be shown that, in dealing with these variances, one can characterize the waveform as being clocked as opposed to non-clocked. Further, it will be seen that multiplication by a coherent continuous wave will yield what is equivalent to a "sum of weighted sampled-variances." Finally, experimental results using a coherent, continuous multiplying waveform will be reported.

## 4.1 Review of Classical Knowledge

Before considering the statistics of clocked waveforms it is profitable to review briefly the classical information about Gaussian waveforms and the way in which a related type of noise, random-pulse noise, approaches a Gaussian waveform.

It is well known that if a Gaussian waveform is the input to a linear filter, then the output is a Gaussian waveform (Ref. 15). Since a

filtered shot effect is a familiar example of Gaussian noise, and since the conceptual model for the shot effect is a pulse process in which the time of occurrence is random (called random-pulse noise), one can consider the amplitude distribution for a finite random-pulse noise. That is, the pulses are not infinitely dense as they are for the shot effect. Although random-pulse noise is not the same as a clocked waveform, the conclusions reached about this noise are instructive for considering the clocked waveforms.

Middleton (Ref. 16) has derived analytic expressions for the probability densities, of the various orders, for random-pulse noise. As one expects, it is found that the character of the distribution functions depends heavily on the overlapping of the elementary pulses. Further, for heavy overlapping of pulses, the character of the distribution function is little affected by the precise shape and statistics of the elementary pulses--which is justified by considering the Central Limit Theorem. If the average number of pulses per second times duration of a typical pulse is in the range of 10 to $10^4$, the distributions are normal with one or more correction terms. Above this range the correction terms are insignificant.

Hilibrand (Ref. 17) is concerned with a similar situation when studying the approach to a Gaussian distribution of random-pulse noise which is passed through a narrow-band filter. By using a moments technique in the frequency domain, he evaluates the odd-order higher moments (which are zero for Gaussian noise) for random-pulse noise. By such a method it is possible to see the approach to Gaussianness of the distributions of random-pulse noise.

The above comments relate to random pulse noise, where the time of occurrence of the pulses is random. However, for clocked waveforms one would expect the same type of action. For example, with heavy overlapping

of the pulses (high $f_c$), the Central Limit Theorem still specifies that the waveform approach a Gaussian distribution. Thus one can expect the same type of approach to Gaussianness in the clocked case as in the random-pulse case.

Although one could hope to characterize the clocked waveform by evaluating the correction terms by which the amplitude statistics differ from Gaussian, it appears more profitable to make use of the clock information and to search for characteristics that result from the clocking. This point of view has been taken in this investigation. Furthermore, the "non-Gaussian" approach leaves the characterization uncertain as to whether the non-Gaussianness results from clocking or from some other mechanism.

## 4.2 Cyclo-Stationarity of Clocked Waveforms

It was mentioned in Section 2.2 that an ensemble of clocked waveforms, where the clock positions of each sample are "lined up," represents a non-stationary process in the continuous time domain. If one assumes either that one knows the clock rate or that he can find it by a scanning method, it is possible to characterize the clocked waveform by exploiting the particular type of non-stationarity that is exhibited by clocked waveforms (called cyclo-stationarity). We begin by calculating the autocorrelation to exhibit this non-stationarity. The following sections then consider ways to utilize the cyclo-stationarity.

To investigate the non-stationarity, consider the autocorrelation, which is the expected value of $e(t)\, e(t + \tau)$.

$$R_e(\tau, t) = E\left\{e(t)e(t + \tau)\right\} = \text{av}\left\{e(t)e(t + \tau)\right\} \qquad (4\text{-}1)$$

where:

$R_e(\tau, t)$ = autocorrelation of ensemble $\left\{e(t)\right\}$.

If one lets e(t) be given by

$$e(t) = \sum_{n=-\infty}^{\infty} a_n h(t - \frac{n}{f_c}) , \tag{4-2}$$

Then the autocorrelation $R_e(\tau, t)$ is given by:

$$R_e(\tau, t) = av\left\{ \sum_{m=-\infty}^{\infty} a_m h(t - \frac{m}{f_c}) \sum_{n=-\infty}^{\infty} a_n h(t - \frac{n}{f_c} + \tau) \right\}$$

$$= \sum_{m=-\infty}^{\infty} \sum_{n=-\infty}^{\infty} av[a_m a_n] \, h(t - \frac{m}{f_c}) h(t - \frac{n}{f_c} + \tau) \tag{4-3}$$

$$= \sum_{m=-\infty}^{\infty} \sum_{n=-\infty}^{\infty} R(m - n) h(t - \frac{m}{f_c}) h(t - \frac{n}{f_c} + \tau) ,$$

where:

$$R(m - n) = av[a_m a_n].$$

For the process to be stationary, Eq. 4-3 would have to be independent of t. To show that $R_e(\tau, t)$ is not independent of time, merely substitute $t + 1/f_c$ for t in Eq. 4-3. The result is:

$$R_e(\tau, t) = \sum_{m=-\infty}^{\infty} \sum_{n=-\infty}^{\infty} R(m - n) h(t - \frac{m-1}{f_c}) h(t - \frac{n-1}{f_c} + \tau) . \tag{4-4}$$

If we now let m' = m-1, and n' = n-1, it is quickly seen that Eq. 4-4 is identical to Eq. 4-3. Thus $R_e(\tau, t)$ is periodic in t with period $T = 1/f_c$. Bennett (Ref. 18) has termed a process having such a periodic autocorrelation as "cyclo-stationary." He also states the conditions necessary for this periodicity to vanish--which would result in a stationary process. If one expands $R_e(\tau, t)$ as a Fourier series:

$$R_e(\tau, t) = \sum_{k=-\infty}^{\infty} d_k e^{i2k\pi f_c t} , \tag{4-5}$$

then $d_k$ is given by:

$$d_k = f_c \sum_{m=-\infty}^{\infty} R(m)F(\tau + \frac{m}{f_c}, kf_c) \quad , \tag{4-6}$$

where:

$$F(\tau, f) = \int_{-\infty}^{\infty} h(t)h(t + \tau)e^{-i2\pi ft}dt \quad .$$

For the process to be stationary it is necessary that $d_k$ be zero for all values of $kf_c$ except zero. In general, this will never be true.

## 4.3 Calculation of Sampled Variance

The realization that a clocked waveform sampled at the clock rate results in a stationary process leads one to investigate the statistics of such sampled functions. In particular, we will calculate the variance of a sampled, clocked waveform. Consider the notation used in Fig. 4-1. We will calculate the variance of $e_2(t)$ as a function of $\beta$, where $\beta$ is the phasing

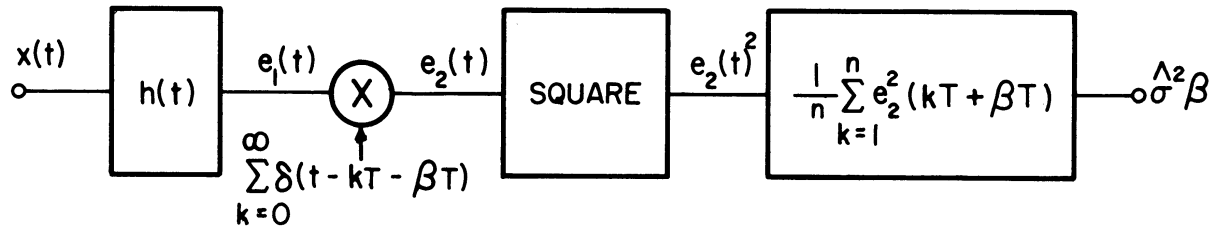


Fig. 4-1. Depiction of calculation and measurement of sampled variance.

of the sampling with respect to the clock ($0 \leq \beta < 1$). First write $e_1(t)$ as:

$$e_1(t) = \sum_{i=-\infty}^{\infty} a(i)h(t - \frac{i}{f_c}) = \sum_{i=-\infty}^{\infty} a(i)h(t - iT) \quad , \tag{4-7}$$

where:

$$T = \frac{1}{f_c} \quad .$$

After sampling, $e_2(t)$ appears as:

$$e_2(t) = 0 \quad \text{for} \quad T \nmid (t - \beta T), \quad 0 \leq \beta < 1 \ ,$$

and, by letting $\frac{t - \beta T}{T} = k$: (4-8)

$$e_2(kT + \beta T) = \sum_{i=-\infty}^{k} a(i)h([k-i]T + \beta T) \quad \text{for } T|(t - \beta T) .$$

Since $h(t) = 0$ for $t < 0$:

$$e_2(kT + \beta T) = \sum_{i=-\infty}^{k} a(i)h([k-i]T + \beta T) \ . \tag{4-9}$$

Let $k - i = n$:

$$e_2(kT + \beta T) = \sum_{n=0}^{\infty} a(k - n)h(nT + \beta T) \ . \tag{4-10}$$

One can now evaluate the variance of $e_2(kT + \beta T)$:

$$\text{Variance} = E\left\{e_2^{\,2}(kT + \beta T)\right\} = \sigma^2(\beta) \ . \tag{4-11}$$

Since the a(n)'s are mutually independent, and also independent of $h(n/f_c)$, one can write:

$$E\left\{e_2^{\,2}(kT + \beta T)\right\} = \sum_{n=0}^{\infty} E\left\{a^2(k - n)\right\} E\left\{h^2(nT + \beta T)\right\}$$

$$= \sum_{n=0}^{\infty} E\left\{a^2(n)\right\} E\left\{h^2(nT + \beta T)\right\} \ . \tag{4-12}$$

Letting $a(n) = +1$ or $-1$, the $E\left\{a^2(n)\right\} = 1$; therefore:

$$E\left\{e_2^{\,2}(kT + \beta T)\right\} = \sum_{n=0}^{\infty} h^2(nT + \beta T) = \sigma^2(\beta) \ . \tag{4-13}$$

The important result here is that, with independent a(n)'s, the variance of the sampled, clocked waveform is a function only of the impulse response of the filter. Further, the variance will, in general, vary with $\beta$, the angle between the clock position and the sampling function. If there is a

detectable change in $\sigma^2(\beta)$ as $\beta$ is varied, one may characterize the filter input as being clocked, since sampling true noise should not show any change in $\sigma^2(\beta)$ as $\beta$ is varied. A useful way to exploit this is to take measurements at two $\beta$'s, and subtract them. If one chooses $\beta_1$ and $\beta_2$ properly for the particular filter, a non-zero difference will exist for the clocked case, whereas zero is expected for true noise. A practical implementation of this idea would appear as in Fig. 4-1. The waveform $e_1(t)$ is first sampled, then squared, and an estimate of the sampled variance obtained by summing a large number of terms:

$$\hat{\sigma}^2(\beta) = \frac{1}{n} \sum_{k=1}^{n} e_2^2(kT + \beta T) \quad \text{for large } n \ , \qquad (4\text{-}14)$$

where:

$\hat{\sigma}^2(\beta)$ = estimate of the sampled variance.

If this process were done for two values of $\beta$, and the results subtracted, the differences noted above will result.

Since two sampled experiments are to be conducted, and their results subtracted, one can view this as multiplying the square of $e_1(t)$ by a single sampling function whose samples are alternately positive and negative. This is depicted in Fig. 4-2.

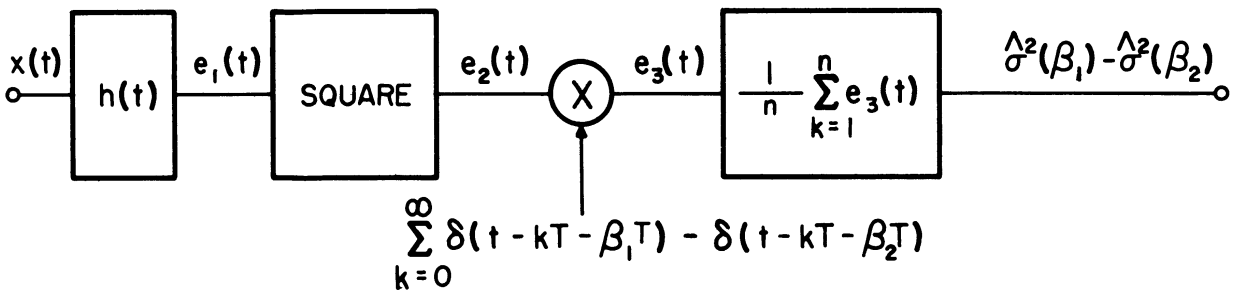


Fig. 4-2. Implementation of measuring difference in sampled variance.

As an example of this method we will calculate the $\sigma^2(\beta)$ as a function of $\beta$ for a simple exponential filter. In general, when taking the difference, $\sigma^2(\beta_1) - \sigma^2(\beta_2)$, one desires this difference to be as large as possible. Therefore, after calculating $\sigma^2(\beta)$ we will investigate the difference relation as a function of the clock frequency-to-filter frequency ratio.

To begin, let:

$$h(t) = e^{-\alpha t} \cos(\omega_o t + \theta) \quad . \tag{4-15}$$

Then let:

$$T = 1/f_c$$

$$h(nT + \beta T) = e^{-\alpha\beta T} e^{-\alpha nT} \cos(\omega_o nT + \omega_o \beta T + \theta)$$

$$2h^2(nT + \beta T) = e^{-2\alpha\beta T} e^{-2\alpha nT} \left\{ 1 + \cos[2\omega_o nT + 2\omega_o \beta T + 2\theta] \right\} . \tag{4-16}$$

Using Eq. 4-13:

$$2\sigma^2(\beta) = e^{-2\alpha\beta T} \left\{ \sum_{n=0}^{\infty} e^{-2\alpha nT} + \cos(2\omega_o \beta T + 2\theta) \sum_{n=0}^{\infty} e^{-2\alpha nT} \cos 2\omega_o nT \right. \tag{4-17}$$
$$\left. - \sin(2\omega_o \beta T + 2\theta) \sum_{n=0}^{\infty} e^{-2\alpha nT} \sin 2\omega_o nT \right\} .$$

Since each of the infinite summations in Eq. 4-17 forms a geometric series, one can use the summation formula. Doing this, after sufficient algebra the result is:

$$\sigma^2(\beta) = 0.5e^{-2\alpha\beta T} \left[ \frac{1}{1-e^{-2\alpha T}} + \frac{\cos(2\omega_o \beta T + 2\theta) - e^{-2\alpha T} \cos(2\omega_o T[1-\beta] - 2\theta)}{1 - 2e^{-2\alpha T} \cos 2\omega_o T + e^{-4\alpha T}} \right] . \tag{4-18}$$

Considering Eq. 4-18 as a function of $\beta$, it is seen that the term within brackets contains a constant dc term and an ac sine wave term of frequency

$2\omega_o T$. Regarding, for a moment, the exponential term outside the bracket as a constant, and noting that the dc term subtracts out in $\sigma^2(\beta_1) - \sigma^2(\beta_2)$, it is sensible to find the relation between $\omega_o$ (the filter frequency) and T (reciprocal of clock frequency) for maximizing and minimizing the magnitude of the ac term. For the exponential filter (and considering the $e^{-2\alpha\beta T}$ term as constant) this represents the best and worst conditions, since the maximum of $[\sigma^2(\beta_1) - \sigma^2(\beta_2)]$ depends on the magnitude of the ac term.

Considering the $e^{-2\alpha\beta T}$ term as constant is very reasonable for a narrow-band filter. Thus if $\alpha T \leq 0.05$, $e^{-2\alpha\beta T}$ varies from 1.0 to 0.9 as $\beta$ goes from 0 to 1. Since the $e^{-2\alpha\beta T}$ term multiplies both the dc term and the ac term within the bracket, regarding it as a constant means that the variance is well approximated by a constant times the dc term plus the ac one within the brackets of Eq. 4-18. We will now find the relation between $\omega_o$ and T for the ac magnitude to be both a maximum and a minimum.

To find the magnitude of the ac term, first rewrite Eq. 4-18 in general terms and let $\theta = 0$; there is no loss in generality for $\theta = 0$ since it serves merely to alter the phase of the ac term and doesn't affect the magnitude.

$$\sigma^2(\beta) = 0.5\, e^{-2\alpha\beta T}\left[K + \frac{\cos x\beta - a\cos(x\beta - x)}{1 - 2a\cos x + a^2}\right] \qquad (4\text{-}19)$$

where:

$$K = \frac{1}{1 - e^{-2\alpha T}} = \frac{1}{1-a}$$

$$a = e^{-2\alpha T}$$

$$x = 2\omega_o T$$

In finding the magnitude of the ac term, one need merely regard the two cosine terms as vectors and find their vector sum. The result is that the ac

term can be written:

$$\frac{\cos x\beta - a\cos(x\beta - x)}{1 - 2a\cos x + a^2} = \frac{(1 - 2a\cos x + a^2)^{\frac{1}{2}}\cos[x\beta + \Phi(x)]}{1 - 2a\cos x + a^2} \tag{4-20}$$

$$= (1 - 2a\cos x + a^2)^{-\frac{1}{2}}\cos[x\beta + \Phi(x)],$$

where:

$\Phi(x)$ = phase angle as function of x.

Hence the magnitude (M) of the ac term is:

$$M = \text{Magn.} = (1 - 2a\cos x + a^2)^{-\frac{1}{2}} . \tag{4-21}$$

The maximum and minimum of this magnitude can be found by differentiating with respect to x and setting the result equal to zero. There are two sets of roots:

$$\begin{aligned} &(1)\ x = 0 \pmod{2\pi} = m2\pi,\ m = 0, 1, 2, 3, - - - \\ &\qquad\qquad\qquad\qquad\qquad\qquad\qquad\qquad \text{are maxima;} \\ &(2)\ x = (2m - 1)\pi \quad m = 0, 1, 2, 3, - - - \text{ are minima.} \end{aligned} \tag{4-22}$$

To establish that the set (1) are maxima and the set (2) minima, the second derivative of the magnitude was taken, and the sign of this expression at values of the critical points was noted. Remembering that $x = 2\omega_o T$ and $T = \frac{2\pi}{\omega_c}$, the following relation between filter frequency $f_o$ and clock frequency $f_c$ is noted, for maximum and minimum magnitude of the ac variance term:

$$\begin{aligned} &\text{Maximum when } f_o = \frac{mf_c}{2} \quad \text{for } m = 0, 1, 2, 3, - - - ; \\ &\text{Minimum when } f_o = \frac{2m-1}{4} f_c = \frac{mf_c}{2} - \frac{f_c}{4} \text{ for } m = 1, 2, 3, - - - . \end{aligned} \tag{4-23}$$

These relations then give the maximum and minimum magnitude of the ac variance term (for $e^{-2\alpha\beta T} \approx$ constant) which in turn give the maximum "difference

in variance" achieved by sampling at two different β points for an exponential filter.

To illustrate the variation of $\sigma^2(\beta)$ versus β for a maximum (exponential filter) condition, consider the following example:

$$f_o = f_c \text{ (clock frequency equals ringing frequency)},$$
$$\alpha T = 0.05,$$
$$\theta = 0, \text{ and}$$
$$h(t) = e^{-\alpha t} \cos \omega_o t \ .$$

Then, using Eq. 4-18 it is found that:

$$\sigma^2(\beta) = e^{-.1\beta} \left\{ 5.26 + 5.26 \cos 4\pi\beta \right\} . \qquad (4\text{-}25)$$

The variation with β is sketched in Fig. 4-3;

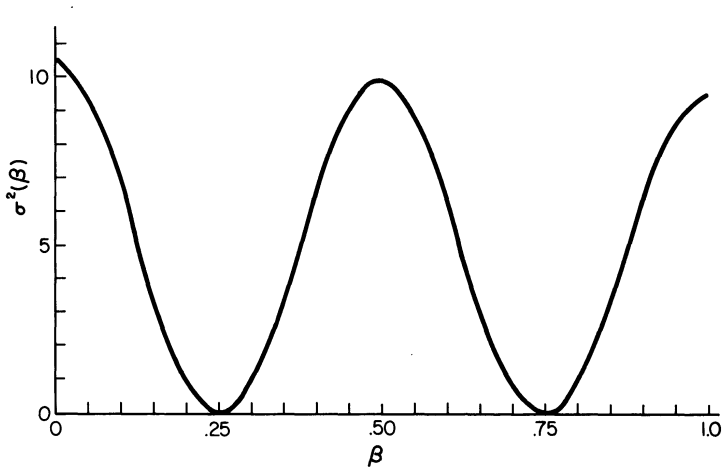


Fig. 4-3. $\sigma^2(\beta)$ vs. β for filter frequency equal to clock frequency.

For this simple exponential case with θ = 0 one notes that the maximum $\sigma^2(\beta)$ occurs at β = 0, and a minimum at β = $\frac{1}{4}$. If the sampling function were successively adjusted to these two values, and the difference taken, the expected result would be:

$$\sigma^2(0) - \sigma^2(\tfrac{1}{4}) = 10.52 \quad . \tag{4-26}$$

Dividing this difference by the initial "mean" of $\sigma^2(\beta)$ gives some measure of the accuracy required of any experimental implementation in the absence of added (non-clocked) noise; in this case the value is 2.

To illustrate the other extreme, a minimum situation for the exponential filter is given by the following example:

$$\begin{aligned} f_o &= \tfrac{5}{4} f_c \qquad (m = 3 \text{ in Eq. } 4\text{-}23) \\ \alpha T &= .05 \\ \theta &= 0 \\ h(t) &= e^{-\alpha t} \cos \omega_o t. \end{aligned} \tag{4-27}$$

Again using Eq. 4-18 it is found that:

$$\sigma^2(\beta) = e^{-.1\beta} \left\{ 5.26 + 0.2625 \cos 5\pi\beta \right\} \quad . \tag{4-28}$$

This variation with $\beta$ is sketched in Fig. 4-4.

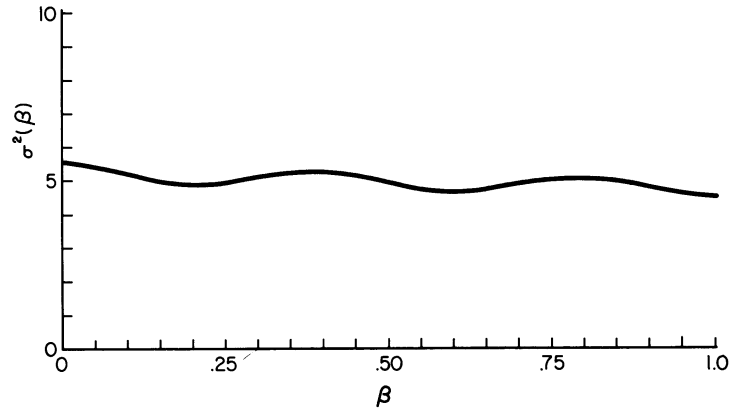


Fig. 4-4. $\sigma^2(\beta)$ vs. $\beta$ for filter frequency equal to 5/4 clock frequency.

For this case, dividing the maximum difference in variance by the initial mean results in a value of 0.1 (as compared to 2.0 for the previous case).

From Eq. 4-18 and from the above two examples one can conclude some general comments regarding the behavior of $\sigma^2(\beta)$ for an exponential filter. If there is an integral relation between $f_o$ and $f_c/2$ then the maximum difference in $\sigma^2(\beta)$ over the range of $\beta$ is the maximum possible. For all such cases $\sigma^2(\beta)$ will have an integral number of cycles in the range $(0 \leq \beta < 1)$; if $f_o = mf_c/2$ then there are m complete cycles in the range. Also, the $\sigma^2(\beta)$ curve will always go to zero for these cases. Finally, the effect of a non-zero $\theta$ is to shift the curve horizontally.

If $f_o$ and $f_c/2$ are not integrally related then the general effect is that the maximum difference in $\sigma^2(\beta)$ over the $\beta$ range shrinks. Also the $\sigma^2(\beta)$ will not have an integral number of cycles for $(0 \leq \beta < 1)$ and will never go to zero.

The maximum difference in $\sigma^2(\beta)$ reaches a minimum when $f_o$ is an odd multiple of one-quarter clock frequency. For all such cases the $\sigma^2(\beta)$ contains an odd number of half-cycles in the range $(0 \leq \beta < 1)$. Since these are the minimum cases, it is expected that they would be the most difficult to deal with in terms of characterizing the filter input as being clocked as opposed to Gaussian noise. It must be remembered that the above conclusions assume that the $e^{-2\alpha\beta T}$ factor of Eq. 4-18 is approximately a constant.

Thus in principle the $\sigma^2(\beta)$ for an exponential filter will always retain a maximum and a minimum value for a clocked waveform, so that it should be possible always to distinguish it from true noise. In general these comments will also be true for all narrow-band filters, as will be discussed below (Section 4.4.1).

It is interesting to compare this "difference of variance" method with the short-time symmetry method of the previous chapter. First of all, to note symmetry effects, energy has to be available at certain positions in

the frequency domain. Here there is no such requirement, but the clock frequency must be known in order to sample properly. Thus this is a coherent measurement; to make the two methods equivalent in this respect it would be necessary to run coherent spectral measurements. Hence, whereas it is expected that noise will quickly wash out any spectral symmetry if there is not sufficient signal energy in symmetrical positions, here, with a coherent measurement, in principle it is possible to extract the presence of clocking no matter now much noise is present.

## 4.4 The Sum of Weighted Variances--A General Method

In the previous section it was seen that, in general, narrow-band clocked waveforms will exhibit two different values of sampled variance, for proper sampling positions $\beta$. For true noise, on the other hand, the two values of variance should be the same.

These results lead one to question whether some continuous coherent multiplying waveforms may be used which give results equal to or better than the sampled variance case. In this section we will consider multiplying by a coherent (possibly phase-bumped) sine wave instead of with a sampling waveform. It will be shown that this procedure is optimum if the sampled variance, as a function of $\beta$, is essentially sinusoidal (which it is for sufficiently narrow-band filters). This result will be obtained by considering the multiplication by a coherent wave as a "sum of weighted variances."

4.4.1 Calculation. We now wish to consider what coherent, continuous waveform results in the best indication of the presence of clocking when considering the variance of the waveform. Consider the block diagram of Fig. 4-5. Whereas in the previous sampled case, depicted in Fig. 4-2,

the multiplying waveform was a sampling function consisting of the subtraction of two basic sampling functions, here the multiplying waveform is a continuous function. We will analyze the effect of this waveform, and the best K(t), by considering the result as a "sum of weighted variances."

Because of this technique the result as to what form of K(t) is best will first appear in terms of $\beta$ as $K(\beta)$, and it will be necessary to convert to K(t). This conversion is straightforward with the idea being that one wishes to multiply by the proper $K(\beta)$ in each clock interval. Thus the K(t) waveform will be a waveform which repeats, in each clock interval, the desired $K(\beta)$.

In order to find the proper $K(\beta)$, the first step is to write the $K(\beta)$ as a sum of impulses; that is, as a sum of rectangular elements taken

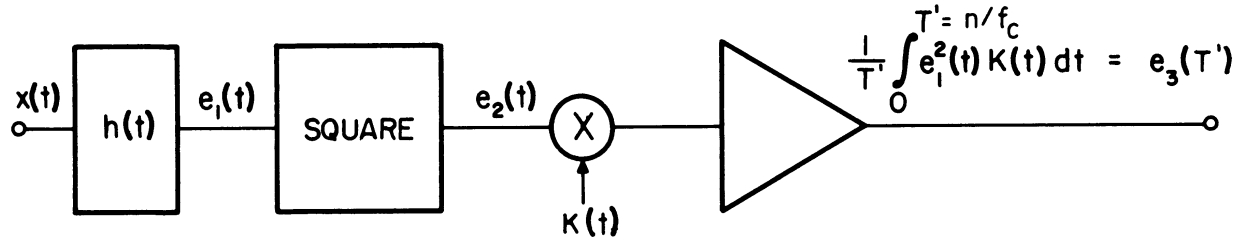


Fig. 4-5. Procedure for measuring the sum of weighted variances.

to the limit. Let $K(\beta)$ be given by:

$$K(\beta) \cong \sum_{k=0}^{1/\Delta\beta} A_k \Delta\beta \, u_o(\beta - k\Delta\beta) , \qquad (4\text{-}29)$$

where: $A_k$ = magnitude of $K(\beta)$ in interval $k\Delta\beta$,

$u_o$ = rectangular area taken to the limit to form impulse, and

$\Delta\beta$ = elementary length of $\beta$.

It is seen that the rectangular impulses have an area which is proportional to the magnitude of $K(\beta)$.

Using this form of $K(\beta)$ [or K(t)] we now seek to write the output of Fig. 4-5 $\left[e_3(T')\right]$ in terms of $\hat{\sigma}^2(\beta)$---the sampled variance. This

can be done by considering $e_3(T')$ as the sum of a parallel bank of units of the type shown in Fig. 4-1. For each such unit one set of rectangular impulses of Eq. 4-29, spaced $1/f_c$ apart, is used to multiply $e_1^2(t)$. To do this first write $e_3(T')$ as the limit of a summation:

$$e_3(T') = \frac{1}{T'} \int_o^{T'} K(t) e_1^2(t)\,dt = \lim_{N \to \infty} \frac{1}{T'} \sum_{i=1}^{M=Nf_cT'} K(t_i) e_1^2(t_i) \cdot \Delta t \qquad (4\text{-}30)$$

where: $N$ = number of elements in a clock interval, $1/f_c$

$M = Nf_cT'$ = total number of elements in time $T'$.

Now divide this total summation into a set of n, where $n = T'f_c$, and where the contributions from each one of the set are spaced $T = 1/f_c$ apart. Also, note that $\Delta t = 1/f_cN$, with N defined above; then:

$$e_3(T') = \lim_{N \to \infty} \frac{1}{T'} \sum_{k=1}^{N} K(t_k) \sum_{r=1}^{n} e_1^2(rT + \beta_k T) \cdot \frac{1}{f_c N} \qquad (4\text{-}31)$$

where: $\beta_k = k\Delta\beta$ = phasing of the sampling with respect to the clock

$t_k = rT + \beta_k T$.

Since $K(t)$ is a repetitive waveform with period T, we can use Eq. 4-29 to substitute $A_k$ for $K(t_k)$:

$$e_3(T') = \lim_{N \to \infty} \sum_{k=1}^{N} A_k \cdot \frac{1}{f_c T'} \sum_{r=1}^{n} e_1^2(rT + \beta_k T) \cdot \frac{1}{N}$$

$$= \lim_{N \to \infty} \sum_{k=1}^{N} A_k \Delta\beta \, \frac{1}{n} \sum_{r=1}^{n} e_1^2(rT + \beta_k T)$$

where: $\Delta\beta = 1/N$ .

But, using Eq. 4-14, it is noted that the second summation equals $\hat{\sigma}^2(\beta_k)$. The resulting limiting value as N, the number of elements in a clock interval, approaches $\infty$ can thus be returned to integral form:

$$e_3(T') = \lim_{N \to \infty} \sum_{k=1}^{N=1/\Delta\beta} A_k \, \Delta\beta \, \hat{\sigma}^2(\beta_k) = \int_o^1 \hat{\sigma}^2(\beta) \, K(\beta)\,d\beta. \qquad (4\text{-}32)$$

The important result here is that the output, when multiplying by a coherent, continuous waveform $K(\beta)$ consists of the area under the product curve of $\sigma^2(\beta)$ and $K(\beta)$. This method of viewing the analyzing process in terms of the sampled variance has been chosen because the behavior of the variance and its difference for clocked waveforms and true noise is known. Also this treatment will allow one to decide upon the best form of $K(t)$.

One can now find what form of $K(\beta)$ is required to exhibit the greatest difference between the case of clocked waveforms $(e_1)$ and true noise.

To do this, it is necessary to consider for a moment the influence of the dc part of $K(\beta)$ versus the ac part in comparing the clocked waveform to true noise with this method. When comparing the waveforms, using Eq. 4-32 one is interested in the quantity:

$$\int_0^1 \sigma_c^2(\beta)K(\beta)d\beta - \int_0^1 \sigma_N^2(\beta)K(\beta)d\beta \ , \qquad (4\text{-}33)$$

where: $\sigma_c^2(\beta)$ = variance of clocked waveform, and

$\sigma_N^2(\beta)$ = variance of noise waveform.

If the waveform $e_1(t)$ is true noise then the expected value of $\sigma_N^2(\beta)$ is a constant or dc value and equals the average power. Since, when comparing the two situations, the power should be equal, the dc value of $\sigma_c^2(\beta)$ (average power) should be equal to $\sigma_N^2$. Thus the integral of the dc contribution of $\sigma_c^2(\beta)$ will be equal to the second integral of Eq. 4-33 and subtract to zero. The term remaining will be the ac portion of $\sigma_c^2(\beta)$, as expressed by:

$$\int_0^1 \sigma_{dc}^2(\beta)K(\beta)d\beta + \int_0^1 \sigma_{ac}^2(\beta)K(\beta)d\beta - \sigma_N^2 \int_0^1 K(\beta)d\beta = \qquad (4\text{-}34)$$

$$\int_0^1 \sigma_{ac}^2(\beta)K(\beta)d\beta \ ,$$

where:

$\sigma_{dc}^2(\beta)$ = dc component of $\sigma_c^2(\beta)$,

$\sigma_{ac}^2(\beta)$ = ac component of $\sigma_c^2(\beta)$, and

$\sigma_{dc}^2(\beta) = \sigma_N^2$.

It is clear that, in seeking the best $K(\beta)$ for distinguishing, one wishes to find the largest value of:

$$\int_0^1 \sigma_{ac}^2(\beta)K(\beta)d\beta \quad . \tag{4-35}$$

Using Schwarz's inequality, which states that:

$$\frac{\int_0^T x(t)y(t)dt}{\sqrt{\int_0^T x^2(t)dt}\ \sqrt{\int_0^T y^2(t)dt}} \leq 1 \tag{4-36}$$

$$\frac{\int_0^T \sigma_{ac}^2(\beta)K(\beta)d\beta}{\sqrt{\int_0^T \sigma_{ac}^4(\beta)d\beta}\ \sqrt{\int_0^T K^2(\beta)d\beta}} \leq 1, \tag{4-37}$$

it will be seen that the largest value occurs when $K(\beta)$ is made equal to $\sigma_{ac}^2(\beta)$.

Thus it has been shown that the best coherent, continuous waveform $K(t)$ to use as the multiplier in Fig. 4-5 consists of a wave which, in each clock interval, has the form:

$$K(\beta) = \sigma_{ac}^2(\beta) = \sum_{n=0}^{\infty} h^2(nT + \beta T) - \sigma_{dc}^2(\beta) \tag{4-38}$$

where:

$K(\beta)$ = multiplying waveform to characterize clocked input, and

$h(t)$ = impulse response of transmitting filter.

The conversion of $K(\beta)$ to $K(t)$ can be formalized as follows: let

$$\beta = \frac{t}{T} - \left[ \frac{t}{T} \right] , \tag{4-39}$$

where:

$$\left[ \frac{t}{T} \right] = \text{largest integer less than } \frac{t}{T} .$$

Then $\beta$ will always be in the range $(0 \leq \beta < 1)$ as used before. Consequently one can let $t = \beta T$ and:

$$K(t) = K(\beta T) . \tag{4-40}$$

Clearly $K(t)$ is a periodic time function with period $T = \frac{1}{f_c}$ and is of the same form as $\sigma_{ac}^2(\beta)$ in each clock interval. For example, if $\sigma_{ac}^2(\beta)$ is sinusoidal and has an integral number of cycles for $0 \leq \beta < 1$, then $K(t)$ will be sinusoidal. If $\sigma_{ac}^2(\beta)$ is sinusoidal but not integral cycle, then the $K(t)$ would be a phase-bumped sine wave; i.e., it would begin repeating the pattern of $\sigma_{ac}^2(\beta)$ each clock interval.

Consider the proper $K(t)$ for given filters. If $h(t)$ is an exponential filter and is clocked at some multiple of half-clock, then the $\sigma_{ac}^2(\beta)$ is a slightly damped exponential and has an integral number of cycles, as found in Eq. 4-25. The ideal $K(t)$ then would be a sine wave that decays exponentially between clock pulses. For many narrow-band filters a pure undamped sine wave will be quite adequate. If this same filter is clocked other than at some multiple of half-clock, the $\sigma_{ac}^2(\beta)$ will be a damped sine wave, but not having an integral number of cycles. For this case a phase-bumped, damped sine wave would be the ideal $K(t)$. Again, for many purposes a phase-bumped sine wave without damping will be adequate.

For filters other than exponential, the $\sigma_{ac}^2(\beta)$ will be approximately of the sinusoidal form for narrow-band filters. This can be verified

by considering a general impulse response:

$$h(t) = \sum_{m=1}^{r} e^{-\alpha_m t} \cos(\omega_m t + \theta_m) . \qquad (4\text{-}41)$$

For a narrow-band filter the assorted $\omega_m$'s will be close to each other; the result is that the $\sigma_{ac}^2(\beta)$ is made up of a sum of damped sine waves, each of which differs in frequency by only a small amount.

Some comments regarding the relative position of $f_o$(the filter center frequency) and the clock frequency are justified. As in the straight sampled variance case, the best situation occurs when the filter is located at some multiple of half-clock frequency. For then the $\sigma_{ac}^2(\beta)$ is the largest possible. For other frequency positions the $\sigma_{ac}^2(\beta)$ will shrink and K(t) will decrease correspondingly. However, as before, the distinction between $\sigma_{ac}^2(\beta)$ for true noise and clocked waveforms will always remain (no matter what the position of energy) so that, in principle one can always use this method; however, this test, as will all others, becomes more and more difficult as $f_c$ increases indefinitely relative to $f_o$. If the filter is exponential, and if $f_c \leq 2f_o$ so that at least one full cycle of $\sigma^2(\beta)$ occurs in the $\beta$ range, then the minimum situation occurs when $f_o$ is an odd multiple of $f_c/4$, as proved in the previous section.

4.4.2 Comparison of Sampled and Continuous Cases. It is of interest to compare the "difference of sampled variance" method of Section 4.3 with the continuous multiplication method of this section. In comparing a clocked waveform with true noise in the sampled variance case one notes that the quantity:

$$\left\{ \sigma_{max}^2(\beta) - \sigma_{min}^2(\beta) \right\} , \qquad (4\text{-}42)$$

where:

$\sigma_{max}^2$ = maximum of $\sigma^2(\beta)$ for $(0 \leq \beta < 1)$, and

$\sigma_{min}^2$ = minimum of $\sigma^2(\beta)$ for $(0 \leq \beta < 1)$,

is zero for true noise, but is different from zero for clocked waveforms.

In comparing the two waveforms for the continuous multiplication case, it was seen in Eq. 4-35 that the comparison results in:

$$\int_0^1 \sigma_{ac}^2(\beta)K(\beta)d\beta \ , \qquad (4\text{-}43)$$

where:

$K(\beta) = \sigma_{ac}^2(\beta)$ for the best condition.

Hence in comparing the two distinguishing methods, we will evaluate the results of Eq. 4-42 versus those of Eq. 4-43 for the exponential filter.

The $\sigma^2(\beta)$ for the exponential filter is shown in Eqs. 4-18 and 4-19. For the comparison we are concerned with only the ac portion of the $\sigma^2(\beta)$. As before, the term $e^{-2\alpha\beta T}$ is approximately constant over the range $(0 \leq \beta < 1)$ for narrow-band filters. Consequently the second term in the brackets of Eqs. 4-18 and 4-19 will be the $\sigma_{ac}^2(\beta)$. Using this approximation then, $\sigma_{ac}^2(\beta)$ for the exponential filter can be written:

$$\sigma_{ac}^2(\beta) = M \cos [x\beta + \Phi(x)] \ , \qquad (4\text{-}44)$$

where:

$M$ = the magnitude of the cosine term (Eq. 4-21), and

$x = 2\omega_o T$.

Assume for a moment that at least one full cycle of $\sigma_{ac}^2(\beta)$ occurs in the range $(0 \leq \beta < 1)$. If this is true, Eq. 4-42, for the sampled variance case, results in "2M" for the clocked waveform and zero for the noise case. Thus the difference is 2M. The condition that at least one full cycle of $\sigma^2(\beta)$ occurs corresponds to $f_o \geq \frac{f_c}{2}$. If this is not true, the value may be less than 2M, depending on the portion of a cycle that appears and on $\Phi(x)$.

Evaluating the continuous case, Eq. 4-44 is substituted into Eq. 4-43. For general results one must again use the restriction $f_o \geq \frac{f_c}{2}$;

otherwise the value of Eq. 4-43 will depend on the portion of a cycle in $(0 \leq \beta < 1)$ and on $\Phi(x)$. With this restriction the result is:

$$\int_0^1 M \cos [x\beta + \Phi(x)] \cos [x\beta + \Phi(x)] d\beta = M \left[ \frac{1}{2} + \frac{f_c}{16\pi f_o} \sin \frac{8\pi f_o}{f_c} \right] , \tag{4-45}$$

where:

$$x = \frac{4\pi f_o}{f_c} .$$

Since it was assumed that at least one full cycle of $\sigma_{ac}^2(\beta)$ appears, the result is independent of $\Phi(x)$ and thus $\Phi(x)$ plays no part in the above integral. For moderate values of $f_c/f_o$, it is seen that the value is M/2.

Thus, for the sampled variance case the comparison results in a value 2M, and for the continuous multiplication case a value M/2. This is to be expected since in the sampled case one is taking the difference of two extreme values, whereas in the continuous case one obtains an "average" of all values over the $\beta$ range. However, this comparison has meaning for only an ideal "noiseless" case; that is, a clean variance signal $\sigma_{ac}^2(\beta)$ is available. In any realistic situation one should take account of added noise in the clocked case. In this situation it is a fundamental theorem of Signal Detectability that the continuous multiplication case is the optimum test.

4.4.3 Experimental Results. In order to exhibit experimental evidence of the method of using a coherent, continuous multiplying waveform a series of experiments were run. For the first set of experiments an exponential filter was used with clock frequencies that provided maximum, intermediate, and minimum variance situations. A similar set of three experiments was run using a non-exponential filter.

The general idea of all the experiments is depicted in Fig. 4-5. The K(t) in each case was chosen to approxate the $\sigma_{ac}^2(\beta)$, as specified by

Eq. 4-37 and run in synchronism with the clock. Since the integrator output [$e_3(t)$ of Fig. 4-5] is itself a random process, for a finite integrating time, this output was analyzed by measuring the cumulative distribution curve. In some cases the difference in mean between the "noise" and the "clocked waveform" situations was so great that the particular analyzing equipment could not be used. For these cases, photographs of the integrator output were taken, and prove conclusive.

The analyzing equipment used to obtain the cumulative distributions consisted of a special purpose simulator called "SIMulated Receiver And Recorder" (SIMRAR). This equipment essentially assigns the integrator output, with a gated-and-dump operation, to one of ten slot intervals. The cumulative data consisting of the number of times the output rises above a given level are totalized on relay counters. At the end of a "run" the counters provide the data for drawing the histograms to approximate the cumulative distribution (see Section 6.4 for experimental description).

Two sets of counters and the switching arrangements are available for alternately measuring one waveform, then the other. With this operation the relative counter totals are independent of drifts which may occur in the discriminators and operational amplifiers. This feature was used in our experiments with true noise as one input and a clocked waveform as the other.

The experimental results using the exponential filter[1] are shown in Fig. 4-6. Three different clock frequencies were used, and the analyzing results for the three cases are shown in the left-hand column. Pictures of the time waveform for each of the three cases appear to the right of the

---

1 The impulse response and bandpass of the exponential filter are shown in Chapter 6, Fig. 6-7, p. 109.

corresponding results. The picture at right-center shows the time waveform when noise was passed through the filter. This picture is to be compared with each of the three clocked time waveforms.

In the first case, Fig. 4-6(a), the $f_c = f_o$. From Section 4.3 it is remembered that this is a case in which the magnitude of $\sigma_{ac}^2(\beta)$ is a maximum. Thus the variance $\sigma_c^2(\beta)$ for this case is of the form shown in Fig. 4-3. Although the ideal $\sigma_c^2(\beta)$ is slightly damped (Eq. 4-19), the K(t) waveform used was an undamped sine wave (no phase-bumping was required since $\sigma^2(\beta)$ has an integral number of cycles). For this particular filter the approximation is very good.

Since this is a maximum case the difference in the mean of the integrator output, for the noise case versus the clocked case, was too great to use SIMRAR. For this reason a picture of the output is shown in part (a). The three ramps shown correspond to the integrator output when the input is clocked; the two intervening waveforms show the output when noise is the input. The integrator is gated and dumped at the end of each interval. Considering the end of each integrating period, the difference between the clocked and noise situations is quite obvious. Comparing the time waveform of part (a) to that of noise (d) it is seen that they are recognizably different; exponential envelope segments appear frequently in the clocked case. This will be true for all cases of $f_o = mf_c/2$ for an exponential filter; these situations can be considered as singular cases in which the time waveform itself is not very noiselike.

Part (b) is an intermediate case (between maximum and minimum) in which the $f_c$ was chosen to achieve as noiselike a time waveform as possible. Comparing the time waveform of (b) to (d) shows that they are quite similar. The analyzing results for part (b) show the cumulative distribution for

Analysis results | Clocked time waveforms | True noise waveform

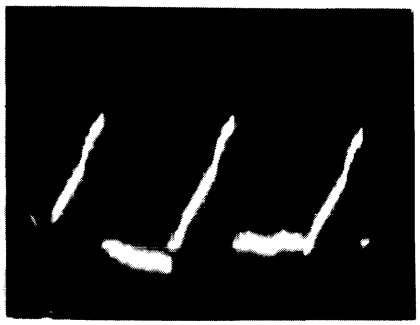


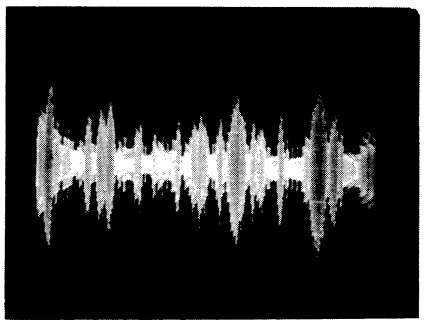

(a) $f_o = f_c = 3908$ cps

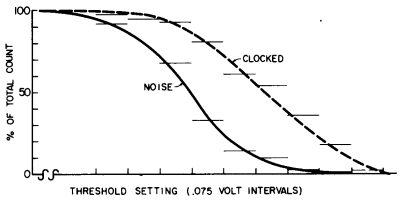


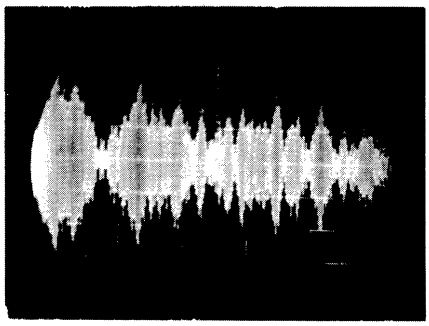

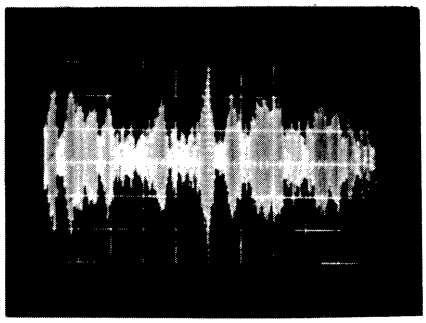

(b) $f_c < f_o$; $f_c = 3525$, $f_o = 3908$

(d) Noise

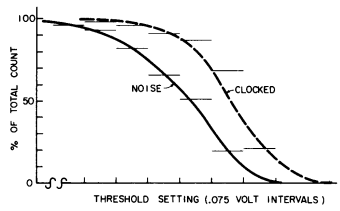


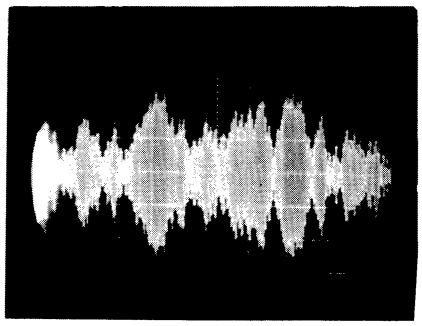

(c) $f_o = 5f_c/4$; $f_c = 3129$, $f_o = 3908$

Fig. 4-6. Analysis results for exponential filter.

both noise and clocked cases of the integrator output. For convenience, the actual curves plotted are "1 - cumulative distribution." This allowed plotting the data directly in terms of gate setting and counts. Thus these are the cumulative data of the integrator values at the end of the integrating time. Since $\sigma_{ac}^2(\beta)$ has a non-integral number of cycles for this case a phase-bumped sine wave was used. A "photoformer" arrangement (see Section 6.4) was used to obtain this phase-bumped curve. Comparing the results to part (a), it is remembered that there the noise and clocked curves were separated too far to permit using the analyzing equipment. Hence, for part (a) the curves would be similar but separated much farther. It should be noted that the horizontal scale on all the distribution curves is not absolute; that is, each pair of curves may be moved to the right or left. This position is actually determined by the bias used in the experiment: the equipment can analyze only positive voltages. Since, for the noise case, negative values are equally probable as positive ones, a common bias must be used for both noise and clocked cases. For all the curves, the same bias was used.

For part (c) the $f_c$ was chosen to implement a case where the magnitude of $\sigma_{ac}^2(\beta)$ is a minimum. Thus, $f_o$ was made an odd multiple of $f_c/4$; in this case $f_o = \frac{5}{4} f_c$. The variance curve for this case is of the form shown in Fig. 4-4. As in the previous case, the $\sigma_{ac}^2(\beta)$ has a non-integral number of cycles in the range $(0 \leq \beta < 1)$, hence a sine wave whose phase is bumped at every clock interval was used; in this case the phase-bump was $180^\circ$. It is seen that the noise and clocked distributions are closer than for part (b), but still clearly discernible. Comparing the time waveform to the noise one, it is seen that the waveform is again very noiselike.

In conclusion, Fig. 4-6 shows the action that occurs when the

best, intermediate, and worst clocking conditions are used. This depicts the results, then, for the exponential filter, with the method of multiplying by a coherent continuous wave which is a good approximation to the $\sigma_{ac}^2(\beta)$.

The equivalent set of results for a non-exponential filter (whose impulse response and bandpass is given in Chapter 6, Figs. 6-9 and 6-10) are shown in Fig. 4-7. For these experiments a sine wave or a phase-bumped sine wave was used as the multiplying waveform K(t). Thus the $K(\beta)$ in this case is a poorer approximation to the actual $\sigma_{ac}^2(\beta)$ than was true for the exponential filter. Although this filter is not strictly narrow-band ($Q \approx 3$), this does not affect greatly the quantities of interest here.

For the first case, Fig. 4-7(a), the $f_c = f_o$. Here again the resultant difference in the mean of $e_3(t)$ was too great to use the analyzing equipment. As before every other interval in (a) is a clocked portion, and the intervening ones are noise. In comparing the time waveform of (a) to the noise waveform of (d) it appears that the clocked waveform has a more liny construction. One would expect some singular action in the time waveform for the singular cases of $f_o = mf_c/2$, but the non-regular impulse response tends to destroy this.

In the second case, Fig. 4-7(b), an intermediate $f_c$ was chosen ($f_c = 3866$, $f_o = 4265$). This case was chosen to coincide with a case in the next chapter, where zero-crossing interval distributions were measured. Whereas, as shall be seen later, there is little difference in the zero-crossing interval distribution, here the difference between the clocked and the noise cases is clearly discernible. The height of the ramp in this case is about one-half that of the previous case. By comparing the time waveform with that of noise (d), it is seen that the waveform is very noiselike.

Analysis results | Clocked time waveforms | True noise waveform

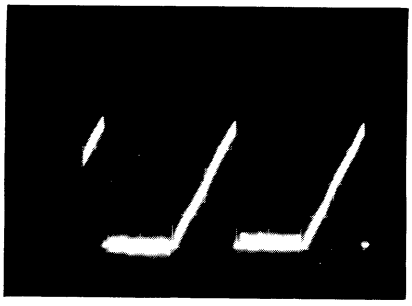

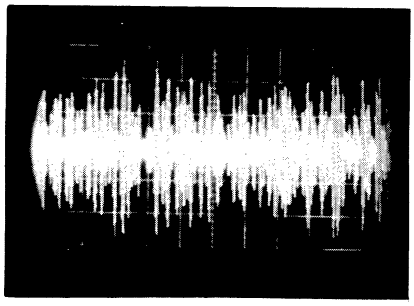

|NOISE|CLOCK|

(a) $f_o = f_c = 4265$ cps

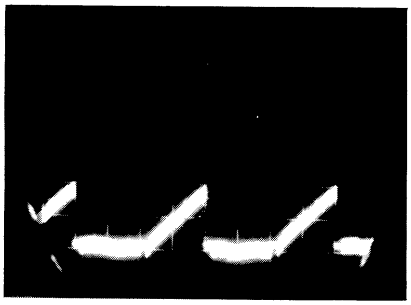

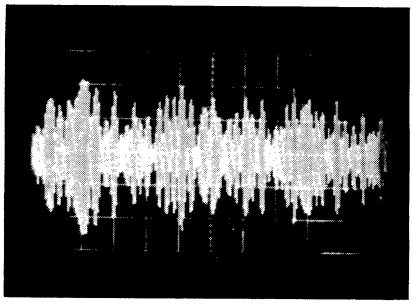

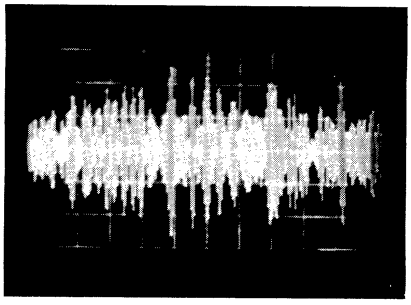

|NOISE|CLOCK|

(b) $f_c < f_o$; $f_c = 3866$, $f_o = 4265$

(d) Noise

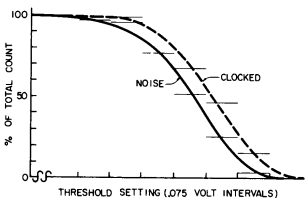


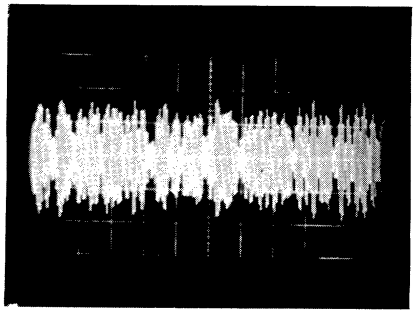

(c) $f_o = 5f_c/4$; $f_c = 3412$, $f_o = 4265$

Fig. 4-7. Analysis results for nonexponential filter.

For the third case, part (c), the $f_o = 5/4\ f_c$. This represents an approximately minimum situation since this ratio would be minimum for an exponential filter. From the cumulative distribution of part (c) it is seen that this situation is the least detectable of the cases treated. The time waveform of part (c) indicates a lower peak-to-rms ratio than appears for true noise (d). Thus the time waveform shows the evidence of a singular relation between the clock and filter frequency.

As is always the case with statistical measurements, the accuracy depends upon the number of trials. For the data given here there are two questions to ask: (1) how significant are the true $e_3(T')$ data; and (2) how significant is the measurement or estimation of these true data?

The true $e_3(T')$ data depend upon the length of integration time T'. If T' is increased the mean-to-standard deviation of $e_3(T')$, for different samples, will improve for both clocked and noise situations. In the graphs of Figs. 4-6 and 4-7 an increasing T' would cause the cumulative distribution curves to become more vertical; if $T' \to \infty$ the clocked and noise curves would be two vertical lines. A T' of 1 second was used in our experiments. Using the respective filter bandwidths, this corresponds to about 200 independent waveform samples (2WT') for the exponential filter and 1300 samples for the non-exponential case. In terms of "signal-detectability," the curves of Fig. 4-6(c) (the worst exponential case) exhibit a d' of 1.3; this corresponds roughly to a signal-to-noise ratio of 2.3 db. Since, for independent values, this can be expected to improve in proportion to increased T', a T' of 10 sec. would have yielded an equivalent output signal-to-noise ratio of 12.3 db.

The measurement of the true $e_3(T')$ data is dependent upon the number of thresholds used and the number of trials. For our measured data 10 thresholds and 500 runs were used. The number of runs necessary to provide a given "estimation" accuracy can be approximated by considering the data for each threshold as a series of n Bernoulli trials. For n sufficiently large the data probability "estimate" will coincide with the true probability of the data; for n much smaller the data estimates will vary about the true mean, for different runs, and thus their probability estimates will exhibit a distribution.

To illustrate the effect of n, let us specify that the clocked and noise distributions of the probability estimates intersect at their respective $3\sigma$ points. Then:

$$p_1 - p_2 = 3\sigma_1 + 3\sigma_2 = 3\sqrt{\frac{p_1(1-p_1)}{n}} + 3\sqrt{\frac{p_2(1-p_2)}{n}}, \quad (4\text{-}46)$$

where: $p_1$ = true probability of clocked case exceeding a given threshold,

$p_2$ = true probability of noise case exceeding the same threshold, and

$n$ = number of runs or trials.

Suppose the true probabilities were .50 and .32, respectively; then 129 trials are required to meet the specified criterion. If the smooth curves which approximate the histograms on Fig. 4-7(c) are used for the probability estimate, the values of .50 and .32 occur for a threshold position. From the above this means that our n of 500 is sufficient to provide a good estimate of the true data. By such methods the statistical significance of the data can be evaluated.

# CHAPTER V

# ZERO-CROSSING CONSIDERATIONS

In the previous section the analysis of clocked waveforms and the method for characterizing such waveforms utilized the amplitude statistics of the waveform. In this section we will ignore all amplitude information and study the characteristics of the zero-crossings of clocked waveforms. In general we will be interested in looking upon any properties of the zero-crossings which may be gleaned from the fact that the waveform is a clocked process. Toward this end it is profitable first to review the classical literature concerning zero-crossing information for true Gaussian noise. We will then portray special properties of the zero-crossings for the exponential filter. Both calculations and experimental results will be shown. The last section will discuss general narrow-band filters and show experimental results.

## 5.1 Review of Classical Knowledge

It is well known that if a true Gaussian waveform is passed through a narrow-band filter, the output can be expressed as:

$$e(t) = V(t) \cos [\omega_o t + \varphi(t)] , \qquad (5\text{-}1)$$

where:

$V(t)$ = slowly varying envelope, and

$\varphi(t)$ = slowly varying phase.

This representation can be applied even when the waveform is not limited to a narrow-band, but then the envelope and phase functions do not have a useful physical significance. With this representation, the zero-crossings are determined by the combination of $\omega_o t$ and $\varphi(t)$.

A statistical description of the zero-crossings of a random process, in general, is given by the probability distribution of the distance between successive zero-crossings. Rice (Ref. 19) was the first to attempt to find analytically this probability distribution for the distance between successive zero crossings for Gaussian noise. He succeeded in finding the probability that the random noise record will pass through zero in the interval $(\tau, \tau + d\tau)$ with a negative slope when it is known that it passes through zero at $\tau = 0$ with a positive slope. The resulting distribution is very close to the desired interval distribution for short intervals. Rice's distribution departs from the actual desired distribution in that this function will include even numbers of intermediate crossings between the desired crossings which do not properly belong there. However, it has been experimentally shown that his results very closely approximate the actual measurements made on Gaussian noise, except for the longer intervals. In fact the actual process of determining a complete distribution function for the distance between successive zeros is still an outstanding problem in random noise theory. McFadden (Ref. 20) has achieved some success in this direction by determining the relation between the zero-crossing interval probability density and the autocorrelation function of the infinitely-clipped waveform which leaves invariant the zero crossings. It is shown that this probability density function is closely related to the autocorrelation function of the clipped noise signal.

A number of experimental investigations have been devoted to measuring the probability distributions for the zero-crossings of Gaussian noise. Kohlenberg (Ref. 21), White (Ref. 22), and Blötekjaer (Ref. 23) are some of the investigators in this area.

## 5.2 Exponential Filter

It will be the general purpose in these calculations and experiments to find whatever information is possible about the zero crossings of the clocked narrow-band waveforms. The technique will be to glean any possible information from the fact that the clocked narrow-band waveforms are made up of regularly-spaced sums of the impulse response of the filter being used. Information will be obtained about the distribution of the intervals between zero-crossings and also about the time behavior of certain intervals. The object in this latter case is to take advantage of the fact that the impulse responses which are being summed are in a definite time relationship with each other. Therefore, making use of time properties of the axis-crossing intervals involves more information than the distribution function alone contains since it lumps all intervals of a given length together.

5.2.1 Concerning Distribution of Zero-Crossing Intervals. First we will consider the probability distribution of the intervals between successive zero-crossings for the simple exponential filter. The impulse response is:

$$h(t) = e^{-\alpha t} \cos (\omega_o t + \theta) , \qquad (5\text{-}2)$$

where:

$h(t)$ = impulse response of the transmitting filter.

As before write the output waveform $e(t)$ as the summation of impulse responses:

$$e(t) = \sum_{n=0}^{N(t)} a_n \, h(t - \frac{n}{f_c}) \quad \text{for } t \ni N < t < N + 1 , \qquad (5\text{-}3)$$

where:

$a_n$ = +1, -1, depending upon binary sequence $x(t)$.

Substituting the particular impulse response of Eq. 5-2 one finds:

$$e(t) = \sum_{n=0}^{N(t)} a_n e^{-\alpha(t - \frac{n}{f_c})} \cos\left[\omega_o(t - \frac{n}{f_c}) + \theta\right] . \qquad (5\text{-}4)$$

From Eq. 5-4 one can note the zero-crossing action when the filter frequency ($f_o$) is any multiple of half-clock frequency. For this case the cosine term can be brought outside the summation and e(t) can be written, depending upon whether $f_o$ is an even or an odd multiple of $f_c$, as:

$$e(t) = \sum_{n=0}^{N(t)} a_n e^{-\alpha(t - \frac{n}{f_c})} \cos(\omega_o t + \theta - n2\pi) = \cos(\omega_o t + \theta) \sum_{n=0}^{N(t)} a_n e^{-\alpha(t - \frac{n}{f_c})} \qquad (5\text{-}5)$$

for even multiple, and

$$e(t) = \sum_{n=0}^{N(t)} a_n e^{-\alpha(t - \frac{n}{f_c})} \cos(\omega_o t + \theta - n\pi) = \cos(\omega_o t + \theta) \sum_{n=0}^{N(t)} a_n (-1)^n e^{-\alpha(t - \frac{n}{f_c})}$$

for odd multiple.

In Eq. 5-5, zero-crossings will be contributed both by the cosine (carrier) term and the summation (envelope) term. The first conclusion is that, for such synchronism between $f_o$ and a multiple of $f_c/2$, zero-crossings will occur at spacings of $1/2f_o$ for all time. This occurrence of zero-crossings at regular intervals is depicted in Fig. 5-1 below. For this picture an exponential filter centered at 3908 cps was used with an input sequence at $f_c$ = 1117 (3908/1117 = 3.5). The scope trace was triggered in synchronism with the clock. The fact that all the corresponding zero-crossings coincide exhibits the regularity, through-out-time, of these crossings when the filter is at a multiple of half-clock frequency.

Zero-crossings of the envelope may occur between the "carrier"

crossings, and thus the intervals between successive zero-crossings will be affected by these crossings also. In general, the zeros of the summation term will be of a much smaller number than those of the cosine term in Eq. 5-5 if $f_o$ is greater than $f_c$. Thus one would expect practically all of the zero-crossing intervals to be of length $1/2f_o$, in the zero-crossing interval distribution, for such synchronous, exponential filter cases.

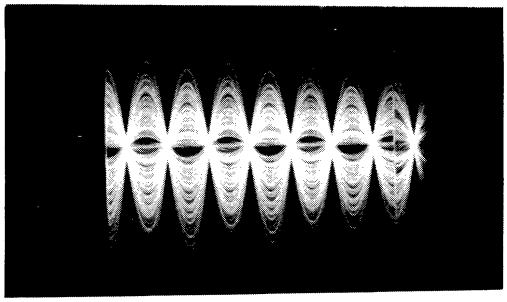

Fig. 5-1. Demonstration of regular zero-crossings when $f_o$ is a multiple of $f_c/2$ for an exponential filter.

An experimental test was run to measure the zero-crossing interval probability density curve for the synchronous case, $f_o$ equal to $f_c$, and the results are shown in Fig. 5-2. The experimental apparatus consisted essentially of clipping the waveform, forming a monotonically increasing voltage whose height is proportional to the zero-crossing interval, and then counting the total number of intervals that exceed a given length. From these cumulative data, adjacent values were subtracted and divided by the abscissa interval to form the density curve of Fig. 5-2. Also shown, for comparison, is the measured density curve for Gaussian noise with the same filter. The abscissa is normalized and is plotted as:

$$\varphi = 2\pi f_o \tau \,, \tag{5-6}$$

where:

$\tau$ = zero-crossing interval.

The advantage of this is that the plot is normalized with respect to frequency so that the results are valid for a filter with the same characteristics

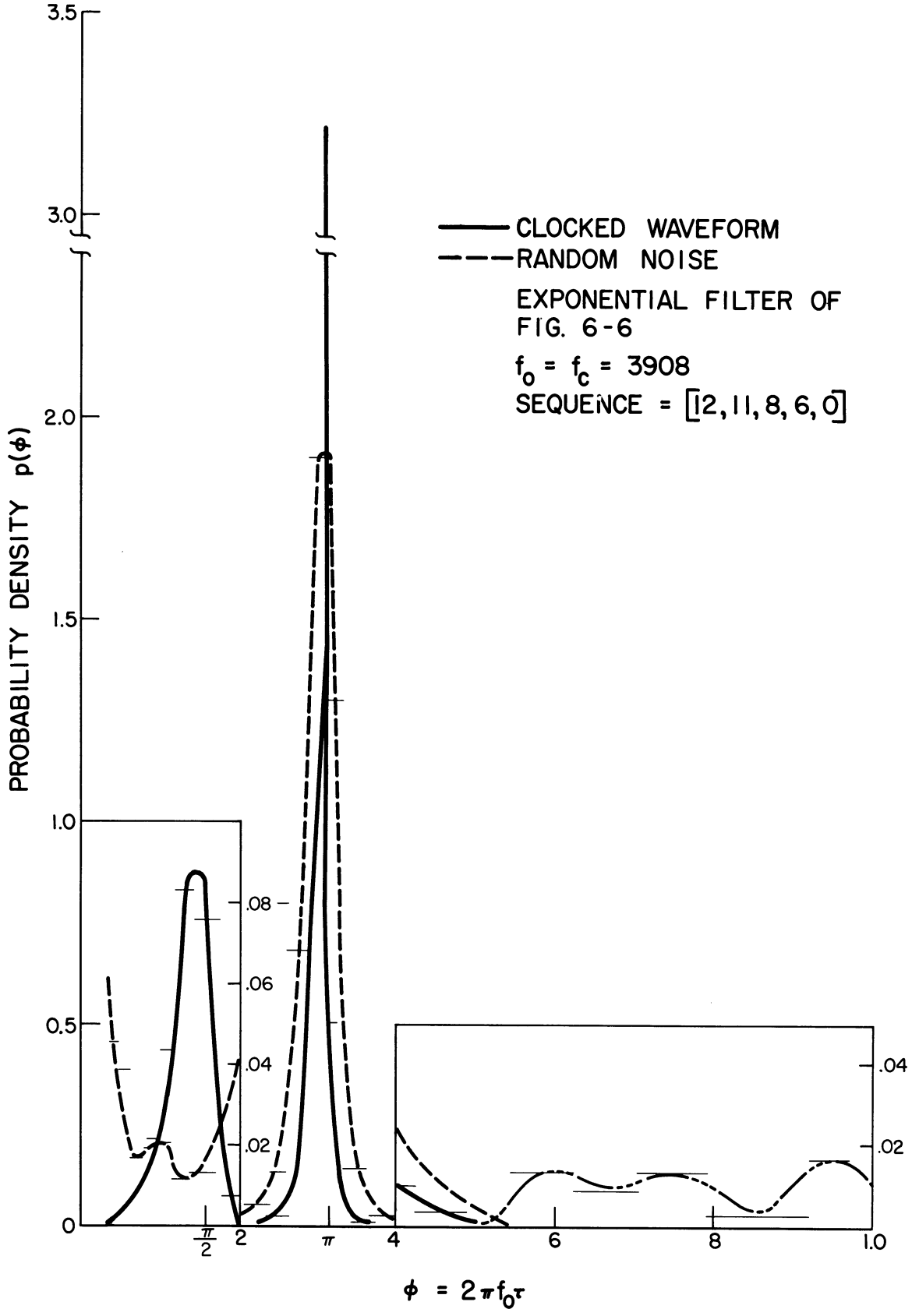


Fig. 5-2. Probability distribution of the intervals between successive zero-crossings for the synchronous, exponential filter.

at any center frequency. The ordinate values have been divided by the total count, so that they read the probability density---the total area under each curve is 1.0. To summarize the above, the treatment of the data can be itemized as follows: (1) the $\tau$ being measured by a given setting was determined by a calibration procedure (described in Section 6.5); (2) $\varphi = 2\pi f_o \tau$ was calculated for each setting; (3) $\Delta\varphi$, the difference in two adjacent settings, was then calculated; (4) the difference in "counts" for the two adjacent settings was determined; (5) this difference in "counts" was divided by $\Delta\varphi$; (6) this value, divided by the number of counts for the lowest setting (highest count), was plotted as $p(\varphi)$.

The first thing to note in Fig. 5-2 is the high "spike value" centered at $\pi$. Although ideally this should be a spike with no skirts, the inevitable error in zero-crossing measurement and slight drifts in frequency are responsible for the finite skirts. Also, the filter impulse response, for large t, departs somewhat from the ideal response of Eq. 5-2, and the result of this is to put slight perturbations on the zero-crossing intervals.

Another important action in Fig. 5-2 is the zero-crossings at $\pi/2$---shown in an expanded scale on the figure. The intervals here result from the envelope crossings of Eq. 5-5, in conjunction with the $\omega_o t$ crossings. These intervals result from successive crossings $1/4f_o$ apart, and Fig. 5-3 shows a typical interaction between envelope and carrier crossing. This action at $1/4f_o$ is peculiar to the clocked situation and, in conjunction with the high peak at $1/2f_o (2\pi f_o \tau = \pi)$, can be considered as characterizing a clocked waveform in which there is an integral relation between the filter frequency $\omega_o$ and a multiple of half-clock frequency.

Another phenomenon of Fig. 5-2 is the readings which appear above

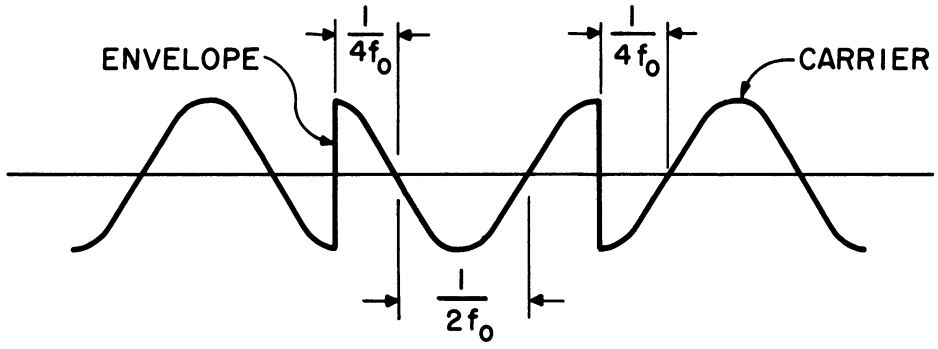


Fig. 5-3. Interaction between envelope and carrier crossing for clock frequency equal to filter frequency.

the spike at $\pi$ (also shown on an expanded scale). As can be seen from Eq. 5-5, theoretically there are no intervals greater than $1/2f_o$ since a zero always occurs for $\omega_o t + \theta = (2k + 1)\frac{\pi}{2}$. In the experiment, however, readings for intervals longer than this were obtained, shown by dashed lines in Fig. 5-2. The reason for these erroneous readings are that, when clocked at filter frequency, at some places the waveform hovers extremely close to zero and fails to operate the zero-crossing circuit. Hence, in actuality these values should be added to the values at $\pi$ and $\pi/2$. They are only of the order of five per cent, however, so the data are plotted as they were recorded. This problem is prevalent only for the case where $mf_c = f_o$; the reason for conducting this experiment was to note the spike at $\pi$ and the unique subsidiary one at $\pi/2$.

The same distribution measurements were made for true noise, using a General Radio random-noise generator. The results shown in Fig. 5-2 were compared with experimental results by Blötekjaer (Ref. 23). Although his results covered Q's only up to 3, and the Q here was 43, his results, when

extrapolated, agreed closely. In Section 5.3 measurements were taken for a filter having a Q of about 3; although the skirts are not as sharp as those in Ref. (23), the results are comparable and show good agreement.

The next experiment was run for the case in which $f_c$ is appreciably less than $f_o$. Figure 5-4 shows these results where $f_c$ = 460 cps and $f_o$ = 3908 cps. Because of this frequency ratio there are approximately nine crossing intervals of $\omega_o t$ between each possible envelope zero. The result is a nearly ideal spike at $\pi$, as shown in Fig. 5-4. Due to the incommensurability of $\omega_o$ and $\omega_c$, there is not the problem of erroneously reading long intervals as was the case in Fig. 5-2. Also, there is no especial action at $\pi/2$ as previously. This is because the envelope crossings are so infrequent relative to the carrier crossings.

A final experiment with the exponential filter was run with $\omega_o \cong \omega_c$, but not equal. Figure 5-5 shows the results for $f_c$ = 3668 cps with $f_o$ = 3908 cps. For this case it is seen that the probability density curve begins to approach the curve for Gaussian noise. The skirts are wider than before, and the spike at $\pi$ is reduced. Again no significant error at large intervals is encountered.

The above three experiments and basic theory exhibit the properties of zero-crossing intervals when a sequence of clocked pulses is passed through an exponential filter. If the filter frequency $f_o$ is a multiple of half-clock, zero-crossings will appear regularly at intervals of $1/2f_o$, with envelope zeros between. Considering the distribution, a spike appears at $\pi$ and a subsidiary spike at $\pi/2$. If $f_c << f_o$, the spike at $\pi$ increases and no action at $\pi/2$ is noted. As $f_c$ approaches and exceeds (but is not equal to) $f_o$ the distribution becomes more and more like that of Gaussian noise.

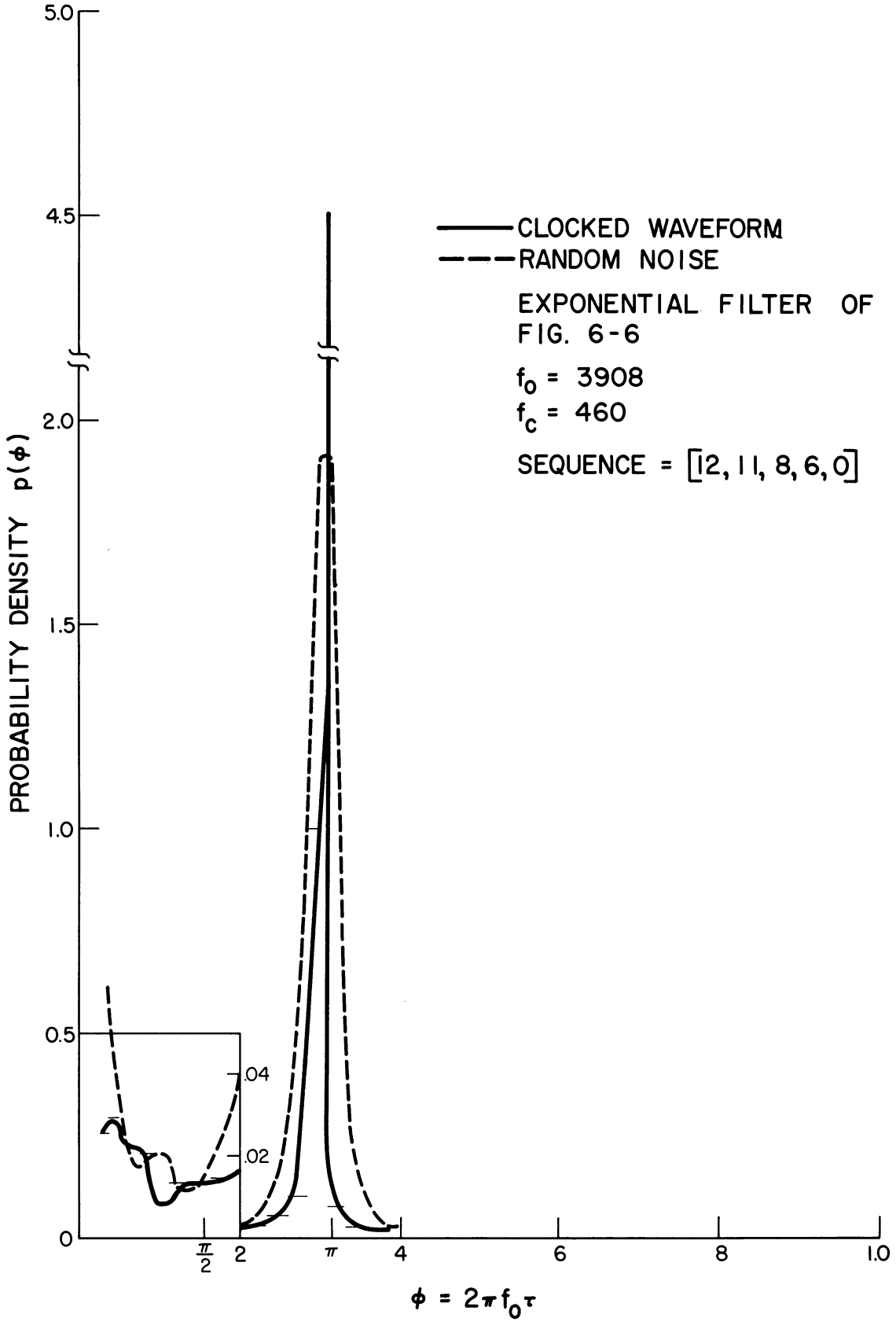


Fig. 5-4. Probability distribution of the intervals between successive zero-crossings for the exponential filter with $f_c < f_o$.

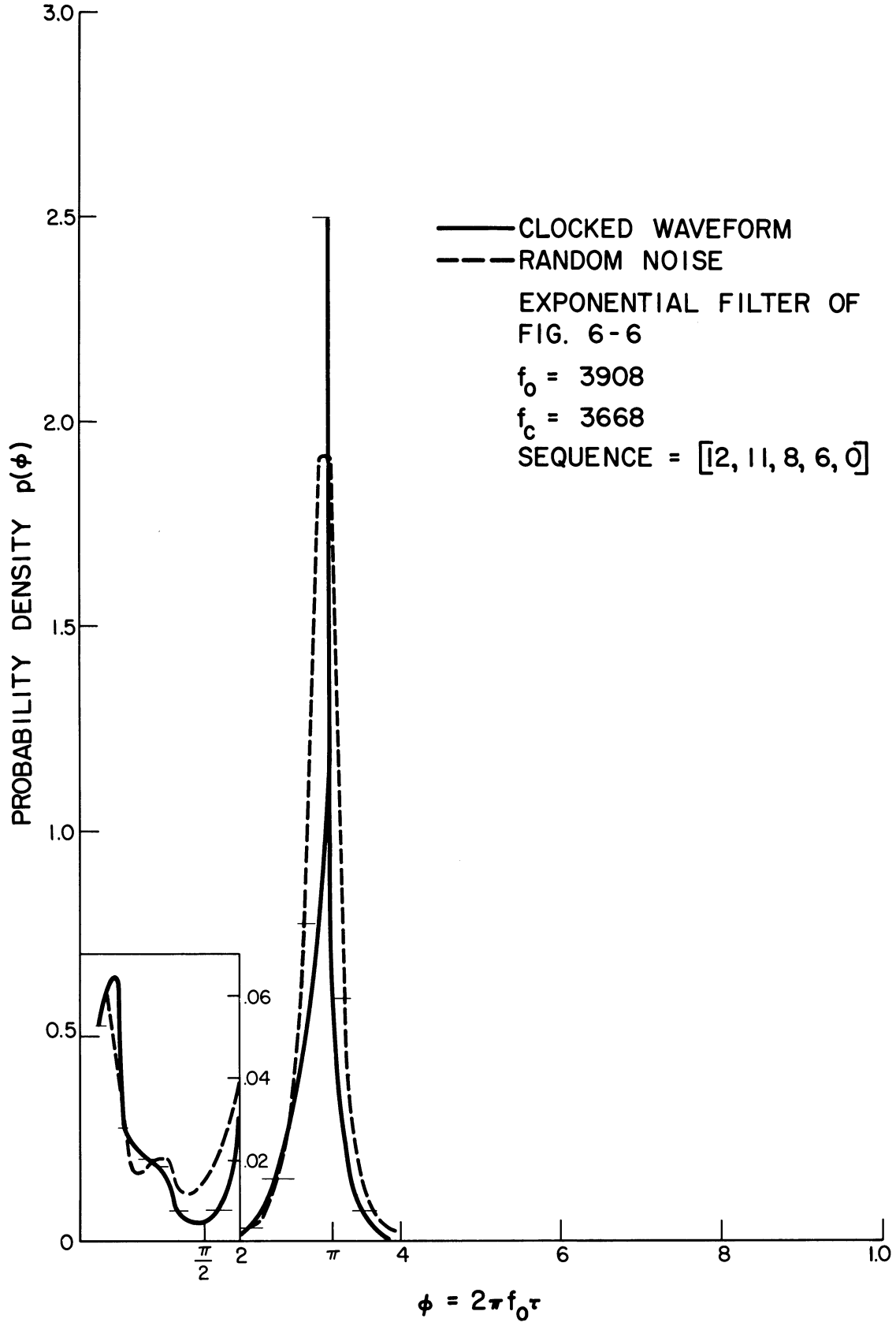


Fig. 5-5. Probability distribution of the intervals between successive zero-crossings for the exponential filter with $f_c \approx f_o$.

5.2.2 Regularity Between Pulses. From Eq. 5-5 above it was noted that, if an exponential filter has a ringing frequency at a multiple of half-clock, there will be regularly-spaced zero-crossings at intervals of $1/2f_o$. For other frequency positions this does not occur. However, a regularity of zero-crossings does occur between pulses (if $\omega_o > \omega_c$) for all filter positions. This can be seen as follows.

In general the N(t) in Eqs. 5-2, 5-3, and 5-4 increases with t. Let us consider N(t) as being fixed and thus note the action only within a given interval between pulses. Using Eq. 5-4 and denoting N' as a particular value of N(t), one writes:

$$e(t) = e^{-\alpha t} \sum_{n=0}^{N'} K_n \cos(\omega_o t + \theta - \varphi_n) = e^{-\alpha t} A_{N'} \cos(\omega_o t + \Phi_{N'}) \quad \text{for } t \ni N' < t < N' + 1, \tag{5-7}$$

where:

$$K_n = a_n e^{\alpha \frac{n}{f_c}},$$

$N'$ = particular value of N(t),

$$\varphi_n = \frac{n\omega_o}{f_c}, \text{ and}$$

$\Phi_{N'}$ = phase angle of a particular sum of sine terms.

Similarly, one can write the e(t) for the next pulse interval:

$$e(t) = e^{-\alpha t} \sum_{n=0}^{N'+1} K_n \cos(\omega_o t + \theta - \varphi_n) = e^{-\alpha t} A_{N'+1} \cos(\omega_o t + \Phi_{N'+1}) \quad \text{for } t \ni N'+1 < t < N' + 2 . \tag{5-8}$$

One can write the output of Eq. 5-8 as the sum of the previous output and the new contribution:

$$e(t) = e^{-\alpha t}\left[A_{N'}\cos(\omega_o t + \Phi_{N'}) + K_{N'+1}\cos\left(\omega_o t + \theta - \frac{(N'+1)\omega_o}{f_c}\right)\right] \quad \text{for } t \ni N'+1 < t < N'+2 \ . \tag{5-9}$$

From Eqs. 5-7, 5-8, and 5-9 it is seen that regular crossings occur between pulses (if $\omega_o > \omega_c$) and that "phase bumps" may occur only in conjunction with clock pulses. A neat way to demonstrate this phenomenon consists of triggering a scope trace at the zero-crossing immediately following a clock pulse. An experiment was set up to depict this property and the results are shown in the following figures.

Figures 5-6(a) and 5-6(b) are oscilloscope pictures taken when a sequence of pulses was driving an exponential filter at 1200 cps (a) and 1807 cps (b). The filter frequency was 3908. The trigger was arranged so that the trace began at the first negative-going zero-crossing after a clock pulse. As seen in part (a), all the zero-crossings "line-up" for two complete cycles. Then the extraneous crossings appear and, for the rest of the picture, are spread out. Considering the frequency ratio of $f_o$ (3908) to $f_c$ (1200) one would expect three complete cycles of superimposed crossings. The reason there are only two such cycles is because the trigger circuit is capable of triggering on only one slope; hence being limited to "negative-going zero-crossings after a clock pulse" means that in many cases the trace begins at the second zero-crossing after a clock pulse. For this reason, then, some extraneous crossings appear one cycle earlier.

The same conditions apply to part (b), where the clock frequency is 1807 cps. For comparison, Gaussian noise was passed through the same exponential filter and the triggering was established as above for 1200 cps. The result is shown in part (c). As expected, the zero-crossings are

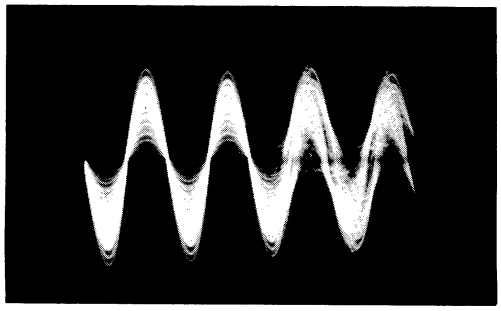

(a) Clocked;
$f_c$ = 1200 cycles.

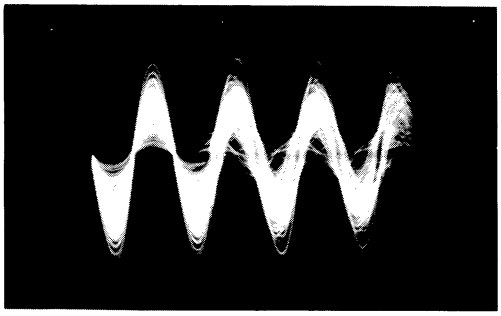

(b) Clocked;
$f_c$ = 1807 cycles.

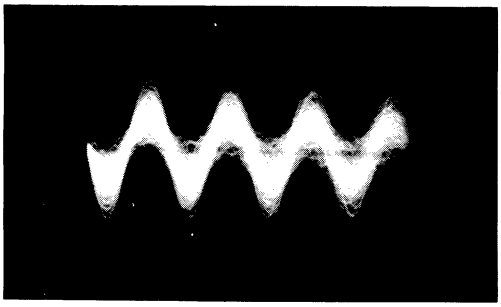

(c) Noise (scope triggered at 1200 cycles).

Fig. 5-6. Depiction of regularity of zero-crossings between clock pulses for exponential filters.

now dispersed.

It is interesting to note the behavior of the zero-crossings if the trace is always started with a clock pulse. One now expects a purely random zero-crossing situation, for the clocked case, and this is shown in Fig. 5-7(a) where the clock was 1200 cps ($f_o$ = 3908). This shows that, although there are regular spacings between clock pulses, these blocks of spacing occur randomly on the time scale. It was seen before that when $f_o$ is a multiple of half-clock these blocks of regular spacings themselves appear regularly so that there are coherent zero-crossings at intervals of $1/2f_o$ throughout time. In Fig. 5-7(a) note that the second clock pulse is faintly discernible at the right. For comparison, the result when Gaussian noise was inserted, and the trace still triggered with the 1200 cycle clock, is shown in 5-7(b). It is seen that the two pictures are much the same.

(a) Clocked waveform. (b) Gaussian noise.

Fig. 5-7. Depiction of the irregularity of zero-crossings when taken over many clock intervals.

## 5.3 General Filter

For the exponential filter above it was found that the zero-crossing interval distribution tends to have a spike at the interval $1/2f_o$, depending upon the $f_o/f_c$ ratio. If $f_o$ is any multiple of half-clock a definite spike appears; for other $f_o$'s this effect is diminished. Further, for this exponential filter, there are regularly-spaced zero-crossings between clock pulses if $f_o > f_c$; if $f_o$ is a multiple of half-clock, these spacings are coherent throughout time.

In general one can say that any narrow-band filter will tend to exhibit the behavior reviewed above for the exponential filter. In this section we will write the equations for the general filter and see how the various results depart from those of the exponential filter. Experimental results will also be given.

One begins by again writing the output as a sum of impulse responses:

$$e(t) = \sum_{n=0}^{N} a_n \, h(t - \frac{n}{f_c}) \qquad \text{for } t \ni N < t < N + 1 \, . \qquad (5\text{-}10)$$

Any general h(t) can be written in either of two forms:

$$h(t) = \sum_{m=1}^{r} e^{-\alpha_m t} \cos(\omega_m t + \theta_m) , \qquad (5\text{-}11)$$

where:

r = number of poles in upper, left-half plane,

or:

$$h(t) = F(t) \cos[\omega_o t + \theta(t)] . \qquad (5\text{-}12)$$

Equation 5-11 expresses the impulse responses in terms of the contribution from each pole-pair. Since, for any realizable filter, the poles will occur as complex conjugates, one need only look at the poles in the upper left-half complex frequency plane. Equation 5-12 uses the narrow-band representation which is valid for any narrow-band waveform. One can use either Eq. 5-11 or 5-12 to substitute in 5-10 in order to seek zero-crossing properties. Below we will use Eq. 5-12.

Substituting Eq. 5-12 into 5-10, one has:

$$e(t) = \sum_{n=0}^{N} a_n F(t - \frac{n}{f_c}) \cos\left[\omega_o t - \frac{n\omega_o}{f_c} + \theta(t - \frac{n}{f_c})\right] . \qquad (5\text{-}13)$$

Consider first the case where $f_o$ is a multiple of half-clock frequency; for an even multiple one has:

$$e(t) = \sum_{n=0}^{N} a_n F(t - \frac{n}{f_c}) \cos\left[\omega_o t + \theta(t - \frac{n}{f_c})\right] . \qquad (5\text{-}14)$$

It is obvious that one can take the cosine term outside the summation (as was done in Eq. 5-5) only if $\theta(t)$ of Eq. 5-12 is constant.

For frequencies $f_o$ other than a multiple of half-clock, only general comments can be made. Both the F(t) and the $\theta(t)$ will contribute to departures from the situation of "regularly-spaced crossings between clock pulses," as was true for the exponential filter. Considering the F(t), an

F(t) other than an exponential will cause the summation of Eq. 5-14 to consist of a sum of sine waves whose amplitudes are functions of time. Now a sum of sine waves of constant amplitude will result in another sine wave. A sum of sine waves of slowly varying amplitude will yield a perturbed sine wave; and this is the effect of F(t) in Eq. 5-14. The $\theta(t)$ will also, of course, influence or disturb the zero-crossings.

Based on the foregoing, one expects the same general phenomena for the general filter as for the exponential, but with each characteristic more like that of noise. Figure 5-8 shows the measured interval distribution for the case where the non-exponential filter of Figs. 6-8 and 6-9 is clocked at its ringing frequency. As seen, for this synchronous case there is a spike at $\pi$, but the skirts of the spike are wider than those of the corresponding exponential case (Fig. 5-2). Note that here also the action at $\pi/2$ is present; this action is peculiar to clocked, synchronous waveforms. The action above $\pi$, shown by the dashed line, is again due to the fact that the waveform, for this synchronous case, sometimes hovers very near the axis and fails to operate the zero-crossing circuit.

Figure 5-9 shows the distribution when the filter is clocked close to, but not integral with, the filter frequency. Here it can be seen that the distribution does not differ essentially from that of Gaussian noise. Although the Q of this filter is only 3, and differences could be expected to be greater for a higher Q, this does indicate that the zero-crossing distrubution does not serve as a reliable characterization for the clocked waveforms treated here. The case shown here is identical to the case treated in Fig. 4-7b of Section 4.4.3, where the difference was detectable.

Pictures to indicate the regularity of crossings between clock

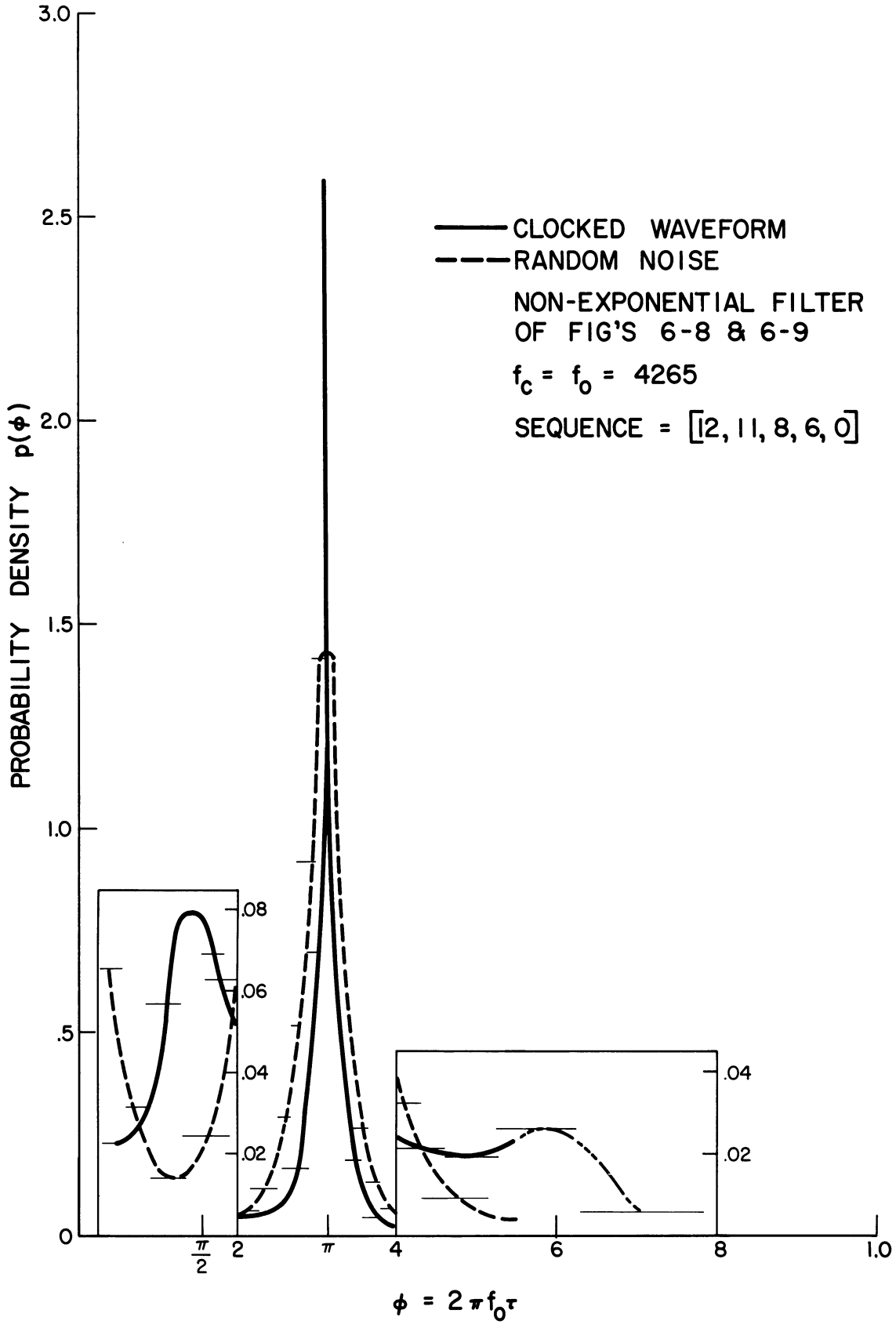


Fig. 5-8. Probability distribution of the intervals between successive zero-crossings for a non-exponential filter with $f_c = f_o$.

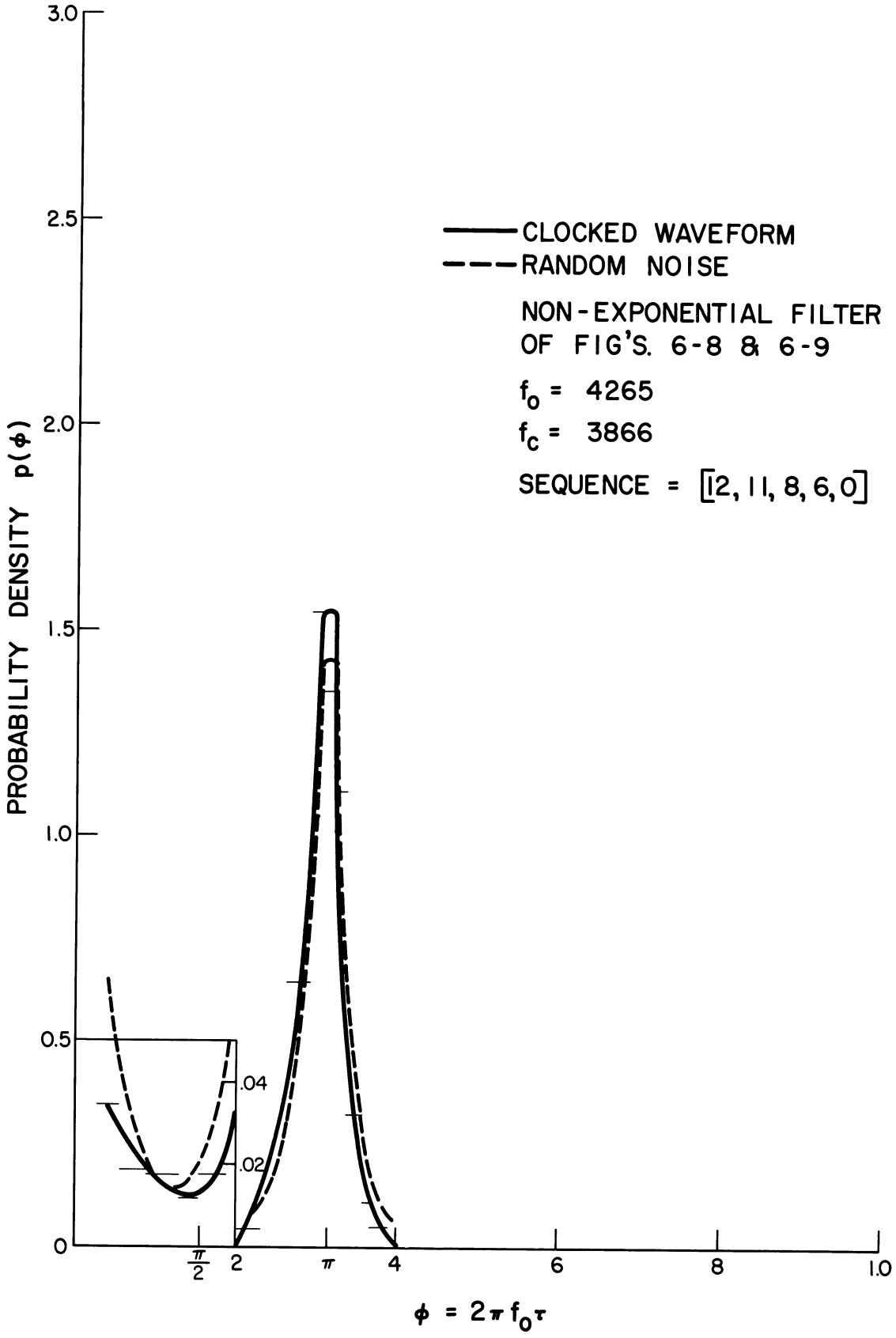


Fig. 5-9. Probability distribution of the intervals between successive zero-crossings for a non-exponential filter with $f_c \approx f_o$.

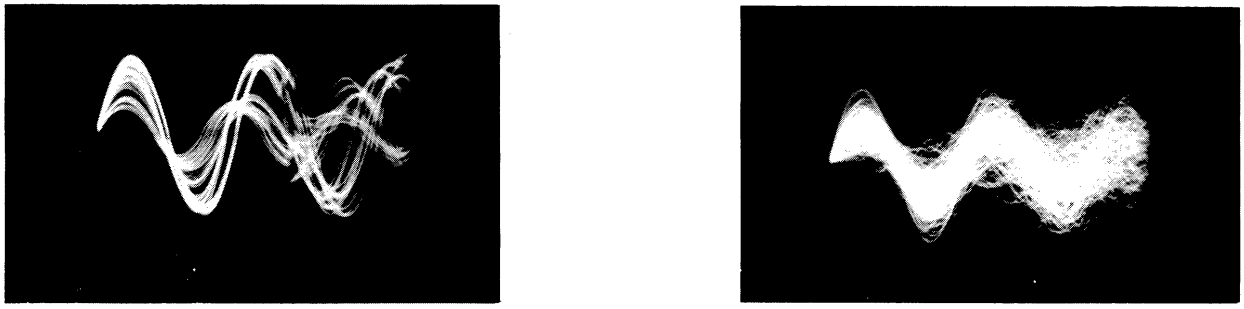

(a) Clocked (b) Noise

Fig. 5-10. Regularity of zero-crossings between clock pulses; $f_c \approx 1987$.

pulses (comparable to Fig. 5-6 above) are shown in Fig. 5-10. It is seen that, although the crossings are more coherent than for those of noise, the perturbations make the characterization difficult.

# CHAPTER VI

# DESCRIPTION OF EXPERIMENTS

It will be the objective of this chapter to describe the experiments, the results of which were reported throughout the previous material. Since the data were presented previously, this chapter will not repeat these data but will present the necessary descriptions, circuit diagrams, and procedures used for the experiments. In each case reference will be made to the proper section of the preceding material.

## 6.1 Method of Obtaining Clocked Waveforms

As indicated in Section 1.2 the clocked waveforms used throughout this study were generated by passing the pulses from a maximal shift-register generator through a narrow-band, high Q filter. As is shown in Fig. 6-1 the shift-register generator itself is driven by the clock. The output

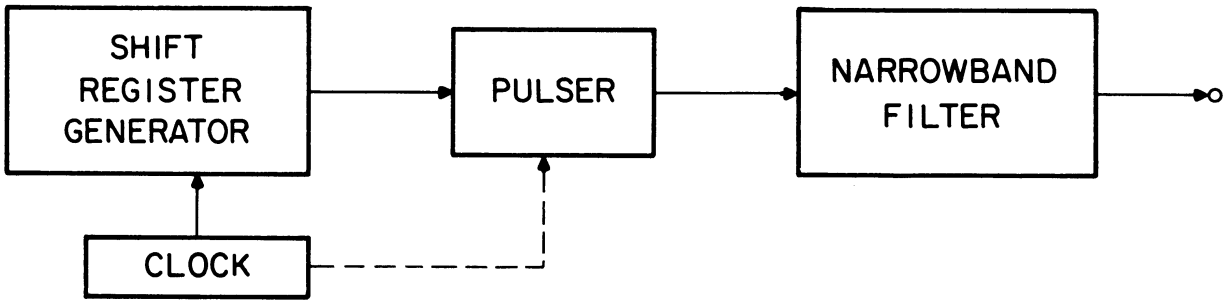


Fig. 6-1. Generation of clocked waveforms.

of the generator is a "square wave" waveform, and this waveform is converted into a pulse waveform in synchronism with the clock. The result, then, is a sequence of pulses whose sign at any clock interval is determined by the generator state in that interval. This sequence of pulses is then passed through the narrow-band filter.

6.1.1 Obtaining Clocked Pulses. For the data reported in the previous material, the combination of the clock, the shift-register generator, and the pulser of Fig. 6-1 were all obtained with the use of "Harvey-Wells Digital Data Blocs." This equipment consists of flexible, transistorized, basic digital items, the major items being flip-flops, "and/or" gates, and a clock.

As mentioned in Section 1.2, a shift-register generator is composed of a basic shift-register to which modulo-two feedback is attached. Figure 6-2 shows the function diagrams for all of the components used to form a shift-register generator with Harvey-Wells equipment (Ref. 24). The gates associated with the flip-flop units are for the purpose of allowing flexible logical decisions. The Logic A configuration can be used to form either an "and" gate or an "or" gate. The Logic B unit is used primarily as an "or" gate but may also form an "and" gate.

The basic shift-register is formed by a cascading of flip-flops. The panel connections to form a shift-register with the flip-flops shown in Fig. 6-2 are shown in Fig. 6-3. Also shown in this figure is the panel connection for the modulo-two adder and the method in which it is combined with the basic shift-register. In addition, the connections which provide a sync signal are also shown in Fig. 6-3.

The essential idea in forming the basic shift-register is to connect the output of a flip-flop to the input gates of the next flip-flop. The input gates are also connected to the clock. Thus the input gates act as a coincidence device between the clock pulses and the previous flip-flop level. In this way the content of any given stage is made to travel to the succeeding stages in the manner of a shift-register.

Because of loading considerations, the clock is connected in a

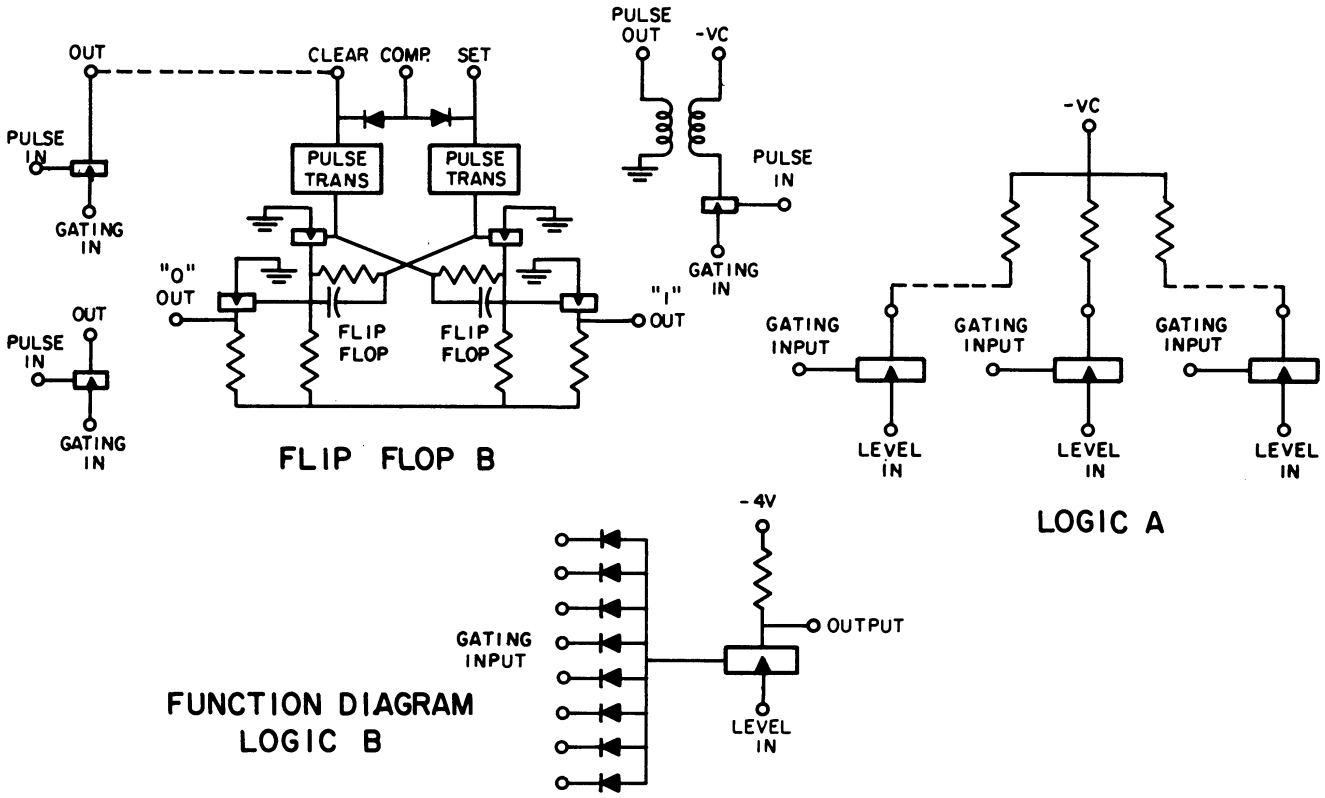


Fig. 6-2. Functional diagram of generator components.

pyramid arrangement (not shown in Fig. 6-3) through the "output gates" of the flip-flop units. A sync signal was obtained by noting when the register contained all "ones!" This was implemented, as shown in the figure, by connecting all "one" outputs of the flip-flops to a Logic B circuit acting as an "and" gate. This sync signal allowed any experiment to be synchronized with the period of the maximal sequence of the shift-register generator.

A modulo-two adder is formed by interconnecting two gates, such as in the Logic A unit (Fig. 6-2). The emitters are connected to the opposite "inputs" and the collectors are connected together with a common load resistor. The functional diagram is shown in Fig. 6-4. With this arrangement, both transistors will be "off" if the inputs are the same,

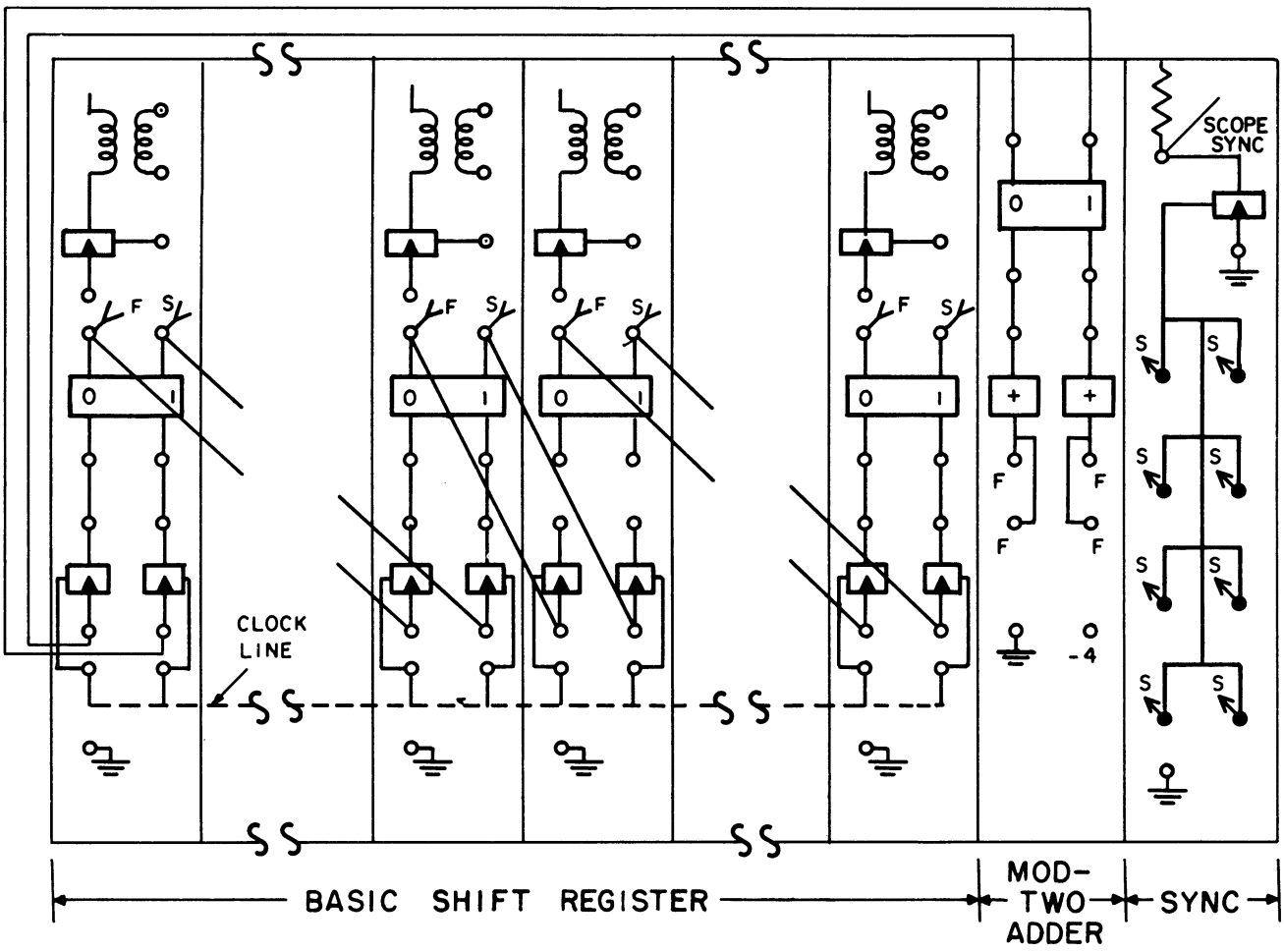


Fig. 6-3. Panel connections for shift-register generator.

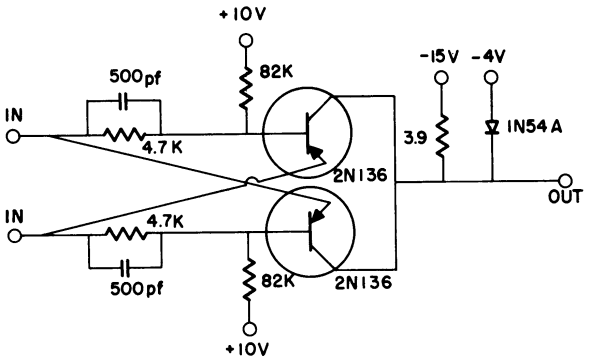


Fig. 6-4. Functional diagram of modulo-two adder.

and one of the transistors will be "on" if the inputs differ. In this way the modulo-two function is implemented. To handle more than two feedback taps, such modulo-two units can be pyramided. Some units allowing four feedback taps were built, and the panel is shown in Fig. 6-3. The manner in which the modulo-two unit is connected to the basic register is shown; the mod-two inputs are connected

to the desired flip-flop outputs. Since the mod-two output is levels (rather than pulses) this mod-two output feeds the first flip-flop in the same manner as the other flip-flops are fed.

This, then, is the way in which the basic shift-register of Fig. 6-1 is realized.

For the pulser of Fig. 6-1, the objective is to obtain a positive pulse if the output flip-flop is in state "one," and a negative pulse for state "zero." A pulse will occur at each clock pulse interval. A circuit to realize this with the digital components of Fig. 6-2 was evolved by forming a monostable multivibrator which is used in a coincidence arrangement with two other gates. The functional diagram is shown in Fig. 6-5. The clock drives the monostable circuit and the width of the output pulse is determined by the external capacitor C. This pulse then forms coincidence

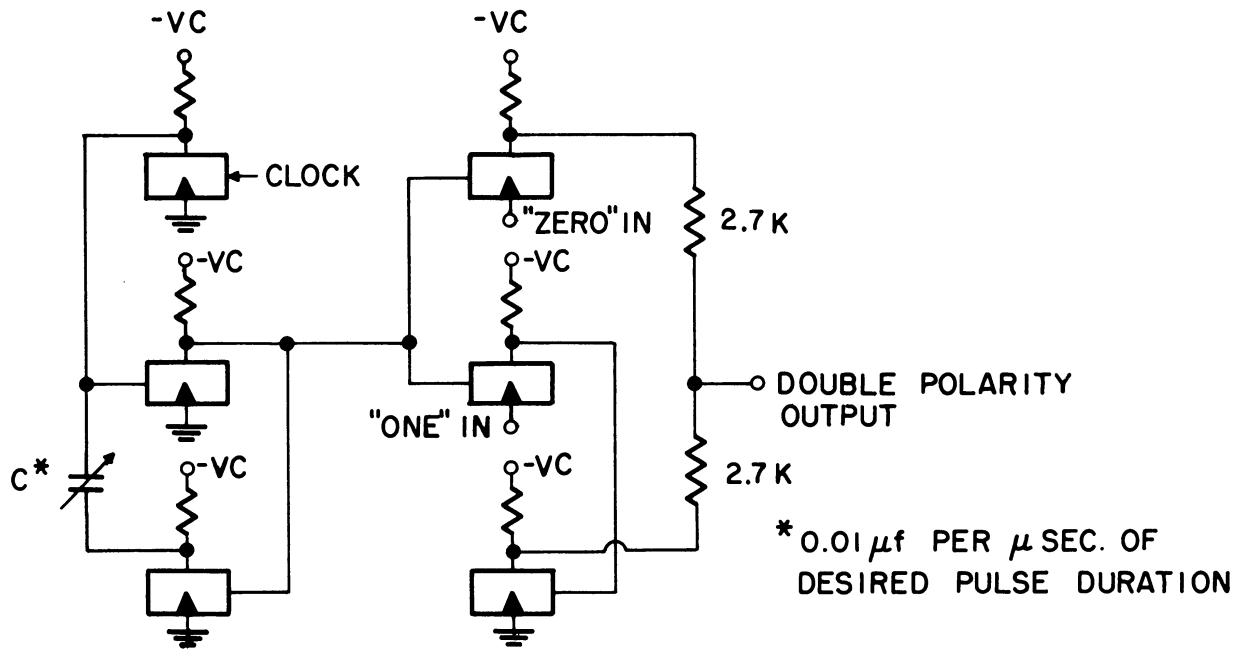


Fig. 6-5. Functional diagram of double polarity pulser.

with two gates; one gate is driven by the "one" level of the output flip-flop and the other by the "zero" level. An inverter stage is required on one gate. The collectors of the two gates are connected by an external resistance circuit so that the double polarity pulse can be achieved. As mentioned, the output of this pulser is a sequence of pulses in which the sign of each pulse is determined by the state of the shift-register output stage in that clock interval. The combination of the basic shift-register and this pulser, then, provided the desired sequence of pulses for performing all the experiments of this report.

Although all the experimental data of this report were obtained using the above equipment it may be noted that the earlier experiments were done with a vacuum tube shift-register generator which was adapted from a digital computer. Sync circuits, modulo-two circuits, and special purpose circuitry were adapted to this basic shift-register to perform various experiments. However, the equipment mentioned above superseded this equipment since it is much more flexible and has a much higher frequency range.

6.1.2 Narrow-band Filters. The various narrow-band filters used in this study will now be described. For the exponential filter described throughout this report the filter was constructed as shown in Fig. 6-6. Essentially this is a pentode with a parallel resonant circuit as the load. The pentode is biased in the active region so that both positive and negative pulses will be treated with approximately equal gains by the ringing stage. Because of low signal level at the plate this section is followed immediately by an extremely linear amplifier, and then a cathode follower provides the necessary reduction in impedance to drive other experimental apparatus. This filter has a center frequency of 3908 and a Q of about 43. When this filter was used in an experiment it was followed

by a Krohn-Hite Hi-pass filter whose lower cutoff was set at 200 cycles to reduce the inevitable ripple which occurred in the output. The impulse response and the bandpass characteristic of this filter, with the Krohn-Hite filter included, is shown in Fig. 6-7.

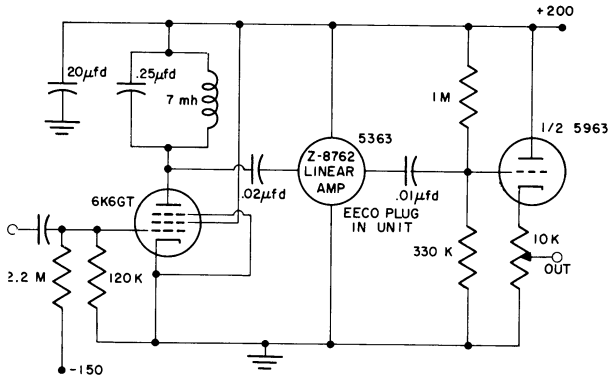


Fig. 6-6. Circuit diagram of exponential filter.

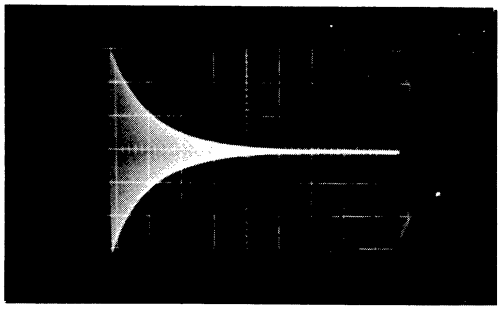

(a) Total impulse response.

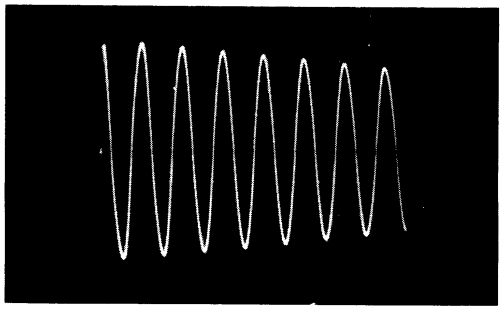

(b) Expansion of impulse response.

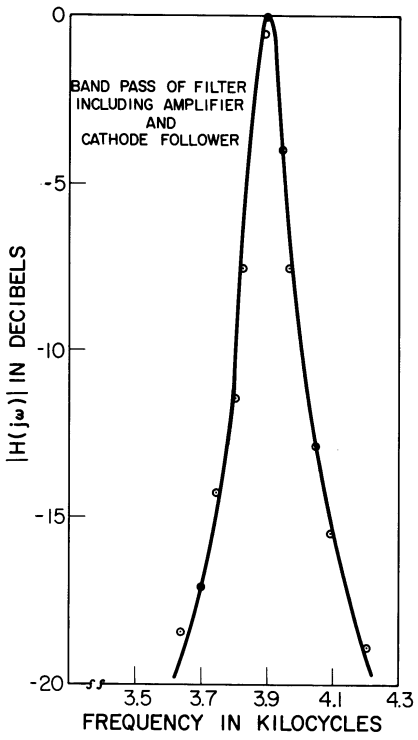


(c)

Fig. 6-7. Impulse response and bandpass of exponential filter.

For the nonexponential filter a 4-pole, Tschebyscheff-designed, maximally flat filter was used. The prototype bandpass network is given

in Fig. 6-8. Filters based on this design were available from the range

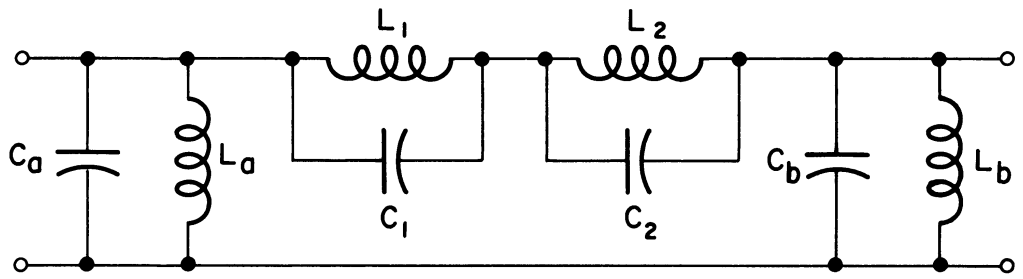


Fig. 6-8. Prototype bandpass network.

of 200 cycles to 7 k with 10 filters covering this range. The bandwidths of the filters themselves were actually designed to optimize the frequency breakdown for the Vocoder audio system. Throughout this work various of the filters were used depending upon the particular experiment. However, all of these had the same prototype network as shown in Fig. 6-8. The actual bandpass characteristic of the filter used most often is shown in Fig. 6-9.

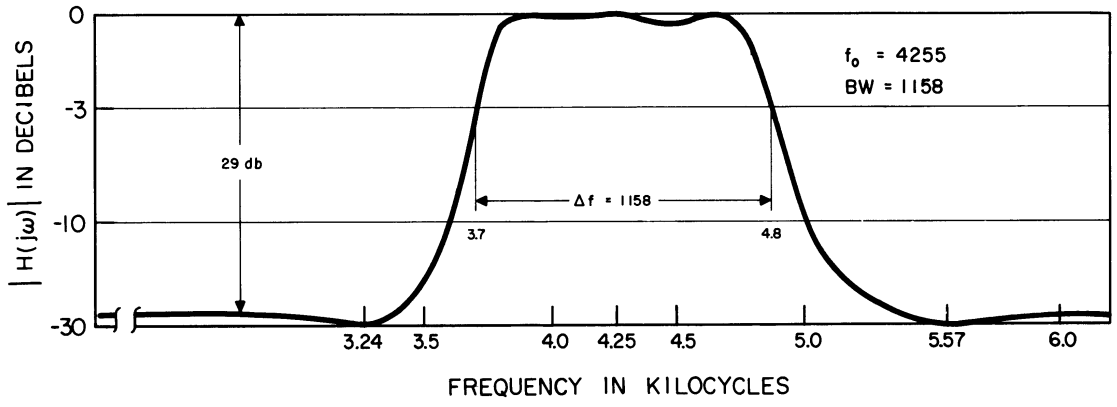


Fig. 6-9. Bandpass of 4-pole Tschebyscheff filter.

The impulse response which corresponds to this is shown in Fig. 6-10.

Although these Tschebyscheff filters do not actually qualify as high-Q filters, this fact and their distinctly nonexponential impulse response provided a stringent test of the results derived in this report--which were directed primarily toward high-Q filters.

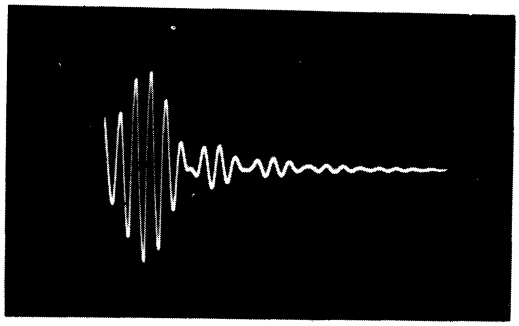

Fig. 6-10. Impulse response of 4-pole Tschebyscheff filter; $f_o$ = 4255, BW = 1200.

With the circuits described in this section, then, the narrow-band clocked waveforms were generated for the various experiments.

## 6.2 Sound Spectrograph Experiments

The use of the sound spectrograph in this work consisted of portraying the "half-clock spectral symmetry" treated in Section 3.1. The sound spectrogram is an instrument which portrays, as a function of time, the short time spectral density of the audio input waveform. Thus it analyzes, on a short time basis, the frequency composition of the input waveform. The output is an intensity-modulated "frequency vs. time" graph marked on electrically sensitive Teledeltos paper as depicted in Figs. 3-3 and 3-5.

The particular sound spectrograph used here was of the heterodyne type. It employs a fixed-band filter, with a variable oscillator and modulator system by which any portion of the sound spectrograph can be brought within the frequency range of the filter. The spectrograph can be grossly depicted as shown in Fig. 6-11.

In operating the sound spectrograph, the signal to be analyzed

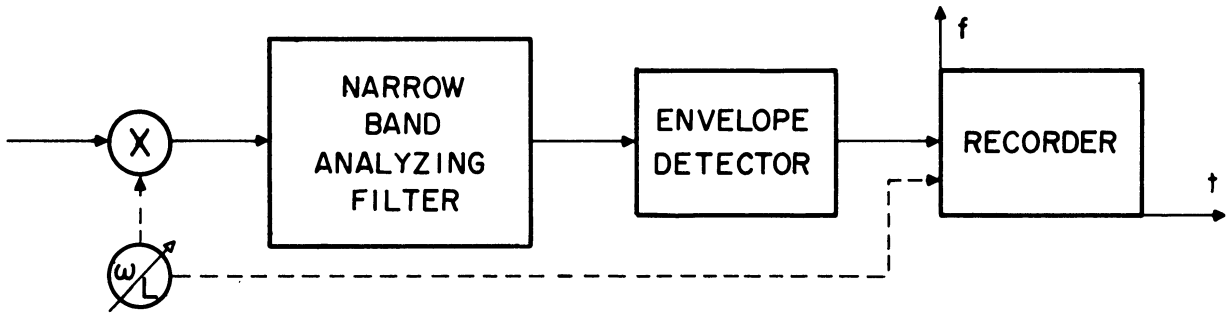


Fig. 6-11. Block diagram of basic operation of sound spectrograph.

is recorded on a continuous-loop magnetic tape. This loop is then driven by a synchronous motor, which also drives the "spectrogram pattern recorder." This recorder consists of Teledeltos paper mounted on a 4" diameter drum, and the associated pen for recording.

In essence, the operation is as follows: the magnetic tape loop is turned one revolution for a given setting of local oscillator, a given position of the recording pen, and one revolution of the recording drum. Within this revolution, the output of the analyzing filter (see Fig. 6-11) appears on the recording pen and forms a single-line imprint on the paper. Then the local oscillator is changed incrementally, the recording pen is shifted vertically, and another revolution of both tape loop and recording drum is undergone. This stepped procedure is continued for the frequency range of the instrument. In this way a "frequency vs. time" graph is obtained as shown in Figs. 3-3 and 3-5.

The basic parameters of the instrument are as follows (Ref. 25): the frequency range is 100-3500 cps; there are two analyzing filter bandwidths with an effective 45-cycle width on "narrow" position and 300-cycle width on "wideband" position. Further, the intensity of blackness on the graph itself is grossly proportional to the magnitude-squared or the power of the analyzing filter output. The marking range of the paper is about 12 db.

For each of the two filter settings there is an AGC-type control available. The narrow-band control circuit is a series arrangement which may be switched in ahead of the analyzing filter. It has the effect of amplifying low level detail in the output signal and then compressing it to the dynamic range of the paper. With the wideband setting a full band control is available and it is a shunt arrangement. This also has the general effect of providing an AGC action. A block diagram of the entire analyzing operation is shown in Fig. 6-12.

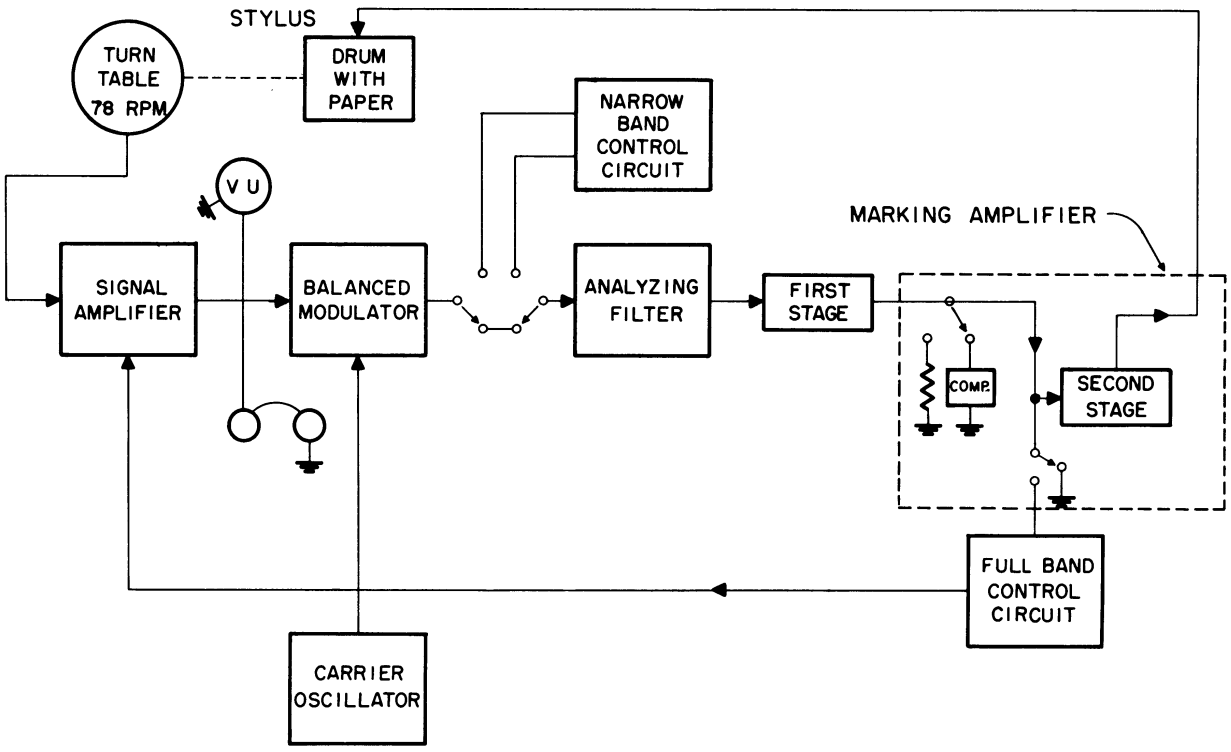


Fig. 6-12. Spectrograph components arranged for reproducing and analyzing.

Although the range of frequencies mentioned above is the basic range, other frequencies can be analyzed by using different speeds in the recording of the tape-loop and reproducing of that loop. For example, to get a range of 200-7000 instead of the 100-3500 range one can originally

record the desired signal at x inches per second and then play this signal onto the spectrograph tape-loop at x/2" per second. The tape loop would then be reproduced at the same speed as it was recorded. To get a ratio of 3 to 1 resulting in a frequency range of 300 to 10,500, one can record the tape-loop at the same speed as the originally recorded signal but then speed the reproduction of this tape-loop by a factor of 3. With these various features the sound spectrograph represents a very flexible piece of equipment.

The experimental procedure consisted of first recording the desired signal on a commercial tape-recorder. This recording was then played back onto the magnetic tape drum of the sound spectrograph. The machine was switched to the reproduce position and the spectrogram made. The VU meter provided with the spectrograph was monitored for the correct levels of recording and reproducing to insure a minimum of distortion. All the spectrographs were made using the NB analyzing filter and the narrow-band control circuit.

## 6.3 Experiments to Measure Envelopes

The envelope experiments were used to portray the half-clock, quarter-clock, and one-eighth clock symmetries in Sections 3.1, 3.2, and 3.3. The essence of these experiments is that each envelope depicts the time behavior of the short time spectrum at a single frequency of the sound spectrograph. Whereas the sound spectrograph records the time behavior of the waveform at all frequencies within a certain range, the envelope experiments consisted of looking only at two predetermined symmetrical frequencies and recording the envelopes detected at these specific frequencies.

The block diagram for these experiments is shown in Fig. 6-13.

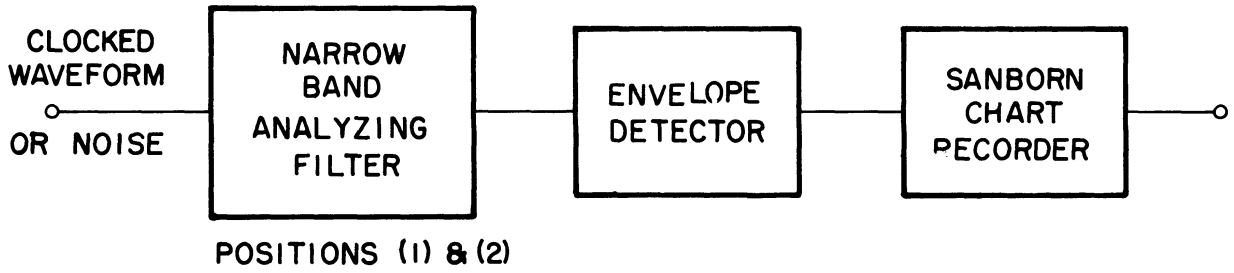


Fig. 6-13. Block diagram of envelope experiments.

In our particular experiment the analyzing filter was the filter of a commercial harmonic analyzer. The envelope was recorded on a Sanborn Recorder.

The filter used in these experiments was obtained by using a portion of the Hewlett-Packard Harmonic Wave Analyzer, Model 300 A. The signal was taken out after the filter and before entering the averaging circuit of the commercial analyzer. This harmonic analyzer is of the heterodyne type and hence the various filter positions were obtained by using different values of the local oscillator; the heterodyned signal then passed through the fixed bandpass filter. This particular filter has a minimum bandpass of 3.5 cycles at the 3 db points and in this position is only 30 cycles wide at the 40 db points.

The detector was of the simple passive RC peak-reading type. The circuit diagram of this detector is shown in Fig. 6-14.

In running the experiments the first item was to calibrate the "filter" to the desired frequency. This was accomplished by inserting a sine wave of the desired frequency as an input to the harmonic analyzer.

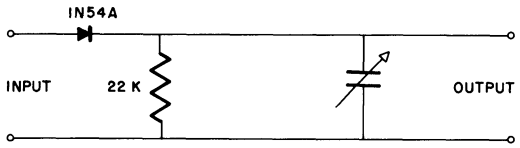


Fig. 6-14. Detector circuit for envelope experiments.

An electronic counter was placed on the output of the local oscillator of

this harmonic analyzer, which was then tuned to show a maximum output meter reading. Having determined the nominal frequency of the sine wave input by the counter, the counter was then used to accurately set up the desired symmetrical frequency. By thus attaching the counter to the local oscillator instead of measuring the input directly, more accuracy was obtained. Also it provided a direct measure of the drift in the harmonic analyzer as the experiment was run. It was found that the drift was unappreciable.

In this experiment it was necessary to align the envelopes so that the envelopes at the two symmetrical frequency positions would be coming from the same signal interval. For the clocked waveforms this was directly possible by using a sync signal which appeared at the end of each period of the maximal sequence. This sync signal was then used to insert a sync marker on the Sanborn chart. For the case of true noise, a magnetic-tape loop was made and a special saturating signal was put on at one point in this loop in order to provide the same marking action. Thus the envelopes of the two symmetrical frequencies could be aligned when presenting the data.

Using these techniques, then, the envelopes of Figs. 3-6, 3-8, and 3-10 were obtained.

## 6.4 Variance Experiments Using Coherent Multiplication

The purpose of this experimentation was to depict experimentally a method of characterizing a clocked waveform. On the basis of the analysis in Section 4.4, this method is called "the sum of weighted variances."

The essential idea, shown in Fig. 6-15, is to multiply the square of the waveform by a coherent wave which is given in each clock interval approximately by:

$$K(\beta) \cong \sum_{n=0}^{\infty} h^2(nT + \beta T) \ . \qquad (6\text{-}1)$$

The time waveform K(t) is a periodic wave with a period the same as that of the clock. This product waveform is then integrated for some period of time T'. Since the output of this integrator is itself a random process, the sensible method of analyzing the output is to measure the distribution. With a clocked waveform input this distribution will have a nonzero mean, while the mean will be zero for true Gaussian noise. For the experiment

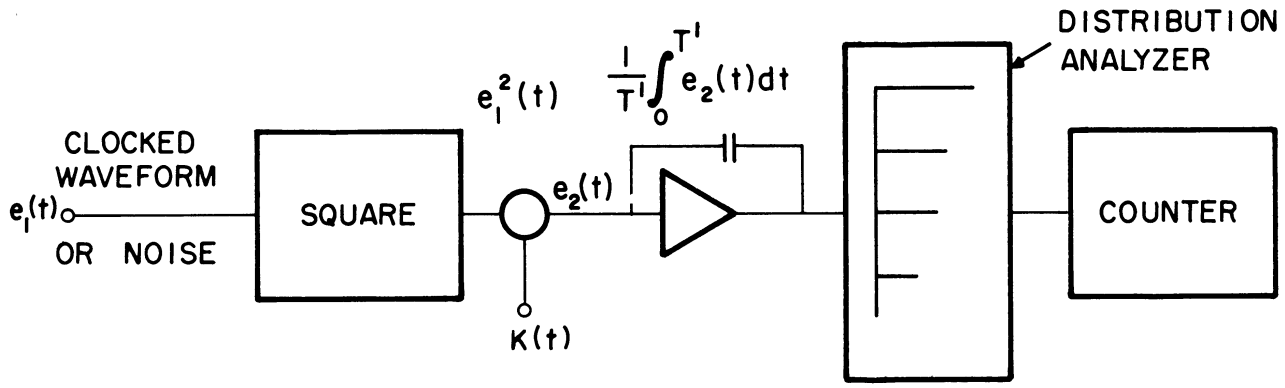


Fig. 6-15. Condensed block diagram of method to characterize clocked waveforms.

here, the distribution was obtained by using a special purpose simulator. The direct output of this simulator is the data used for drawing the histograms to approximate the distribution.

A more complete block diagram of the experiment is shown in Fig. 6-16. Referring to this figure, the first part shows the equipment used to generate the clocked waveforms, as described earlier. The Kron-Hite is used to remove the inevitable ripple. The synchronization between the clocked and the coherent multiplying waveform K(t) was obtained by having the basic clock oscillator drive a pulser which in turn drove a "photoformer."

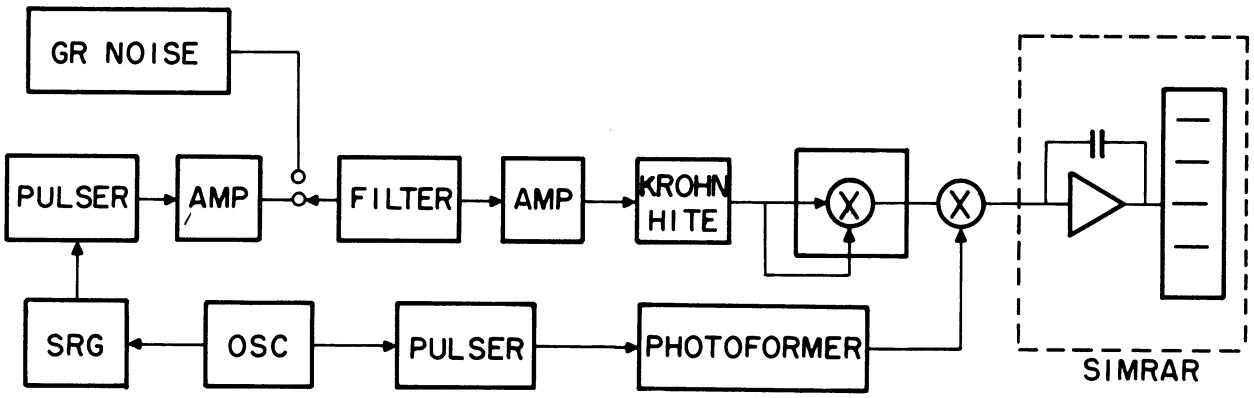


Fig. 6-16. Block diagram of variance experiments.

This photoformer is a general function generator which will reasonably reproduce the waveform specified by a mask on the face of an oscilloscope. The desired waveform was produced by cutting a suitable mask, and this waveform was synchronized with the clock by simply triggering the horizontal oscillator of the oscilloscope with the clock pulses. The analyzing equipment, denoted as "SIMRAR," essentially integrates the waveform for a given interval and then assigns the resulting value to one of ten slot intervals. The cumulative data consisting of the number of times the output waveform of the integrator falls within a given slot are then recorded on relays. At the end of an experiment, then, the cumulative curve for the distribution of the output can be read directly from the totals on the ten counters.

All the equipments shown on Fig. 6-16 have been discussed before, except the photoformer, the multipliers, and the SIMRAR equipment. We will now briefly describe these items.

The photoformer consists essentially of a feedback loop attached

to an oscilloscope which has the objective of causing the electron beam to ride along the edge of a mask. A mask cut to the desired waveshape and a photocell are attached to the scope face. The signal from the photocell passes through a feedback network to the vertical deflection plates. With a suitable feedback network and proper bias voltages, the beam can be made to follow the edge of the mask---within the frequency restrictions of the loop---and a voltage having the same form as the mask is available at the photocell output. Using the horizontal drive of the oscilloscope, a repetitive waveform of the desired type is then available. It was by this means, then, that the K(t) voltage described in Sections 4.4.1 and 4.4.3 was obtained.

Since all the K(t)'s were either sine waves or phase-bumped sine waves the mask was cut in the form of a sine wave. The desired number of cycles (within a clock interval) was achieved by adjusting the oscilloscope horizontal amplifier and position. By triggering the sweep with the clock pulses, any sine wave or phase-bumped wave was obtainable. A pulser with a variable delay was used to change the phase position of K(t) with respect to the clock.

Concerning the multipliers, both of the multipliers were constructed earlier by CEL for use in a special purpose analog computer. They are based on a design developed at the instrumentation laboratory of MIT (Ref. 26). The multipliers are designed to produce a continuous approximation to the product of two independent variables by instrumenting the identity:

$$(x^2 + 2xy + y^2) - (x^2 - 2xy + y^2) = 4xy \,, \qquad (6\text{-}2)$$

where:

x,y = two independent variables.

If this is simplified and solved for the product of xy one obtains

$$xy = \frac{(x + y)^2}{4} - \frac{(x - y)^2}{4} \quad . \tag{6-3}$$

In instrumentation the sum (x + y) and the difference (x - y) of the two inputs are obtained from two independent summing amplifiers. The squaring of the sum and difference is then accomplished by four square-law shapers with two more summing amplifiers being used to combine and correct the polarity of the output of the shapers. In addition, they provide a low impedance output for the multiplier. A block diagram of these multipliers is shown in Fig. 6-17.

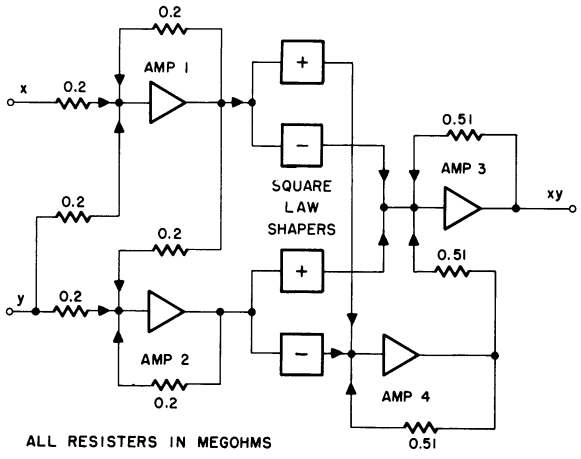


Fig. 6-17. Block diagram of multiplier and squarer.

In using SIMRAR, which stands for "SIMulated Receiver And Recorder," the essential idea is to measure automatically the histogram which approximates the cumulative distribution curve of the output random process. For our experiments an integrator in SIMRAR was also used. Considering the output of this integrator in Fig. 6-15, this voltage trips a counter when the voltage exceeds a preset threshold level which is variable from 0 to 60 volts. Since the counters are sensitive to only positive voltages, a bias is necessary if any negative voltages may be encountered. Figure 6-18 below shows a block diagram of SIMRAR as it was used in these experiments.

Referring to the block diagram Fig. 6-18, the sections of SIMRAR which were used are: an integrator, 10 amplitude discriminators with two

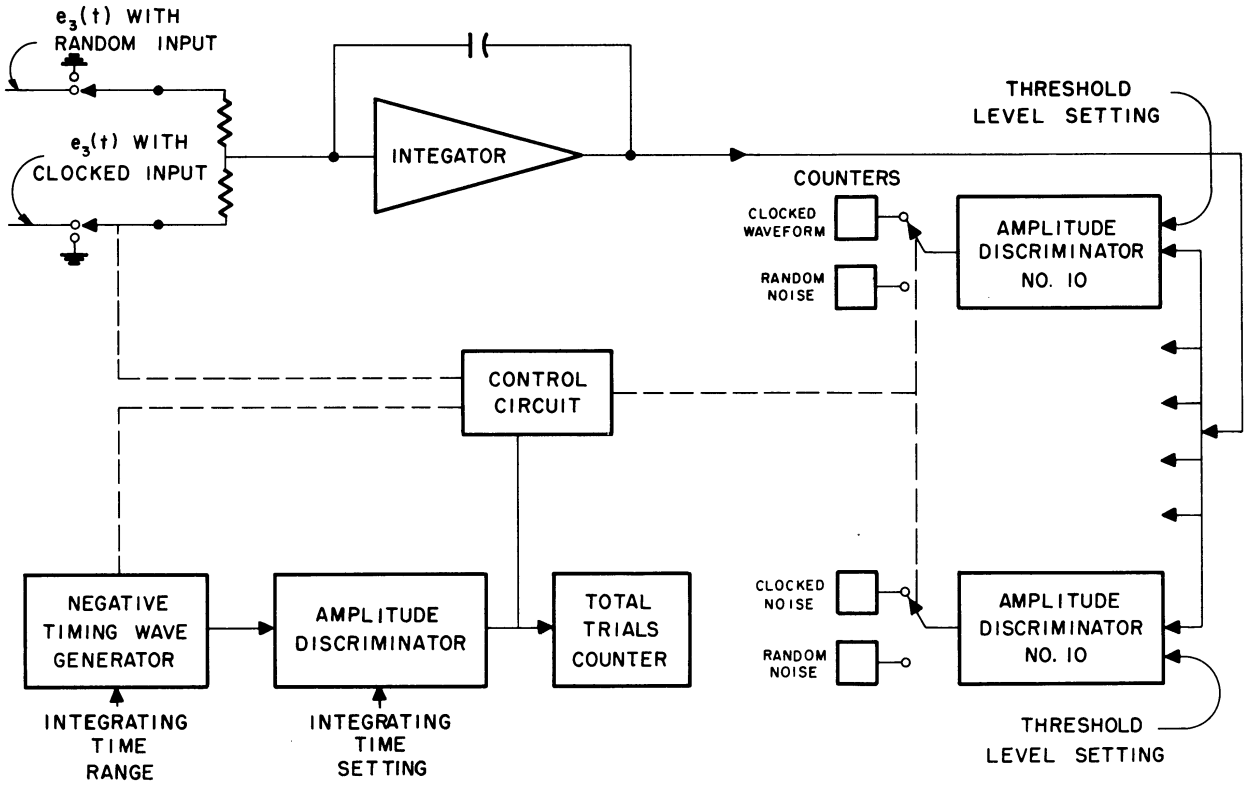


Fig. 6-18. Block diagram of SIMRAR.

counters associated with each discriminator (one counter for each of two possible inputs), a counter to record total samples, a circuit to preset the desired integrating time, a cycling control to select one of two available signals, and a central control circuit to perform all necessary switching operations.

The integrator output is connected to all 10 amplitude discriminators. As mentioned, the voltage output trips a counter when the voltage exceeds a certain preset threshold level which is variable from 0 to 60 volts. Since the counters are sensitive to only positive voltages a bias voltage connected in parallel with the signal (at the input to the integrator) is necessary if any negative integrator outputs may be encountered.

The cycling control is available for alternating between two inputs. The idea here is that one is often testing a given waveform against

another, and by automatically alternating inputs between these two waveforms the output readings are essentially independent of any drift which may occur in the operational amplifier and discriminators. In our case we were interested in comparing a clocked waveform to a true Gaussian noise waveform, and this feature was immediately applicable.

The procedure for running this experiment can now be described by referring back to Fig. 6-15. First of all, the two compared waveforms were made to be as nearly equal as possible by using a Ballantine true rms voltmeter. Next, the K(t) multiplying waveform was adjusted; this operation will now be described.

First the photoformer output was adjusted for the proper number of cycles, using the relation:

$$\text{Number of cycles} = 2\frac{f_c}{f_o} \quad . \tag{6-4}$$

With a repetitive waveform of this number of cycles, obtained by triggering the horizontal drive in sync with the clock, the phase position of K(t) was varied until a maximum difference in integrator output was obtained between noise and the clocked waveforms. This maximum was established by plotting a curve of "counts exceeding a threshold" for both noise and clocked waveforms versus phase angle $\beta$. The resulting $\beta$ was the proper phase relation for the particular filter used. After the phase setting, the number of cycles was then trimmed up for maximum results.

To set up the analyzing equipment, first the threshold levels of SIMRAR were set. The method used was to connect a known dc potential directly to the input of the amplitude discriminators. While cycling the machine (which applies a test signal to the discriminators), the discriminator threshold potentiometer was adjusted for the lowest voltage at which

the counter of the discriminator would still count every sample. The counter would then be tripped whenever the integrator output exceeded this preset level. The dc potential input was then changed to a new value and the next discriminator was set. Similarly, all the discriminators were set to the desired threshold levels. By using a dc battery and a micro-voltmeter with a known dc potential in series with it as a "bucking" voltage the gates can be set to 50 millivolts accuracy over the entire 0-60 volt range.

Because of possible drift it was necessary to measure the threshold levels of each amplitude discriminator both before and after each set of trials. Also, it was desirable to allow a suitable warm-up time to stabilize all the circuits as much as possible. The integrator was calibrated by adjusting the output to zero volts while the input was shorted.

After checking all components of the system for correct operation and calibration a preset counter control was set to stop the machine after the desired number of cycles. The input wave and integrator output was monitored to ensure continued correct operation. After the completion of the desired number of cycles the number of counts registered on each counter was taken as data for the histograms.

These are the equipments and procedures, then, which were used to perform the variance experiments reported on in Figs. 4-6 and 4-7. The equipment used for the experiments is shown in Fig. 6-19.

## 6.5 Zero-Crossing Distribution Experiments

The objective of these experiments was to obtain zero-crossing interval distributions for both clocked waveforms and Gaussian noise. The method for doing this is shown in Fig. 6-20. The method consists of first converting the zero-crossing interval into a monotonic height. The Schmidt

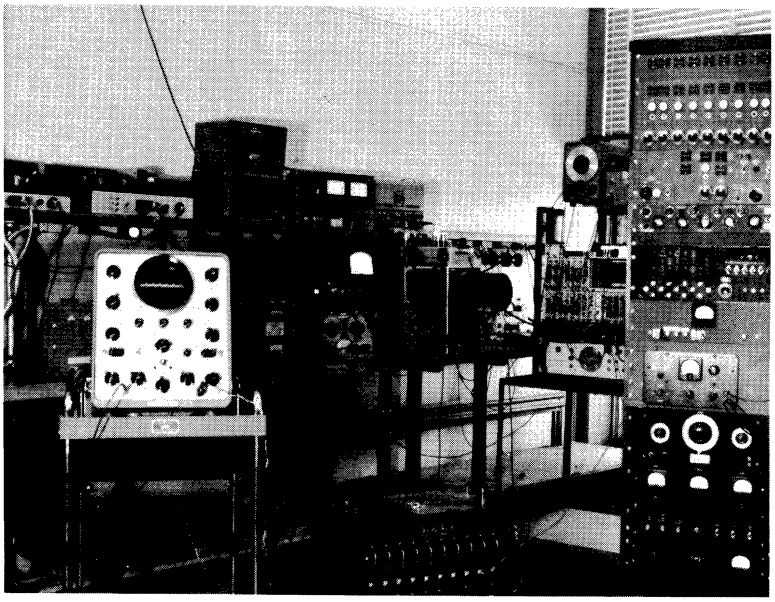

Fig. 6-19. Equipment used in variance experiments.

trigger was then set at the greatest height and the count recorded. The trigger was then reduced by successive incremental amounts, with a count

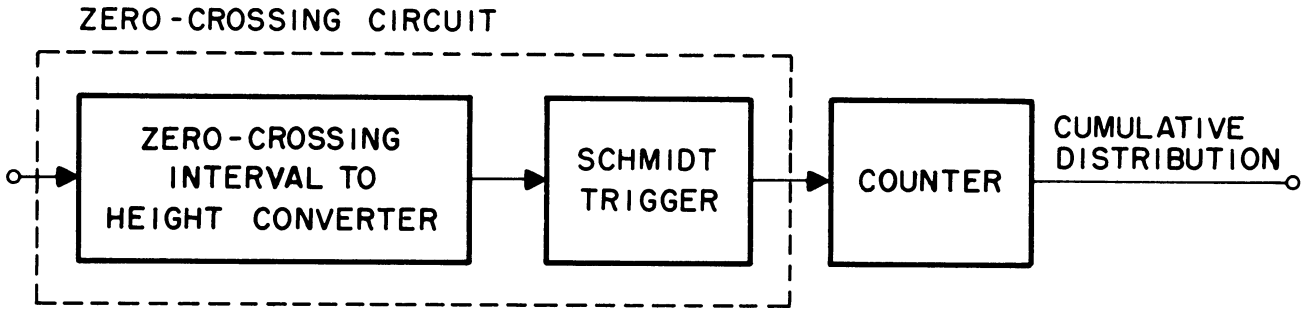


Fig. 6-20. Block diagram of zero-crossing interval distribution experiments.

being taken at each setting. This operation is depicted graphically in Fig. 6-21.

The resulting counts versus length of zero-crossing interval constitute the cumulative distribution curve.

Referring to Fig. 6-20 we shall refer to the combination of the "zero-crossing interval to height converter" and the Schmidt trigger as constituting the "zero-crossing circuit." A special zero-crossing circuit was built for these experiments, the circuit diagram of which is shown in Fig. 6-22. The general idea here was to implement the operations shown in Fig. 6-21. The first operation was to convert the noise waveform into a square wave; thus the interval between zero-crossings of the square wave was directly equal to the interval between zero-crossings of the noise waveform. These square waves were then converted into a monotonic slope so that the height or voltage of this waveform was proportional to the original zero-crossing interval. This varying-height voltage was then fed to a Schmidt trigger which in effect operated on all heights that exceeded a given set level.

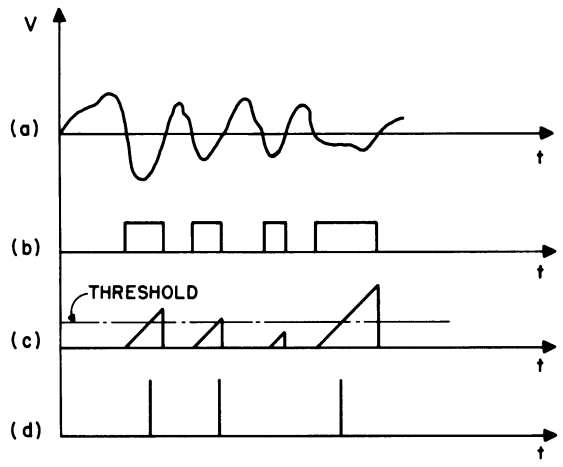


Fig. 6-21. Graphical depiction of distribution measurements.

The first operation of converting the noise waveform into a square wave was accomplished by first limiting (with parallel diodes), then amplifying, and then using this waveform to operate a bistable multivibrator. The reason for using a multivibrator was that it is much easier to obtain good transient response and a constant, flat-topped wave with it than, for example, by attempting to build a good video amplifier to do this job. For accuracy it is necessary to have a non-decaying square wave. The circuit, then, is as follows: the clipping diodes are followed by a grounded emitter amplifier. An emitter follower then feeds the triggering circuits for

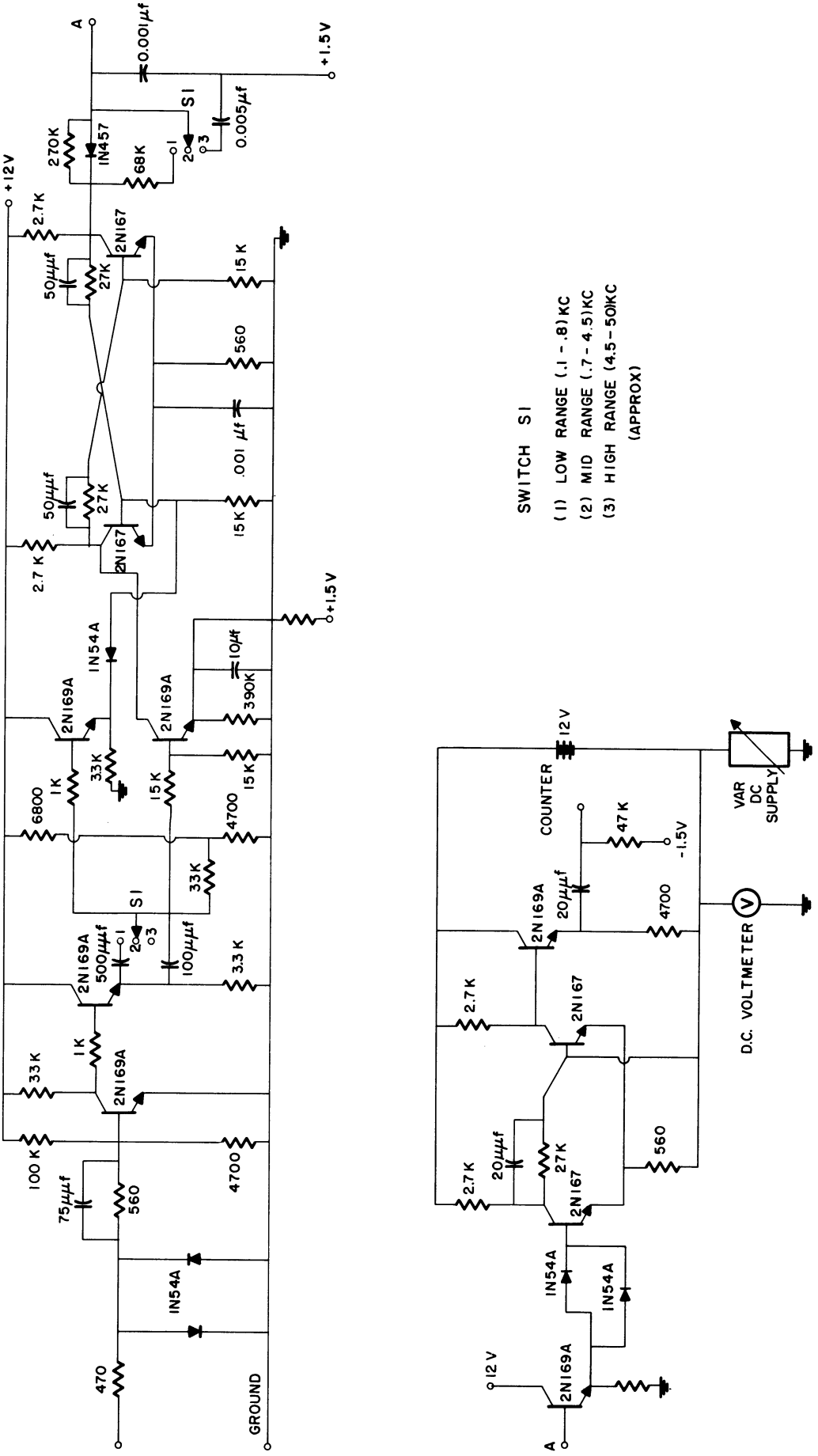


Fig. 6-22. Circuit diagram of zero-crossing circuit.

the bistable multivibrator.

To convert the square waveform into monotonic heights, a simple RC integrating circuit was used. A diode was placed in parallel with the resistor to provide fast recovery time. Thus the waveform now consists of a series of "charge curves" with rapid decay times. The height reached by any particular charge curve is proportional to the time between "off and on" of the square wave--which in turn is equal to the interval between zero-crossings of the input waveform.

An emitter follower then isolates this RC charge circuit from the ensuing Schmidt trigger. The Schmidt trigger is actually a monostable multivibrator in which the triggering voltage is varied by the simple means of varying the common terminal of the multivibrator with respect to ground. This varying voltage was provided by a sensitive potentiometer across a dc battery. Finally an emitter follower was used to couple the monostable output to a counter.

Thus, whenever a charging curve from the RC circuit exceeds the trigger level of the multivibrator, an output pulse is counted by the counter. In this manner the number of times which a zero-crossing interval exceeds a given length is obtained. These "cumulative distribution" data were then converted to "density" data by subtracting adjacent counts.

Because of the use of mercury batteries as power supplies for this entire circuit many problems that are caused by the use of dc power supplies were avoided. Concerning accuracy, one of the most critical components is a silicon diode type 1N457 which is part of the RC charging curve. Even though silicon is much less sensitive to temperature changes than germanium, it was found in early experiments that the RC charge curve varied with different levels of rms voltage coming into the charging circuit.

Therefore a fan was continuously directed toward the silicon diode to keep it at a constant temperature.

To depict the procedure used in this experiment a block diagram of the entire experimental apparatus is shown in Fig. 6-23. For the case where clocked waveforms were the input, a synchronizing pulse was used at the beginning of each period of the shift-register generator so that this period determined the length of the counting time.

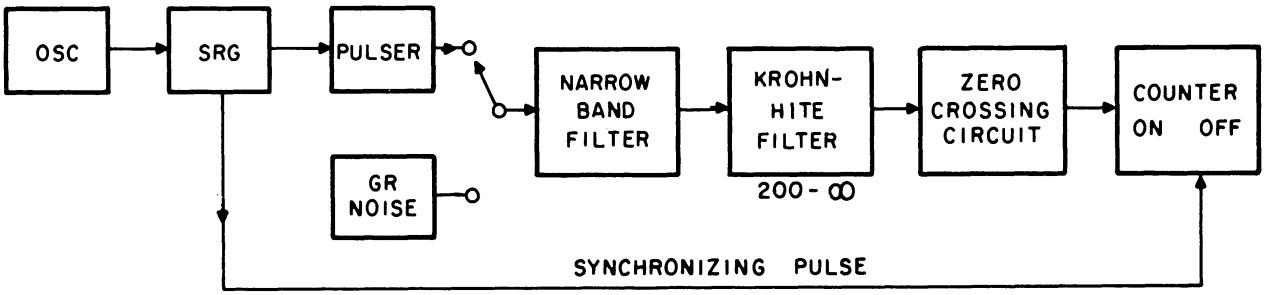


Fig. 6-23. Block diagram of zero-crossing distribution experiments.

Since a simple monotonic curve was used to convert the time intervals into voltage height, the entire experiment's accuracy depended upon the calibration method used. For this reason, a good deal of care was taken with the calibration method, which is described below. The zero-crossing circuit was calibrated at the beginning of a particular run and then immediately afterwards. If the two calibrations differed by only a small amount, the average of the two was taken as the true calibration. If they differed by a large amount, the data were rejected and corrections were made. The calibration procedure itself consisted of using a sine wave oscillator and two counters. One counter was connected to the input sine wave and one to the output of the zero-crossing circuit. The frequency of the oscillator was increased until the two counters differed. If the

oscillator were raised a few cycles above this point where the counters differed, the zero-crossing circuit counter stopped entirely. Thus there were only a few cycles of ambiguity regarding the length of the zero-crossing interval.

In order to make a valid comparison between clocked and true noise waveforms, the rms value of the two waveforms were made equal by measurements with a Ballantine true rms voltmeter. The signal waveform was made as large as possible without saturating and resulted in an rms voltage of about 7 volts. The objective in having the waveform as large as possible, of course, is to define the zero-crossing as well as possible.

The experimental data which resulted from these experiments were recorded in Chapter 5, Figs. 5-2 through 5-9.

## 6.6 Zero-Crossing Oscilloscope Experiments

The purpose of the zero-crossing oscilloscope experiments in Sections 5.2 and 5.3 was to depict, in a visual manner, the regularity and irregularity of the zero-crossings under given conditions. The essential part of the experiment consisted of devising a circuit to trigger the scope trace in the desired manner. The block diagram of the system is shown in Fig. 6-24. The pictures shown in Chapter 5 were taken with one of the following triggering methods: (1) triggering on the first negative-going zero-crossing after a clock pulse; (2) triggering on a clock pulse; (3) triggering on zero-crossings, regardless of clock.

In obtaining the triggering on the first zero-crossing after a clock pulse, the necessary triggering circuit was obtained essentially by modifying the Harvey-Wells digital equipment. The functional diagram of how this was accomplished is shown in Fig. 6-25. The essential idea is to

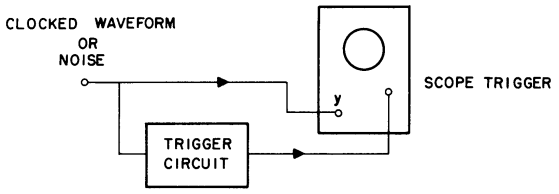


Fig. 6-24. Block diagram of zero-crossing oscilloscope experiments.

use a bistable multivibrator in which the "one" state is controlled by the clock pulse and the zero state is activated by an output from the zero-crossing circuit. It was arranged that the multivibrator stay in its zero state until the next clock pulse, at which it is again returned to its "one" state. The threshold setting of the zero-crossing circuit described in the previous section was set at a low value in order to specify the

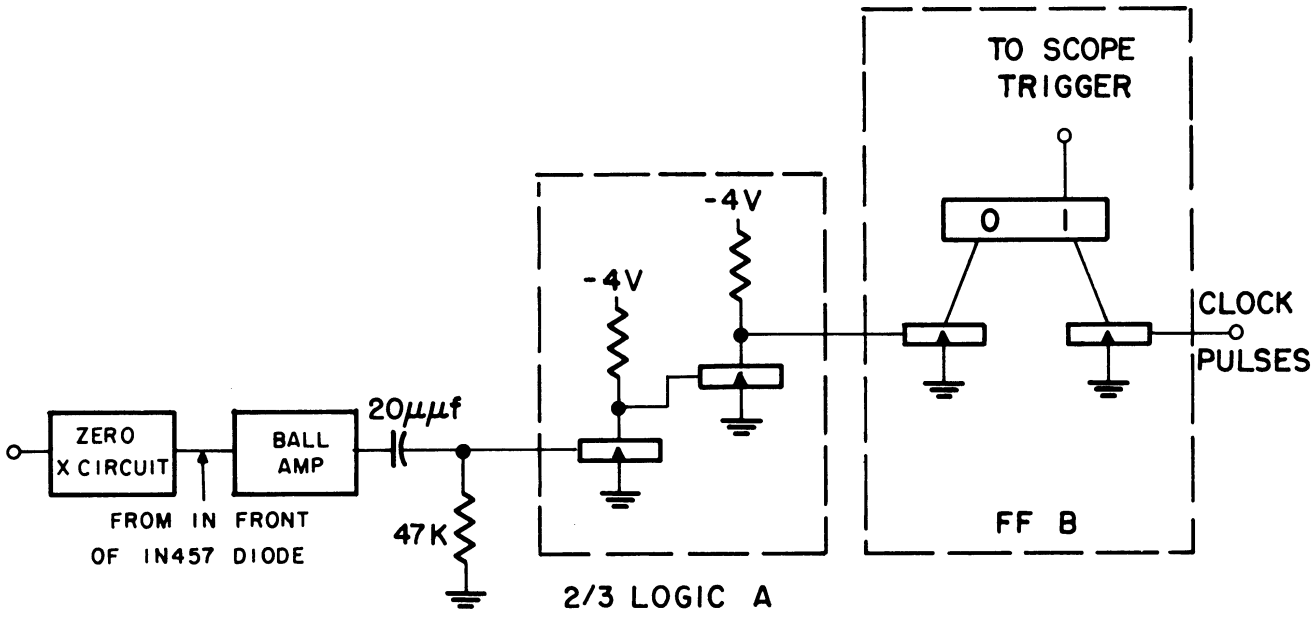


Fig. 6-25. Functional diagram of "triggering" circuit for zero-crossing oscilloscope pictures.

zero-crossings. The result is a pulse at each negative zero-crossing of proper duration and polarity to trigger the multivibrator. Thus an output pulse was achieved whenever a negative zero-crossing was encountered.

Assuming that the clock frequency is less than the ringing frequency of the filter, the waveform out of the multivibrator which is used to trigger the scope is shown in Fig. 6-26. Since the zero-crossing

circuit is producing an output pulse only for negative crossings, it is clear that the triggering circuit will operate on "the first negative crossing after a clock pulse." For this reason, as explained in Chapter 5, irregularities appear earlier than if the circuit were operating on the first crossing (positive or negative after a clock pulse. This is not detrimental as long as the clock frequency is less than the ringing frequency by an amount large enough to enable one to see the regularities in the zero-crossings for a few cycles.

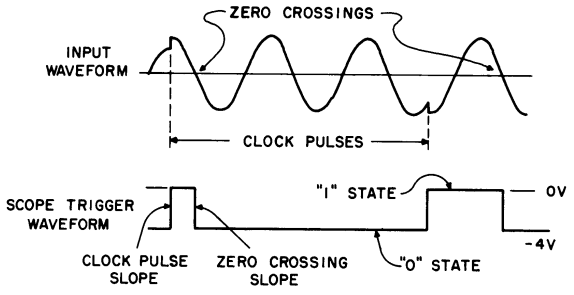


Fig. 6-26. Operation of triggering circuit.

A Dumont Oscilloscope Record Camera Type 299 with Polaroid type 42 film was used in making the photographs. The circuit is first connected as shown in Fig. 6-25. The input waveform must be as large as possible without clipping to ensure triggering the zero-crossing circuit at every zero-crossing. The oscilloscope setting to operate with the circuit described above is as follows: the scope sync selector must be on "external," and the trigger slope selector in the positive-going slope position and at approximately -2 volts. This was the method, then, to implement the triggering circuit for obtaining "triggering on the first negative-going zero-crossing after a clock pulse." The pictures of Figs. 5-1, 5-6, and 5-10 were taken using this method.

For the pictures of Chapter 5 which were taken by triggering on a clock-pulse no special triggering circuit was required; here one merely fed the clock pulses into the external sync terminal of the scope and the trigger-slope setting was negative. The trigger level was set at

approximately -2 volts; Fig. 5-7 was taken with this method.

To trigger on zero-crossings irrespective of position with respect to clock, it was again unnecessary to use the external triggering circuit described above. Here one merely set the oscilloscope to trigger on a zero-crossing. The scope trigger-slope selector was set for either positive or negative and 0 volts.

# CHAPTER VII

## CONCLUSIONS AND RECOMMENDATIONS

This investigation is both an analytical and an experimental study which seeks to find those properties of narrow-band waveforms which characterize the waveform as being clocked instead of Gaussian noise, where the waveforms are generated by hard-filtering sequences of constant amplitude clocked pulses having a random (positive or negative) sign. The properties which were studied and the principle results fall into four categories: (1) ordinary spectrum, (2) short time spectrum, (3) coherent sampled variance, and (4) zero-crossing properties. The results in each of these areas and their significance will be discussed below.

The ordinary spectrum treatment considers two cases: (1) the case where the waveform stems from a periodic clocked sequence and (2) the case where the waveform is the result of a random sequence of pulses in which there are no period considerations. The waveform spectrum was calculated by first finding the spectrum of the sequence of pulses and then using the usual filter-transfer magnitude relation.

For the periodic case the sequences were limited to linear maximal sequences and the long-time spectrum was calculated in terms of the common autocorrelation of these sequences. The sequence spectral result is a series of lines spaced $\frac{f_c}{L}$ apart and having an envelope which is the transform of the major component of the autocorrelation function of the maximal sequence. If the sequence were short enough so that the analyzing equipment had an effective integrating time of the order of 10 or more times the period, one should be able to identify the filtered sequences as a clocked phenomenon as opposed to Gaussian noise. This situation will rarely occur in practice however.

For the case of a random sequence of pulses the spectrum was calculated by what is known as the "direct method." If the pulse sequence values are independent and have a zero mean, this results in a continuous power spectral density which is similar to the envelope of the frequency components of the periodic case. Under these conditions the power spectral density of the sequence of pulses is determined, except for a constant, by the spectrum of the unit pulse itself. If the pulse sequence values have a non-zero mean the power spectral density will contain discrete contributions at multiples of the clock frequency.

The short-time spectrum properties of clocked waveforms are analyzed by writing the output of an analyzing filter (through which the clocked waveform is passed) as a sum of pulses and regarding the short-time spectrum as the square of the output envelope of this analyzing filter. Using this procedure the output envelopes exhibit half-clock symmetry, which means that the two varying envelopes are identical in time if two analyzing filters are placed symmetrically on both sides of any multiple of half-clock frequency. This property was experimentally verified and sound spectrographs depicting the symmetry are shown. A restriction on this result, of course, is that clocked waveform energy must be available on both sides of some multiple of half-clock frequency in order to observe the symmetry. Two other symmetrical situations were studied: one-quarter clock and one-eighth clock relations. For the quarter-clock case it was found that the envelopes of the two symmetrical positions behave according to two different sequences, where the one sequence is the precise complement of the other (the sign of every other pulse is reversed). Although this is a firm relation between the effective inputs for the two envelopes no quantitative relation between the resulting envelopes has been found. It

is recommended that, should this case be of interest for a particular application, this envelope relation be explored in a refined statistical manner to seek a reliable distinguishing characteristic (from the measured noise envelopes). Much the same applies to the one-eighth clock relation. Although the two envelopes can be written as the sum of related quantities no simple quantitative relation between the envelopes is evident. Therefore, any discernible characteristic will have to result from a refined statistical study.

In dealing with statistical amplitude properties of clocked waveforms the main concern was with the sampled variance, where the samples are taken coherently with the clock. For independent values of the pulse sequence this sampled variance of the clocked waveform is a function only of the impulse response of the filter. Of course, it also varies with the phase position of the sampling with respect to the clock. Thus if one knew the clock frequency and could sample coherently with it, one could in principle always distinguish a clocked waveform from a noise waveform by sampling at two proper phase positions and determining the two variances. For a clocked case there will be a non-zero difference if proper phase positions are chosen while for the noise case they should be zero. Since the behavior of the sampled variance as a function of phase position depends upon the relation of the filter frequency to the clock frequency, a maximum and a minimum behavior were calculated for an exponential filter. It was found that, for filter frequencies which are any multiple of half-clock frequencies, the sampled variance shows a maximum variation over the range of the sampling phase position. A minimum for this variation is shown whenever the filter frequency equals an odd multiple of quarter-clock frequency. Another property is that the sampled variance, over the range

of the sampling phase position, has an integral number of cycles whenever the filter frequency is any multiple of half-clock frequency. For any other relation the sampled variance does not have such an integral number of cycles.

Instead of utilizing the sampled variance directly to distinguish the clocked waveform from noise, as described above, a method using a "sum of weighted variances" was evolved. This permitted using a continuous multiplying waveform rather than a sampling procedure. The question of what continuous multiplying waveform is best was answered by expressing the output in terms of the sampled variance. A multiplying waveform of the same form as the varying component of the sampled variance was found to be best. Thus, in implementing this distinguishing method, the clocked waveform is first squared and then multiplied by a coherent, repetitive waveform (with period equal to the clock interval) of the above form. This product is then integrated for a time much longer than the clock interval. For a sufficiently long integrating time the output will be non-zero for the clocked case, and zero for a noise waveform.

The proper multiplying wave for a narrow-band exponential filter is a coherent sine wave, if the filter frequency ($f_o$) is any multiple of half-clock frequency ($\frac{f_c}{2}$), and a phase-bumped sine wave for any other frequency relation. Since this method uses the sampled variances, the maximum and minimum relations noted before hold here: for an exponential filter with $f_c \leq 2f_o$ the most difficult distinguishing situation will occur for the filter frequency equal to an odd multiple of quarter-clock frequency, and the easiest situation will occur for the filter frequency equal to a multiple of half-clock. Although this is precisely true only for exponential filters, it will hold approximately for non-exponential,

narrow-band filters. Experimental tests run in the range $f_c \leq 2f_o$ using both an exponential and a non-exponential filter verified that, if the multiplying waveform is run coherently with the clock and if the integrating time is sufficiently long, the given clocked waveform can be distinguished from noise in the stated range of clock frequencies.

The advantage of this method is that it is not dependent on particular filter frequency-to-clock frequency positions, as are the above symmetry properties. Note also that, with coherent tests, external noise in principle will not ruin the test whereas it would be expected to quickly wash out the above symmetry properties. The limitations, however, are that the clock frequency must be known, the tests must be run coherently with the clock, and the filter's variance-versus-phase must be estimated. Also, as is true for any distinguishing method, the test will become more and more difficult as clock frequency increases indefinitely relative to the filter frequency. Since knowledge of the clock frequency is required, it is desirable to extend this study to find a suitable scanning procedure.

The zero-crossing investigation consisted of a basic analytical approach and experimental measurements of the zero-crossing interval probability distributions. Again, the case of the exponential filter provides the only means of showing precise properties but these properties have significance also for non-exponential narrow-band filters. If an exponential filter frequency is any multiple of half-clock frequency the zero-crossings exhibit a regularity throughout time which, of course, provides an easily discernible case. The zero-crossing interval distribution for this case consists of a spike at $\pi$ (for a normalized interval) and a small subsidiary spike at $\frac{\pi}{2}$. If the filter frequency is higher than the clock frequency the zero-crossings exhibit a regularity within a clock interval,

but these sets of crossings move with respect to each other from interval to interval. Thus, this might be considered as a local regularity; these regularity properties were demonstrated experimentally with oscilloscope pictures. The zero-crossing interval probability distribution again shows a high spike at $\pi$ but no action at $\frac{\pi}{2}$. As the filter frequency becomes equal to and less than the clock frequency no regularity of zero-crossings can be derived and the zero-crossing probability distribution begins to approach that of a Gaussian noise case. For a general non-exponential filter the above regularity properties are essentially perturbed both by the time varying envelope and phase of the filter's pulse response. Also, the zero-crossing distribution appears to much more rapidly approach that of the Gaussian case. Hence, it is concluded from experimental evidence that the zero-crossing distribution does not serve as a reliable characterization for the clocked waveforms unless one is dealing with special cases of exponential filters.

In addition to the suggested extensions noted above it is recommended that the coherent distinguishing method based on the sampled variance be pursued to find what properties remain if the clocked waveform is first limited and then filtered again. Another area is to explore the autocorrelation of zero-crossings, both analytically and experimentally. The general idea here is to look for statistical action at time delays which are multiples of the clock interval. Finally, where symmetry properties are desirable and applicable, it is recommended that the short-time autocorrelation of the clocked waveform (the transform of a special case of the short-time spectrum dealt with herein) be explored. Since any information available in one domain of a transform is available in the other, it is desirable to ascertain whether the time domain case is more convenient for using short-time properties to characterize the clocked waveform.

LIST OF REFERENCES


1. S. O. Rice, "Mathematical Analysis of Random Noise," Bell System Technical Journal, XXIII, XXIV, p. 177.

2. J. H. Laning and R. H. Battin, Random Processes in Automatic Control (New York: McGraw-Hill Book Co., Inc., 1956), p. 154.

3. J. Hilibrand, "Characterization of Probability Distribution for Excess Physical Noises," Research Laboratory of Electronics Technical Report No. 276, Massachusetts Institute of Technology (September 1956).

4. D. A. Middleton, "On the Theory of Random Noise. Phenomenological Models I and II," Journal of Applied Physics, XXII, No. 9 (September 1956).

5. B. Mazelsky, "Extension of Power Spectral Methods of Generalized Harmonic Analysis to Determine Non-Gaussian Probability Functions of Random Input Disturbances and Output Response of Linear Systems," Journal of Aeronautical Sciences, XXI, No. 3 (March 1954).

6. T. G. Birdsall and M. P. Ristenbatt, "Introduction to Linear, Shift-Register Generated Sequences," Cooley Electronics Laboratory Technical Report No. 90, The University of Michigan Research Institute (October 1958).

7. S. W. Golomb, Sequences with Randomness Properties (Advance printing; New York: Glenn L. Martin Co., June 1955).

8. W. B. Davenport and W. L. Root, Random Signals and Noise (New York: McGraw-Hill Book Co., Inc., 1958), p. 90.

9. Ibid., p. 70.

10. Ibid., p. 59.

11. W. R. Bennett, "Statistics of Regenerative Digital Transmission," Bell System Technical Journal, XXXVII, No. 6 (November 1958).

12. J. S. Bendat, Principles and Applications of Random Noise Theory (New York: John Wiley and Sons, Inc., 1958), p. 63.

13. R. B. Blackman and J. W. Tukey, "The Measurement of Power Spectra from the Point of View of Communications Engineering. Parts I and II," Bell System Technical Journal, XXXVII, Nos. 1 and 2 (January and March 1958).

14. R. M. Fano, "Short-Time Autocorrelation Functions and Power Spectra," Journal of Acoustical Society of America, XXII, No. 5 (September 1950).

15. Laning and Battin, Op. cit., p. 156

16. Middleton, Loc. cit.

LIST OF REFERENCES--Continued

17. Hilibrand, Op. cit., pp. 17-24.

18. Bennett, Loc. cit.

19. Rice, Loc. cit.

20. J. A. McFadden, "The Axis-Crossing Intervals of Random Functions. Parts I and II," IRE Transactions on Information Theory; IT-3, No. 4; IT-4, No. 1 (December 1957 and March 1958).

21. A. Kohlenberg, "Notes on the Zero-Crossing Distribution of Gaussian Noise," Lincoln Laboratories Technical Memorandum No. 44, Massachusetts Institute of Technology (October 1953).

22. G. M. White, "Experimental Determination of Zero-Crossing Distribution W(NT)," Cruft Laboratory Technical Report No. 265, Harvard University (June 1957), and "An Experimental System for Studying the Zeros of Noise," Cruft Laboratory Technical Report No. 261, Harvard University (May 1957).

23. K. Blötekjaer, "An Experimental Investigation of Some Properties of Bandpass Limited Gaussian Noise," IRE Transactions on Information Theory, IT-4, No. 3 (September 1958).

24. Digital Products Catalog, Harvey-Wells Electronics, Inc., Research and Development Division, West Roxbury, Massachusetts.

25. W. Koenig, H. K. Dunn, and E. Y. Laey, "The Sound Spectrograph," Monograph B-1415, Technical Aspects of Visible Speech, Bell Telephone System Technical Publication.

26. S. Giser, "An All Electronic High Speed Multiplier," Instrumentation Laboratory Report, Massachusetts Institute of Technology.

DISTRIBUTION LIST

| Copy No. | |
|---|---|
| 1-2 | Commanding Officer, U. S. Army Signal Research and Development Laboratory, Fort Monmouth, New Jersey, ATTN: Senior Scientist, Countermeasures Division |
| 3 | Commanding General, U. S. Army Electronic Proving Ground, Fort Huachuca, Arizona, ATTN: Director, Electronic Warfare Department |
| 4 | Chief, Research and Development Division, Office of the Chief Signal Officer, Department of the Army, Washington 25, D. C., ATTN: SIGEB |
| 5 | Chief, Plans and Operations Division, Office of the Chief Signal Officer, Washington 25, D. C., ATTN: SIGEW |
| 6 | Commanding Officer, Signal Corps Electronics Research Unit, 9560th USASRU, P. O. Box 205, Mountain View, California |
| 7 | U. S. Atomic Energy Commission, 1901 Constitution Avenue, N.W., Washington 25, D. C., ATTN: Chief Librarian |
| 8 | Director, Central Intelligence Agency, 2430 E Street, N.W., Washington 25, D. C., ATTN: OCD |
| 9 | Signal Corps Liaison Officer, Lincoln Laboratory, Box 73, Lexington 73, Massachusetts, ATTN: Col. Clinton W. Janes |
| 10-19 | Commander, Armed Services Technical Information Agency, Arlington Hall Station, Arlington 12, Virginia |
| 20 | Commander, Air Research and Development Command, Andrews Air Force Base, Washington 25, D. C., ATTN: RDTC |
| 21 | Directorate of Research and Development USAF, Washington 25, D. C., ATTN: Chief, Electronic Division |
| 22 | Commander, Wright Air Development Center, Wright-Patterson Air Force Base, Ohio, ATTN: WWAD-Distribution |
| 23 | Commander, Wright Air Development Center, Wright-Patterson Air Force Base, Ohio ATTN: WWRNGW-1 |
| 24 | Commander, Wright Air Development Center, Wright-Patterson Air Force Base, Ohio, ATTN: WCLGL-7 |
| 25 | Commander, Air Force Cambridge Research Center, L. G. Hanscom Field, Bedford, Massachusetts, ATTN: CROTLR-2 |
| 26 | Commander, Rome Air Development Center, Griffiss Air Force Base, New York, ATTN: RCSSLD |
| 27 | Commander, Air Proving Ground Center, ATTN: Adj/Technical Report Branch, Eglin Air Force Base, Florida |
| 28 | Commander, Special Weapons Center, Kirtland Air Force Base, Albuquerque, New Mexico |
| 29 | Chief, Bureau of Ordnance, Code ReO-1 Department of the Navy, Washington 25, D. C. |
| 30 | Chief of Naval Operations, EW Systems Branch, OP-347, Department of the Navy, Washington 25, D. C. |
| 31 | Chief, Bureau of Ships, Code 840, Department of the Navy, Washington 25, D. C. |
| 32 | Chief, Bureau of Ships, Code 843, Department of the Navy, Washington 25, D. C. |
| 33 | Chief, Bureau of Aeronautics, Code EL-8, Department of the Navy, Washington 25, D. C. |
| 34 | Commander, Naval Ordnance Test Station, Inyokern, China Lake, California, ATTN: Test Director-Code 30 |
| 35 | Commander, Naval Air Missile Test Center, Point Mugu, California, ATTN: Code 366 |
| 36 | Director, Naval Research Laboratory, Countermeasures Branch, Code 5430, Washington 25, D. C. |
| 37 | Director, Naval Research Laboratory, Washington 25, D. C., ATTN: Code 2021 |
| 38 | Director, Air University Library, Maxwell Air Force Base, Alabama, ATTN: CR-4987 |
| 39 | Commanding Officer-Director, U. S. Naval Electronic Laboratory, San Diego 52, California |
| 40 | Office of the Chief of Ordnance, Department of the Army, Washington 25, D. C., ATTN: ORDTU |
| 41 | Chief, West Coast Office, U. S. Army Signal Research and Development Laboratory, Bldg. 6, 75 S. Grand Avenue, Pasadena 2, California |
| 42 | Commanding Officer, U. S. Naval Ordnance Laboratory, Silver Springs 19, Maryland |
| 43-44 | Chief, U. S. Army Security Agency, Arlington Hall Station, Arlington 12, Virginia, ATTN: GAS-24L |
| 45 | President, U. S. Army Defense Board, Headquarters, Fort Bliss, Texas |

DISTRIBUTION LIST (Cont'd)

| Copy No. | |
|---|---|
| 46 | President, U. S. Army Airborne and Electronics Board, Fort Bragg, North Carolina |
| 47 | U. S. Army Antiaircraft Artillery and Guided Missile School, Fort Bliss, Texas, ATTN: Electronic Department |
| 48 | Commander, USAF Security Service, San Antonio, Texas, ATTN: CLR |
| 49 | Chief of Naval Research, Department of the Navy, Washington 25, D. C., ATTN: Code 931 |
| 50 | Commanding Officer, U. S. Army Security Agency, Operations Center, Fort Huachuca, Arizona |
| 51 | President, U. S. Army Security Agency Board, Arlington Hall Station, Arlington, 12, Virginia |
| 52 | Operations Research Office, Johns Hopkins University, 6935 Arlington Road, Bethesda 14, Maryland, ATTN: U. S. Army Liaison Officer |
| 53 | The Johns Hopkins University, Radiation Laboratory, 1315 St. Paul Street, Baltimore 2, Maryland, ATTN: Librarian |
| 54 | Stanford Electronics Laboratories, Stanford University, Stanford, California, ATTN: Applied Electronics Laboratory Document Library |
| 55 | HRB-Singer, Inc., Science Park, State College, Penn., ATTN: R. A. Evans, Manager, Technical Information Center |
| 56 | ITT Laboratories, 500 Washington Avenue, Nutley 10, New Jersey, ATTN: Mr. L. A. DeRosa, Div. R-15 Lab. |
| 57 | The Rand Corporation, 1700 Main Street, Santa Monica, California, ATTN: Dr. J. L. Hult |
| 58 | Stanford Electronics Laboratories, Stanford University, Stanford, California, ATTN: Dr. R. C. Cumming |
| 59 | Willow Run Laboratories, The University of Michigan, P. O. Box 2008, Ann Arbor Michigan, ATTN: Dr. Boyd |
| 60 | Stanford Research Institute, Menlo Park, California, ATTN: Dr. Cohn |

| Copy No. | |
|---|---|
| 61-62 | Commanding Officer, U. S. Army Signal Missile Support Agency, White Sands Missile Range, New Mexico, ATTN: SIGWS-EW and SIGWS-FC |
| 63 | Commanding Officer, U. S. Naval Air Development Center, Johnsville, Pennsylvania, ATTN: Naval Air Development Center Library |
| 64 | Commanding Officer, U. S. Army Signal Research and Development Laboratory, Fort Monmouth, New Jersey, ATTN: U. S. Marine Corps Liaison Office, Code AO-4C |
| 65 | President U. S. Army Signal Board, Fort Monmouth, New Jersey |
| 66-76 | Commanding Officer, U. S. Army Signal Research and Development Laboratory, Fort Monmouth, New Jersey<br>ATTN: 1 Copy - Director of Research<br>1 Copy - Technical Documents Center ADT/E<br>1 Copy - Chief, Ctms Systems Branch, Countermeasures Division<br>1 Copy - Chief, Detection & Location Branch, Countermeasures Division<br>1 Copy - Chief, Jamming & Deception Branch, Countermeasures Division<br>1 Copy - File Unit No. 4, Mail & Records, Countermeasures Division<br>1 Copy - Chief, Vulnerability Br., Electromagnetic Environment Division<br>1 Copy - Reports Distribution Unit, Countermeasures Division File<br>3 Cpys - Chief, Security Division (for retransmittal to BJSM) |
| 77 | Director, National Security Agency, Ft. George G. Meade, Maryland, ATTN: TEC |
| 78 | Dr. H. W. Farris, Director, Cooley Electronics Laboratory, University of Michigan Research Institute, Ann Arbor, Michigan |
| 79-99 | Cooley Electronics Laboratory Project File, University of Michigan Research Institute, Ann Arbor, Michigan |
| 100 | Project File, University of Michigan Research Institute, Ann Arbor, Michigan |

Above distribution is effected by Countermeasures Division, Surveillance Dept., USASRDL, Evans Area, Belmar, New Jersey. For further information contact Mr. I. O. Myers, Senior Scientist, telephone PRospect 5-3000, Ext. 61252.